Towards optical quantum information processing using Rydberg dark-state polaritons

DAVID PAREDES-BARATO

Towards optical quantum information processing using Rydberg dark-state polaritons

David Paredes Barato

Abstract

This thesis proposes a novel method to implement universal quantum gates for photonic qubits using the strong dipole-dipole interactions present in a cold gas of Rydberg atoms and the control offered by microwave fields. By means of electromagnetically induced transparency (EIT) we store the information encoded in photonic qubits as Rydberg excitations, and then couple these to neighbouring states using microwaves. Microwaves alter the range of the dipole-dipole interactions between the excitations, and a suitable geometrical arrangement of the excitations in the cloud leads to a controlled π phase shift in the system's wavefunction, the basis of the universal gates proposed. After processing, the excitations in the medium are later retrieved as photons.

A theoretical description of the implementation of a 2-qubit universal gate is presented and a numerical analysis shows the feasibility of its implementation in a cold cloud of Rubidium atoms. A scheme is also proposed to construct more general gates with applications in quantum information processing. These schemes have been made possible by the analysis of recent experiments performed in the group. This analysis is repeated here, along with the characterization of parts of the detection system required to obtain them.

Towards optical quantum information processing using Rydberg dark-state polaritons

David Paredes Barato

A thesis submitted in partial fulfilment
of the requirements for the degree of
Doctor of Philosophy

Department of Physics
Durham University

December 3, 2014

Contents

List of Figures

Declaration

I confirm that no part of the material offered has previously been submitted by myself for a degree in this or any other University. Where material has been generated through joint work, the work of others has been indicated.

David Paredes Barato
Durham, December 3, 2014

Acknowledgements

Everyone who knows me also knows that I have a memory like a sieve (in Spain I would say "I have the memory span of a fish"), so I should apologize beforehand if you have not been included in this brief list. PhD theses in this time and age are rarely a one man's effort, and I have taken inspiration and received help from many people in more ways that I can imagine. Since I like to be thankful for everything that makes an impact in my life, *thank you*, even if you have not been named.

First of all, I would like to express my thanks to Charles Adams and Matt Jones, my supervisors, for their guidance and patience during these past years. Their insight, both in the broad physical concepts, as well as in technical details of the experiments are laudable. I will always be indebted to them for their help during my time in Durham.

I would also like to thank David Szwer for all the help he has given me in these years, both academically and personally. Without his friendship, his technical knowledge, his tea and chocolate(s), this thesis would not have been possible as it is. The previous PhD student working on the blockade project, Daniel Maxwell, helped me during great part of his PhD to understand the experiment in lab 56 and to come to terms with it; I am still learning from his tenacity and I am very grateful to him. I must thank Hannes Busche for his technical expertise and his thoroughness; I wish both him and Simon Ball the best of luck in the new experiment.

I must thank Christophe Vaillant: he is an excellent rubber-duck debugging partner and a nice sports mate; he has taught me pretty much everything I know about dipole-dipole interactions. Both Tommy Ogden and Danielle Boddy have helped me uncountable times, both scientifically and personally, and have been exceptional sports buddies. You have been (and I will consider you) really good friends throughout.

I thank Graham Lochead for his continued support and banter, and for proof-reading the complete manuscript (in just 3 days!). May your future be bright! I should thank both Ifan Hughes and David Petrosyan for providing some (very) important comments which have greatly improved the scientific content of this thesis.

Of course, these years would not have been the same if they were not spent in the AtMol department. Thanks to the very welcoming environment, I have had the most wonderful experience, both inside and outside of the

department. It is because of the friendly atmosphere that I have been able to discuss Physics with a lot of people. In particular, I would like to thank Simon Gardiner, Kevin Weatherill, Christoph Weiss, James Keaveney, Ulrich Kröhn, Liz Bridge, Michael Köppinger, Jon Pritchard, Dan Saddler, Chris Wade, Rob Bettles and Nikola Sibalic for all the big and small scientific contributions that impacted my work, and for always having a smile in your face.
Within the group I have been able to take part in several activities that I love: Fatmol, the amazing group of people sharing cake on Wednesdays; Fitmol, the group of people sharing (good) pain as often as our schedules permitted; the crazy group of people taking part in board games during weekends; and Friday pub, altough you know I am not a keen drinker.
Outside of AtMol, I must thank the people in the DU Judo Club, for their friendship and their help in releasing all the adrenaline built up during the long lab sessions.
I must also thank Rafael Granero for his continued friendship and for embarking himself in crazy scientific projects with me. May this continue for a long time.
Last (but not least) I shall thank my family and friends. I have the tremendous luck of being surrounded by people that I consider exceptional in so many ways that it is impossible for me to give a complete account. Quiero agradecer a mis padres todo lo que han hecho por mi. Siempre han estado allí cuando era necesario y en los no-tan-buenos momentos; así que espero que sigan estando allí y que sigamos compartiendo los buenos tiempos. Los considero un ejemplo de justicia y trabajo duro.
Anche a te, Alice, grazie di tutto. Specialmente, grazie per essere disposta a discutere (con quella passione tua) su ogni tema immaginabile, e per condividere con me il tuo tempo.

To my family and friends:
you have always been there, may you always be there.

E per la mia bella Zingarda.

Chapter 1

Introduction

The aim of this thesis is to show a scheme to implement universal quantum gates that use photonic qubits and Rydberg atoms.

In this Chapter, the relevance of the work is put in the context of classical and quantum information processing (QIP). Then, the reasons for choosing photons as carriers of quantum information (QI) and Rydberg atoms to provide the processing of the information are explained. The Chapter finishes with an overview of the rest of the thesis.

1.1 Quantum information processing

In the same way that people like Babbage, Lovelace, von Neumann, Zuse, Turing, and Shannon [2–5] developed information theory and computing machines during the 19th and 20th centuries, people in this century aspire to harness the power of the quantum world to understand quantum information theory and apply it to solve problems.

The pioneers of classical computing were interested in constructing a general-purpose computing machine able to solve problems, which did not need to be rebuilt every time they changed the problem to solve.

However, some problems that people are interested in solving are hard to compute using current technology. One example of hard simulation is that of a complex, strongly correlated quantum-mechanical system [6]. These simulations are used to design advanced materials such as high temperature superconductors. Simulating a quantum system with a small number of quantum objects is feasible, and scientists do so routinely all around the world using desktop computers; however, as Feynman pointed out [7], increasing the number of quantum objects to simulate also increases the memory and processing requirements to perform computations exponentially, and the specifications of even the fastest supercomputers are rapidly surpassed. Another example of these hard computations is the factorisation of large numbers into their prime number representation [8] - which is a problem in cryptography that many governmental and non-governmental institutions are interested in.

The notable properties of quantum mechanics led Feynman [7] and others to propose a new type of computational device. This type of computer would be able to simulate efficiently any other quantum system: a quantum simulator. Along the same lines, Deutsch [9] proposed a computing architecture that generalises that of Turing's [3], and suggests the use of *quantum gates* in the same way a Turing machine does.

The marriage of quantum mechanics and information and computational complexity theory promises interesting developments. There are many problems in which a quantum computer could surpass the performance of a classical one: Shor's algorithm [10] presents a way to factorise big numbers, which is the key element in current cryptographic systems; Grover's algorithm [11] allows a quadratic speedup in searching an unsorted database[1], etc. [13, 14].

Implementing the ideas behind quantum computation (QC) is a different

[1] Which is only a linear problem but one which has a general interest with the increasing data requirements in business and administration contexts [12].

issue, and a *universal quantum computer* does not exist yet[2]. Di Vincenzo [16] put forward a set of criteria that a physical system needs to fullfil if it is to implement a quantum computer:

- A scalable physical system with well-defined qubits
- The ability to initialise the state of the system to a pure state
- Long decoherence times
- A universal set of quantum gates
- Selective qubit measurement

The three following criteria are of particular importance when deciding on a system to build a quantum computer. One is the identification of well-defined qubits: that is, we need to identify a physical system able to encode QI that abides by quantum mechanical rules. The second one is long decoherence times: the decoherence is a measure of the detrimental effect that the environment has on the preservation of QI and correlations; a long decoherence time is required to perform computations on the QI before decoherence renders it unusable. Finally, we need a universal set of quantum gates, which is one whose elements can approximate any unitary operation with arbitrary precision [17]. The other two criteria are requirements to be able to start a computation (initialise the system to a pure state), and to be able to read the results of the computation (selective qubit measurements).

Although it is still not clear when QC and other related technologies obtain their advantage over classical computation in certain problems, people often talk about "resources" that can be harnessed towards certain tasks. Most of these rely on the coherence properties of joint systems. Examples

[2] Even if building a general purpose quantum computer is hard, it is not necessary to demonstrate, in the mean time, the speed-up offered in the quantum domain in certain hard problems [15].

of these resources are entanglement [18, 19], discord [20, 21], or negative-quasiprobabilities [22].

Of course this is not the only proposal for QC, with other examples being adiabatic QC [23], more similar to Feynman's idea to an analogue quantum computer; or topological QC [24], where the nonlocal encoding of the QI in *multiquasiparticles* makes these machines immune to errors created by local perturbations. However, in this thesis we are interested in the particular mode of computation called *gate based* quantum computation, or the *quantum-circuit model*.

1.2 The role of decoherence: light as an ideal carrier of quantum information

A common drawback of using quantum properties to perform tasks is the irreversibility of the measurement process and the susceptibility of these systems to decoherence. Whenever a measurement of a system is performed, the subtle coherences encoded in the system disappear, and the systems irreversibly collapse to a (classical) state that can be observed[3]. On performing quantum computations, one needs to retain these coherences during the unitary evolution of the system. We need strong measurements to read out the results of a computation, which means a system that interacts strongly upon readout; however, if the coupling between the system and its environment results in quantum information being *leaked* to the environment, those coherences also vanish, damaging the computation process. The loss of these correlations between parts of the system is termed decoherence. In words of Timoty P. Spiller [26]: *"If you keep opening the oven door to see what's happening, or the door fits badly so heat leaks to the environment, your soufflé*

[3] Other type of *weak* measurements are possible [25], but they are beyond the scope of this thesis.

will flop".

Decoherence can be minimised if QI is encoded in physical systems that interact weakly with the environment, such as light. By minimising their interaction, we minimise the information exchange between the important pieces for the computation and the (uncontrolled) rest of the universe. In this sense, photons (elementary excitations of the electromagnetic field modes) are ideal for encoding QI processing: while interacting relatively weakly with non resonant matter, photons can encode QI in many ways (polarisation, orbital angular momentum (OAM), spatial and temporal degrees of freedom, etc.); furthermore, they also travel as fast as it is physically possible, thus allowing easy communication between processing units.

Processing usually involves an exchange of information between different parts of a bigger system, so strong interactions of some kind are required to implement deterministic processors. Other kind of probabilistic processing of photonic qubits is possible [27, 28], in which the nonlinear processing power is achieved via postselection or feedback using auxiliary photons. However, the probability of success of multiqubit gates is strictly less than one [29], which makes concatenating several of these gates very inefficient.

However, strong interactions are not the panacea. For example, it was postulated that *Self-* and *Cross-phase modulation*, based on the Kerr effect [30], could be used to create universal quantum gates [31] when acting on a bipartite degree of freedom of light[4]. In most media these interactions are very weak, which means that we can say different photons *do not interact*. However, when the Kerr effect is so strong that one photon wavepacket could impose a sizeable phase shift[5] to another one, the interaction changes the wavepacket modal structure, which should be preserved for high-fidelity

[4] A bipartite degree of freedom is one that requires two modes for its description, such as polarisation, or the two spatial modes of light after a beamsplitter [32].

[5] We refer here to the phase shift of the electromagnetic field in a given spatio-temporal mode, like the one acquired when the mode traverses a slab of transparent material with an index of refraction different from that of free space [28]. A description of the spatio-temporal modes of a photon wavepacket is given in Chapter 4.

quantum gates [33, 34].

Thus, the realisation of optical QC requires another medium to provide the strong interactions required for QIP.

1.3 Rydberg atoms and strong interactions

Many physical systems present the strong interactions required to implement QI processors: superconducting circuits, nuclear magnetic resonance, trapped ions, atoms in cavities, etc.; however, each of these systems has its advantages and drawbacks, and currently none of them seems to fullfil all of the requirements for scalable QIP when taken alone [35]. This is the reason for the increasing interest in the interfaces between different systems. There is much theoretical and experimental research directed towards harnessing the advantages of strongly interacting systems to perform computations, and combining them with weakly interacting systems (usually light) to solve the problem of communication and long-term storage of QI [36].

In this thesis, Rydberg atoms play the role of a strongly interacting system that can be interfaced with light to implement universal gates, the building blocks for QIP tasks.

1.3.1 Rydberg atoms

Rydberg atoms have been important in the development of quantum theory (e.g. [37, 38]) since Rydberg started studying the spectra of atoms. He discovered a pattern in the spectra of atomic species under certain conditions which allowed him and others to simplify the description of the behaviour of electrons absorbing and emitting radiation in atoms.

While working on a formula to simplify some spectroscopic results Rydberg found that, at least for the simplest spectra, you could write the relationships

between different spectral series in terms of the wavenumbers k of the light emitted [39]. This particular representation was key in the development of quantum mechanics [40], since the wavenumber is proportional to the frequency of light, $E \propto k = \nu/c$, and thus a direct link with electronic energy levels could be made.

An atom in a Rydberg state (or a *Rydberg atom*) is one where one or more electrons have been excited to have a high principal quantum number n. In these states, where the electron is far away from the nucleus and weakly bound, the energies show approximately an inverse square law $E = -R/(n^*)^{-2}$, where $R = 10973731.568\,\mathrm{m}^{-1}$ is the *Rydberg constant* [41], and n^* is called the *effective principal quantum number*. In the (simplest) case of Hydrogen, a positively charged core provides with a $-1/r$ potential for an orbiting single negative charge (the electron), and $n^* = n$. However, in the case of multi-electron atoms, closed electron shells can screen the nuclear charge. Since the orbit of low angular momentum states ($l \leq 3$) is very elliptic, it can penetrate the closed electron shells; therefore, the potential the valence electrons observe is modified from the ideal Coulomb potential at short range. The valence electron can also polarise the inner electrons. Combining these two effects increases the binding energy of the low angular momentum states, and the deviation of the energies with respect to the equivalent Hydrogenic states can be described simply with the introduction of the (l-dependent) *quantum defects* (δ_l) that modify the principal quantum numbers $n^* = n - \delta_l$ [42, 43][6].

This simplicity in the description, alongside the exaggerated properties derived from the large distances between the electrons and the nucleus, have attracted the attention of atomic physicists. In the last quarter of the twentieth century, renewed interest put Rydberg atoms into the focus of research by several groups.

[6] In the rest of this Thesis, the energies of the Rydberg series of Rubidium have been calculated using the quantum defects in [43]

During the 80s, Haroche and others studied the interaction between microwaves and cold atoms in cavities, leading to the field of cavity quantum electrodynamics (CQED) (see, for example, [44, 45]). These, and other experiments, led him to win the Nobel prize in 2012.

Other groups, such as Gallagher's and Pillet's, studied ensembles of cold atoms to reveal the nature of the interactions between these highly excited atoms, and their properties when placed in different kinds of electromagnetic fields [42, 46, 47].

Nowadays, a substantial community of scientist study the properties of Rydberg atoms. First of all, there are studies regarding the properties of the interactions between Rydberg atoms and their detection [48–53] which provide the basic data and models to understand Rydberg phenomenology. Related to these are those which aim at understanding the relationship between Rydberg atoms and their environment [54–56]. Further to these studies, there are groups interested in pairing Rydberg atoms with other Rydberg or ground state atoms to form Rydberg molecules [57–59]. These kind of studies form the basic building blocks of Rydberg Atomic and Molecular Physics.

Additionally, the marriage of the field of Rydberg physics with other areas of physics is a fruitful one. The extraordinary sensitivity of Rydberg atoms to external fields make them very appropriate for applications in metrology [60–62]. The ideas of Rydberg dressing [63–65] and dipole blockade [66–68] provide the basis of many ideas related to QIP (such as universal gates for atomic qubits [69]) and quantum simulation [70–75]. Specially relevant to this thesis is the relatively novel field of nonlinear and quantum optics in Rydberg atom systems [1, 76–88].

1.4 Towards photonic QIP using Rydberg atoms

The idea of exploiting the large dipole-dipole (DD) interactions between Rydberg atoms for photon processing has been analysed theoretically for a variety of scenarios [72, 89–91]. In general this interaction is dissipative, although dissipation can be reduced at the cost of interaction strength by detuning off-resonance [78, 92]. An additional problem is the implicit link between the interaction and propagation, which inevitably leads to a distortion of the photon wave packet and thereby precludes the realisation of high fidelity gates [33, 34]. Quantum gate protocols based on Rydberg atoms have been proposed [93] and realised [94, 95] where the information was encoded in the ground state of the atoms instead of photons.

In a simplified way, the method proposed in this thesis to process photonic qubits in a gas of Rydberg atoms starts with coherently mapping the information carried by the photons onto Rydberg states; then we use the strong dipole-dipole interactions present in the atoms, alongside their strong interactions with microwave fields, to control the effective interactions between the photons; finally, we map the information back into photons, that we measure, and which should have the signature of the interactions.

The first Chapters of this thesis are devoted to the the theory behind the proposal. Chapter 2 is a brief description of the interactions between atoms and light, and provides the basis to understand the interface between photonic qubits and the medium in which they are stored. Chapter 3 reviews some of the properties of Rydberg atoms, especially those related to the strong dipole-dipole interactions they show. In Chapter 4 we review the quantisation of the EM field, and describe the importance of correlation measurements in inferring the quantum nature of the states of light. This Chapter provides the basis to understand some results in Chapter 5 and Chapter 8. Chapter 5 is devoted to a theoretical explanation of the results of recent experiments [1, 86] based on the combination of photon storage in Rydberg states, and

the dynamics generated by microwave fields resonant with a transition in the Rydberg manifold. The main proposal of a universal two-qubit quantum gate [74] is presented in Chapter 6, and an extension to multiple qubits is presented in Chapter 7.

In Chapter 8 we review and characterise a system to obtain the autocorrelation function $g^{(2)}$, which is a fundamental measure of the statistics of the retrieved photons, and a tool to analyse the output of recent experiments performed in the group [1, 86].

Finally, in Chapter 9 we provide a summary of the thesis. We discuss some of the future developments of the experiment, and highlight some outstanding questions in the field.

Chapter 2

Atom light interactions

Our proposal of an all-optical quantum processing unit relies on obtaining nontrivial, controlled photon-photon interactions.

Even if the superposition of photons in a beamsplitter can arguably be seen as a *trivial* or weak[1], probabilistic interaction, it can give rise to non-trivial photon outputs via postselection (see, for example, [27]). However, implementing a full quantum processor using probabilistic gates and postselection becomes inefficient quickly when a large number of gates are needed. This problem can be solved (at least partially) by realising nontrivial photon-photon interactions in a (quasi)deterministic way. We can achieve this objective by mapping the state of the photons into a medium that shows strong, controllable interactions in a deterministic way.

Mapping the state of photons into matter in a reversible way is a known

[1] When indistinguishability is combined with the bosonic nature of the photons, the superposition principle gives rise to interference in the output of a beamsplitter [96]. In the same way we do *not* talk about (water) waves obeying the superposition principle to be "interacting" when they interfere, we consider parts of a subsystem to be interacting when the description of the system cannot be understood by looking at the different components alone (e.g. by adding terms in the Hamiltonian describing the system's evolution). In this sense, quantum statistics is an inherently collective property, which might alter the population of the different energy levels in the system, thus altering the overall energy of the system; however, it does not alter the energy levels themselves, and thus should not be considered as an interaction *per se*. Photon-photon interactions can be considered in QED via the Euler-Heisenberg Lagrangian [97], and optical photons have scattering cross section of $\sigma_{\gamma\gamma} \sim 1.8 \cdot 10^{-69}\,\mathrm{cm}^2$. A small number, indeed.

problem. Using different methods, such as photon-echo, controlled reversible inhomogeneous broadening, the Duan-Lukin-Cirac-Zoller (DLZC) protocol, etc. (see [98]) the state of the light has been stored at the single photon level in solid state (e.g. [99]) and gaseous media (e.g. [100, 101]), with lifetimes up to several minutes [101–104]. Different groups have already stored the states of light encoded in different degrees of freedom like polarisation [105], photon number [106] and orbital angular momentum [107].

One of these methods is electromagnetically induced transparency (EIT), which uses the coherences in three level systems to store photons at the single photon level as "dark-state polaritons" [108–110].

In this chapter, we briefly describe the salient features of two- and three-level systems interacting with electromagnetic fields. We focus our attention on the propagation of light under the conditions of EIT, and the impact of different parameters (such as the detuning, the optical depth and Rabi frequencies) in this process in the phase-gate proposal described in Chapter 6.

2.1 Atom-light interaction basics

When the electric field $\mathbf{E}$ of monochromatic light with frequency ω propagates through a *linear* dielectric medium, the medium acquires a polarisation $\mathbf{P}$ given by

$$\mathbf{P}(\omega) = \epsilon_0 \chi(\omega) \mathbf{E}(\omega), \tag{2.1}$$

where χ is the electric susceptibility of the medium and ϵ_0 is the vacuum permittivity. This constitutive law represents a relationship between the *macroscopic* quantities $\mathbf{E}$ and $\mathbf{P}$. However, it is possible to draw a connection with the *microscopic* behaviour of the (material) system by noting that the polarisation is nothing more than the average dipole moment, $\langle \mathbf{d} \rangle$, per unit volume of the dielectric material, $\mathbf{P} = \langle \mathbf{d} \rangle / V$. electric the

Assuming that wavelength of the light is much larger than the distance between the electron and the nucleus in the atoms (the electric dipole approximation) we can write the Hamiltonian governing the light-matter interaction as

$$H_{\text{int}} = -\mathbf{d} \cdot \mathbf{E}, \tag{2.2}$$

$$\mathbf{d} = \sum_{n} \sum_{m<n} \mathbf{d}_{mn} |m\rangle\langle n| + \mathbf{d}_{nm} |n\rangle\langle m|. \tag{2.3}$$

Depending on the different microscopic models of the material under consideration, it is possible to derive the material's response to the light's electric field by following the von Neumann equation

$$\frac{\partial \rho}{\partial t} = \frac{1}{\mathrm{i}\hbar} [H, \rho] . \tag{2.4}$$

This equation describes the unitary time evolution of the density operator of the system, ρ, generated by the Hamiltonian H. To account for dissipative processes such as spontaneous emission, whilst preserving the normalisation of the density operator, it is possible[2] to convert (2.4) into a master equation by the addition of a Lindblad operator: $\hat{\Gamma}$ [112]

$$\frac{\partial \rho}{\partial t} = \frac{1}{\mathrm{i}\hbar} [H, \rho] + \hat{\Gamma} \ . \tag{2.5}$$

The Lindblad operator

$$\hat{\Gamma} = \sum_{n} \sum_{m<n} \sigma_{mn} \rho \sigma_{mn}^{\dagger} - \frac{1}{2} \left\{ \rho, \sigma_{mn}^{\dagger} \sigma_{mn} \right\} , \tag{2.6}$$

expresses the dissipation of the system coupled to a reservoir. The operators $\sigma_{mn} = c_{mn} \sqrt{\Gamma_n} |m\rangle\langle n|$ are called lowering operators, and represent the transition from $|n\rangle$ to $|m\rangle$. The total decay rate out of state $|n\rangle$ is Γ_n, and $|c_{mn}|^2$

[2] An alternative approach is the Monte Carlo wave function method, based on solving the Schrödinger equation and adding "quantum jumps" to account for dissipation [111].

is the branching ratio of that decay towards state $|m\rangle$.

Therefore, to understand the effect that this propagating electric field has in the system, we should answer the following two questions:

- what is the mathematical description (density matrix ρ) of the system under consideration?
- what is the effect of $\mathbf{E}$ on the Hamiltonian describing the evolution and the susceptibility?

Finally, since (2.4) only provides partial information – namely, the action of light on matter – another equation is required to connect the effect that matter has on the electromagnetic field propagating through it. This is the Maxwell wave equation

$$\left(\frac{\partial^2}{\partial t^2} - c^2\frac{\partial^2}{\partial z^2}\right)\mathbf{E} = -\frac{1}{\epsilon_0}\frac{\partial^2}{\partial t^2}\mathbf{P}. \tag{2.7}$$

The relationship between the properties of propagating light and the microscopic properties of the medium come through the *refractive index* $\hat{n} = \sqrt{1+\chi}$.

Equation (2.1) is a linear response [113] equation, in which the field $\mathbf{E}$ causes a polarisation $\mathbf{P}$of the material, which responds via its susceptibility χ. This reaction depends, as we have said, on the microscopic details of the system via the dipole operator $\mathbf{d}$. Applying a Fourier transform to (2.7) in the time domain, we obtain

$$\left(\frac{\partial^2}{\partial z^2} + \frac{\omega^2}{c^2}\hat{n}^2\right)\mathbf{E}(\omega) = 0, \tag{2.8}$$

with $\omega = 2\pi/t$. The solution of this equation in the monochromatic case is of the form

$$E(z) = E(0)\mathrm{e}^{k_0\int n_\mathrm{I}\mathrm{d}z}\cdot\mathrm{e}^{\mathrm{i}\left(k_0\int n_\mathrm{R}\mathrm{d}z-\omega t\right)}. \tag{2.9}$$

Here, $\hat{n} = n_\mathrm{R} + \mathrm{i}n_\mathrm{I}$, and k_0 is the wavevector in vacuum of the light with

frequency ω. Therefore, the imaginary part of the refractive index affects the amplitude of propagating electric fields, and the real part affects their phase.

If an incoming collimated, monochromatic electric field $E(z = 0) = E_0$ and intensity $I = \frac{\epsilon_0 c \hat{n}}{2} E^2$ enters the medium with homogeneous $\hat{n}$, its intensity decreases exponentially according to the *Beer-Lambert law*,

$$\frac{I(z = L)}{I(z = 0)} = \mathrm{e}^{-\mathrm{OD}}, \tag{2.10}$$

where the *optical depth*, $\mathrm{OD} = 2k_0 n_\mathrm{I} L$, is a measure of the probability of the photons to interact with the medium and being scattered.

Together, (2.5) and (2.7) constitute the Maxwell-Bloch equations[3] of the system, and they describe the evolution for both the system and the field propagating through it

In the following sections we will briefly describe the characteristics of Maxwell-Bloch equations and their solutions in the case of two- and three-level systems.

2.2 Two-Level system

2.2.1 Material system

The simplest material system is that of a two-level system. In our case this system can be the idealisation of an atom in the ground state interacting with a laser field that couples the ground state to an excited state. As the name suggests, it is composed of two levels:$|a\rangle$ is the ground state with energy E_a, and $|b\rangle$ is the excited state, at energy E_b (shown in Figure 2.1 (left)). Their energy difference is $E_{ba} = \hbar\omega_{ba}$. Population in the excited level can spontaneously decay to the ground state with a rate Γ_b. The state of this

[3] Analogous to the Bloch equations, that describe the dynamics of a nuclear spin in a magnetic field.

system is described as $|\psi\rangle = c_a|a\rangle + c_b|b\rangle$, where c_a and c_b are the probability amplitudes of the system being in $|a\rangle$ and $|b\rangle$ (respectively), which satisfy $|c_a|^2 + |c_b|^2 = 1$.

In this simple case, we will assume that the light field (called *probe*) is a single-mode, monochromatic field with angular frequency ω_p and with an amplitude E. The coupling between light and the two-level system is represented by the Rabi frequency $\Omega_p = \mathbf{d}_{ab} \cdot \mathbf{E}/\hbar$.

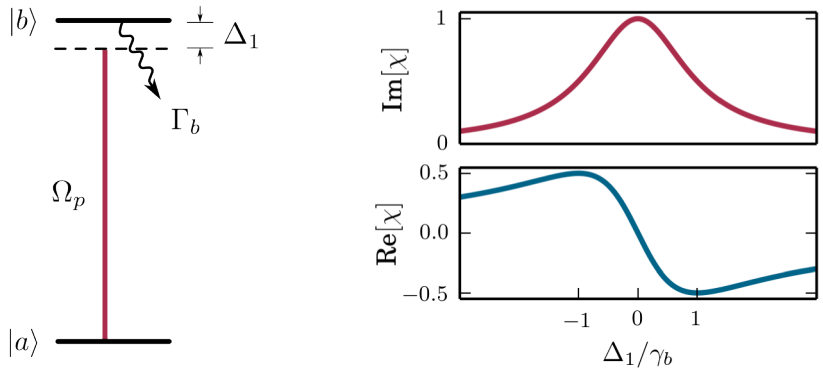

Figure 2.1: (Left) Excitation scheme for a two-level system. A *probe* laser couples levels $|a\rangle$ and $|b\rangle$ with Rabi frequency Ω_p almost resonantly, with detuning Δ_1. The decay from level $|b\rangle$ is Γ_b, and the dephasing from the probe laser γ_p is also accounted for in $\gamma_b = \Gamma_b/2 + \gamma_p$. (Right) Susceptibility of the system. Imaginary (top) and real (bottom) susceptibilities of the system in the weak-probe regime with parameters $\Gamma_a = 100\Omega_p$.

Following (2.5), it is possible to obtain the evolution of the system using the density operator $\rho = |\psi\rangle\langle\psi|$. In this case the polarisation of the medium with a density ρ_0 is its response to the electric field of the incident, monocromatic light

$$\mathbf{P} = \sum \rho_0 \left[\mathbf{d_{ab}} \rho_{ab} \exp(-i\omega_p t) + \text{h.c.}\right], \tag{2.11}$$

where h.c. represents the harmonic conjugate of the term within the brackets.

The energy of an electric dipole in an electric field is

$$H_{\text{int}} = -\mathbf{d} \cdot \mathbf{E}. \tag{2.12}$$

Assuming a real, scalar electric field $E = E_0 e^{\mathrm{i}\omega_p t} + E_0^* e^{-\mathrm{i}\omega_p t}$, this gives rise to rapidly rotating terms in the equation (2.5).

At this point, we resort to an approximation called the *Rotating Wave Approximation* (RWA). You can read more about this approximation in [114], but the basic idea is that, by looking at the dynamics from a frame of reference that is co-rotating with the light field, we can identify and eliminate the fast, counter-rotating terms in the dynamics which violate energy conservation [115], and that, under usual experimental conditions, average out to zero. This introduces a *detuning* in the description, $\Delta_1 = \omega_p - \omega_{ba}$, that measures the difference between the laser frequency and the frequency of the transition, which is zero when the field is resonant. Thus, the Hamiltonian, generator of the unitary evolution in (2.5), becomes

$$H_{\mathrm{2LS}} = \frac{\hbar}{2} \begin{pmatrix} 0 & \Omega_p \\ \Omega_p & -2\Delta_1 \end{pmatrix} . \tag{2.13}$$

The decay in this system is described using the operator $\sigma_{ba} = \sqrt{\Gamma_b}|b\rangle\langle a|$. The off-diagonal dephasing terms in the master equation (2.5), $\Gamma/2$, are affected by the finite linewidth of the probe light γ_p, and we can write them as $\gamma_b = \Gamma_b/2 + \gamma_p$ [116].

In the steady state, when this two-level system is strongly driven, the excited-state population probability distribution is given [117] by the Lorentzian

$$\rho_{bb}^{\mathrm{steady}} = \frac{1}{2} \frac{\gamma_b \Omega_c^2}{\Omega_p^2 \gamma_b + \Gamma_b \left(\Delta_1^2 + \gamma_b^2\right)}. \tag{2.14}$$

This distribution is close to $1/2$ if the driving is much stronger than the linewidth ($\Omega \gg \Gamma_b$) and the field is on resonance ($\Delta_1 = 0$), and close to zero if either the lifetime or the detuning are much bigger than the driving ($\Gamma_b, |\Delta_1| \gg \Omega$).

2.2.2 Rabi oscillations

It is difficult to give closed analytic solutions of (2.5) for the general two-level system with Hamiltonian (2.13) [118]. The dynamics described by (2.13), in the absence of strong damping, leads to oscillations in the population between the ground and excited states, called *Rabi oscillations*. If we neglect the effect of spontaneous emission, $\Gamma_b = 0$, and in the case of the light field being resonant with the the solution of (2.4), when the initial population is in $|a\rangle$, gives an excited state population

$$\rho_{bb}(t) = |c_b(t)|^2 = \sin^2\left(\frac{\Omega_p t}{2}\right). \tag{2.15}$$

This equation shows that the larger the Rabi frequency Ω_p, the faster the cycling of the population between levels $|b\rangle$ and $|a\rangle$.

In this ideal case, a so called 2π pulse (a pulse of light of a certain duration $t_{2\pi}$ and power to give $\Omega_p \cdot t = 2\pi$) sends the population back to the original state, $\rho_{bb}(t_{2\pi}) = \rho_{bb}(0)$. However, even if the population has undergone a full rotation, it is simple to show[4] that the state coefficient changes sign, $c_b(t_{2\pi}) = -1 \cdot c_b(0)$. This change of sign is of paramount importance in the inner workings of the phase-gate, as shall be explained in Chapter 6.

2.2.3 Susceptibility

The two previous sections have dealt with the material two-level system, but we have so far neglected what happens to the light that is propagating. Since for small $|\chi| \ll 1$, $\hat{n} = \sqrt{1+\chi} \approx 1 + \frac{1}{2}\chi$, determining χ determines the response of the system to light via (2.7).

The steady-state of the Maxwell-Bloch equations for the two-level system in the weak-probe regime [114] shows a relationship between the susceptibility

[4] See Appendix B for details.

and ρ_{21} via (2.1) and $\langle \mathbf{d} \rangle = \mathrm{Tr}\{\rho, \mathbf{d}\}$:

$$\chi = -2\frac{d_{ba}^2 \rho_0 \rho_{ba}}{\epsilon_0 \hbar \Omega_p}, \tag{2.16}$$

$$= \frac{d_{ba}^2 \rho_0}{\epsilon_0 \hbar} \frac{i\gamma_b - \Delta_1}{\Omega_p^2/2 + \Delta_1^2 + \gamma_b^2}. \tag{2.17}$$

The imaginary part of the susceptibility, χ_{I}, is a Lorentzian lineshape, with an effective width $\Gamma_{\mathrm{eff}} = \sqrt{\gamma_b^2 + \Omega_p^2/2}$, and centered at $\Delta_1 = 0$. According to the definition of the optical depth, this means that light propagating through the medium is more strongly absorbed when resonant with the two-level transition frequency. Conversely, when the light frequency is far off-resonance ($|\Delta| \gg \max(\gamma_b, \Omega_p)$), the medium shows lower opacity.

Regarding the real part χ_R, the medium shows a region of *anomalous dispersion* near resonance; that is, the refractive index is reduced with increasing frequency ($\mathrm{d}n/\mathrm{d}\omega < 0$). Although it is not relevant in the present case, due to strong absorption present in the region where this occurs, we note that strong anomalous dispersion can give rise to so called *superluminal propagation* [119].

2.3 Three-Level system

The phenomenology associated with three-level systems has been described extensively in the literature. One of these phenomena is *electromagnetically induced transparency* [108–110, 120], which allows for a medium to become transparent on resonance and a resonant *probe* beam to be stored in the medium. In this section we briefly review the salient features of three-level systems interacting with two resonant electromagnetic fields, and describe the conditions under which the quantum state of light can be stored in the medium.

2.3.1 Material system

The system under consideration consists of three levels, $|a\rangle, |b\rangle$ and $|c\rangle$, with energies $E_i = \hbar\omega_i$ for $i \in (a, b, c)$, in a ladder configuration (Figure 2.2); these levels are coupled via the *probe* and *coupling* light beams. The probe beam is almost resonant with the transition $|a\rangle$–$|b\rangle$, with frequency ω_p and detuning $\Delta_1 = \omega_{ba} - \omega_p$. The coupling beam is almost resonant with the transition $|b\rangle$–$|c\rangle$. Its frequency is ω_c, and the two-photon detuning (taking into account the single-photon detuning Δ_1 is $\Delta_2 = \hbar\left(\omega_c - \omega_a - (\omega_c + \omega_p)\right)$. The spontaneous decay rate from level $|b\rangle$ is given by Γ_b, and the metastable state $|c\rangle$ has a linewidth $\Gamma_c \ll \Gamma_b$.

The Hamiltonian evolution is governed by

$$H_{3\mathrm{LS}} = \frac{\hbar}{2}\begin{pmatrix} 0 & \Omega_p & 0 \\ \Omega_p & -2\Delta_1 & \Omega_c \\ 0 & \Omega_c & -2\Delta_2 \end{pmatrix}, \tag{2.18}$$

where the dynamics is described with the rotating wave approximation in the rotating frame of the laser frequencies [121]. The decay terms of the Lindblad operator in (2.5) are written using the operators $\sigma_{ba} = \sqrt{\Gamma_b}|b\rangle\langle a|$ and $\sigma_{cb} = \sqrt{\Gamma_c}|c\rangle\langle b|$. In the rest of the section we discuss the effects this system presents, from the point of view of the matter system and that of the EM field.

2.3.2 Coherent population trapping

The evolution of the three-level system via (2.5) leads, under the condition of two-photon resonance ($\Delta_2 = 0$), to a phenomenon called *coherent population trapping* (CPT) [121, 122].

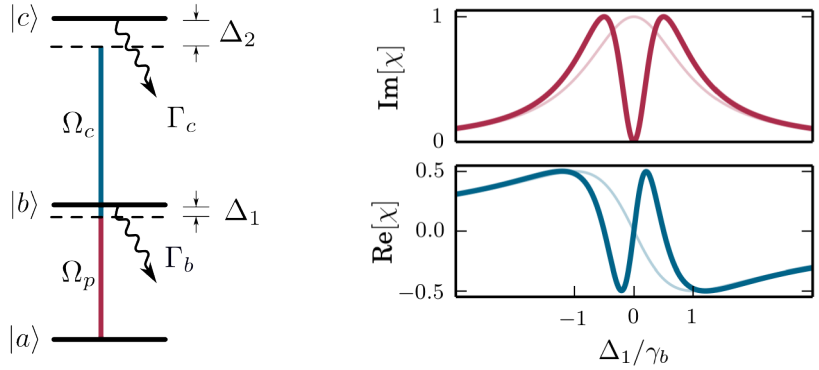

Figure 2.2: (Left) Excitation scheme for a three-level system. It differs from the two-level system in that it adds a *coupling* laser almost resonant with the transition $|b\rangle \leftrightarrow |c\rangle$. The two-photon detuning is Δ_2, and the decay from the upper state is Γ_c. (Right) Susceptibility of the three-level system. The strong lines show the real (top) and imaginary (bottom) susceptibilities of the system with parameters $\Omega_c = \Gamma_b = 100\Omega_p = 1000\gamma_c$, normalised to the maximum of Im[χ]. The weak lines show the susceptibilities of the corresponding two-level system ($\Omega_c = 0$).

This phenomenon can be understood by looking at the eigenstates of (2.18):

$$|B_+\rangle = \sin\theta \sin\phi|a\rangle + \cos\phi|b\rangle + \cos\theta \sin\phi|c\rangle, \tag{2.19}$$

$$|B_-\rangle = \sin\theta \cos\phi|a\rangle - \sin\phi|b\rangle + \cos\theta \cos\phi|c\rangle, \tag{2.20}$$

$$|D\rangle = \cos\theta|a\rangle - \sin\theta|c\rangle, \tag{2.21}$$

where θ and ϕ are the mixing angles defined by [110]

$$\tan\theta = \frac{\Omega_p}{\Omega_c}, \qquad \tan 2\phi = \frac{\sqrt{\Omega_p^2 + \Omega_c^2}}{\Delta_1}. \tag{2.22}$$

The probe laser only couples to the states $|B_\pm\rangle$, which are split in energy by $\lambda_\pm = \frac{\hbar}{2}\left(\Delta_2 \pm \sqrt{\Omega_c^2 + \Omega_p^2 + \Delta_1^2}\right)$ [110, 123]. Under the conditions of two-photon resonance the probe laser is not absorbed because the coupling to the states $|B_\pm\rangle$ have equal magnitude but opposite signs, undergoing destructive interference. Additionally, $|D\rangle$ does not contain any contribution from $|b\rangle$, and thus does not radiate; for this reason, it is sometimes called a *dark*-state. The states $|B_\pm\rangle$ radiate to populate $|D\rangle$ on a timescale of $1/\Gamma_b$, and since

it does not interact with the probe beam anymore, the population becomes *trapped* in this state. When $\Omega_c \gg \Omega_p$, the dark-state is predominantly composed by the ground state $|D\rangle \sim |a\rangle$; once in this state, turning the coupling field off makes the state of the system follow adiabatically the dark-state, which becomes $|D\rangle \sim |c\rangle$. The relevance of this population transfer from $|a\rangle$ to $|c\rangle$ will become relevant in the following two sections.

2.3.3 Electromagnetically induced transparency

As we have mentioned, an *interference of decay pathways* from $|B_\pm\rangle$ prevents resonant probe light from being absorbed by the medium. Thus the medium, previously opaque to the probe light, becomes transparent after the addition of the second, coupling, light field.

Under the conditions of weak-probe, it is possible to neglect the contribution of ρ_{ac} in the susceptibility for the three-level system, and (2.16) applies. Solving the Maxwell-Bloch equation in this case gives [124]

$$\chi = -2\frac{d_{ba}^2 \rho_0 \rho_{ba}}{\epsilon_0 \hbar \Omega_p}, \tag{2.23}$$

$$= \frac{\rho_0 \sigma}{k_0} \frac{i\gamma_b}{\gamma_b - i\Delta_1 + \frac{\Omega_c^2}{4(\gamma_{ca} - i\Delta_2)}}, \tag{2.24}$$

where the effect of the finite linewidth of the probe (γ_p) and coupling (γ_c) lasers have been added to the dephasing terms $\gamma_{ca} = \Gamma_c/2 + \gamma_p + \gamma_c$ [116], and $\sigma = k_0 d_{ba}^2/(\hbar\epsilon_0\gamma_{ac})$ is the resonant absorption cross-section [121]. The real and imaginary parts of this function are shown in Figure 2.1. The main feature in the susceptibility, in the limit of $\gamma_c \to 0$ is that the imaginary part, responsible for absorption, shows a zero on resonance (i.e. transmission increases, $\chi_{\mathrm{R}}(\Delta_1 = 0) = 0$). This effect on resonant light leads to the name *electromagnetically induced transparency* (EIT) [110, 125, 126]. The width

of this transparency window, in the limit when $\gamma_{ca} = 0$, is given by [110]

$$\Delta_{\mathrm{EIT}} = \frac{|\Omega_c|^2}{\gamma_b}. \tag{2.25}$$

We observe that the EIT window depends on Ω_c, being broader the stronger the coupling field. The spectroscopic properties of light propagating through an optically thick medium do not depend *only* on the susceptibility of the medium, but they change with the propagation length according to (2.10):

$$T = \frac{I(z)}{I(0)} = e^{-2k_0 n_{\mathrm{I}} z} = e^{-\chi_{\mathrm{I}} k_0 z}. \tag{2.26}$$

Near resonance ($\Delta_1 = 0$), under EIT conditions in the optically thick medium, the transparency window is described (to lowest order) by a Gaussian with a width given by [121]

$$\Delta_{\mathrm{trans}} = \frac{|\Omega_c|^2}{\gamma_b} \frac{1}{\sqrt{\mathrm{OD}}}, \tag{2.27}$$

where the resonant optical depth $\mathrm{OD} = \rho_0 \sigma L$ corresponds to that of the two-level system $|a\rangle \leftrightarrow |b\rangle$ with absorption cross-section σ. According to the Kramers-Kronig relations [127] (valid under the assumption of a causal connection between $\mathbf{P}$ and $\mathbf{E}$), if an anomaly is present in absorption, an equally important feature appears in the dispersion: the real part of the susceptibility shows strong dispersion within the transparency window. The strong, almost-linear dispersion with positive slope strongly reduces the group velocity of the propagating light, $v_g \ll c$, being

$$v_g = \frac{c}{1 + \frac{\omega}{2} \frac{\partial}{\partial \omega} [\mathrm{Re}\chi(\omega)]}, \tag{2.28}$$

$$= \frac{k^2 \left(\Omega_c^2 + \gamma_{ca}\gamma_b\right)}{6\pi\rho_0 c \Gamma_b}, \tag{2.29}$$

where the last equation is the solution for both lasers being resonant with their respective transitions. As with the EIT transparency window, the group

velocity also depends on the coupling field Rabi frequency. In this case, reducing Ω_c reduces the group velocity in the medium. An inverse relation holds for the density ρ_0 of the medium; where a reduced density increases the group velocity.

In the context of the phase gate in chapter 6, (2.29) shows that decreasing Ω_c slows down the light passing through the medium; besides, as we have seen in section 2.3.2, when the dark-state is populated, reducing Ω_c transfers the population of the atomic system to $|c\rangle$. It is possible to describe these two concomitant effects in the *dark-state polariton* picture.

2.3.4 Dark-state polaritons

When light enters the medium under the conditions of EIT, it is compressed by a factor $c/v_g \gg 1$, but the electric field is constant [128]. The combined action of the probe pulse and the coupling light establishes a coherence between the levels $|a\rangle$ and $|c\rangle$ even at the single-photon level. It is possible to describe the combined state of light and matter in a field called dark-state polariton [109].

If we consider the probe field with quantised electric field $\mathcal{E}(z,t)$ propagating in the z direction, and assume that the operators describing light and matter are suitably averaged over small but macroscopic volumes containing many particles, Maxwell-Bloch equations are analogous to that for the three-level system considered before. In this case, however, we need to define the atom-field coupling constant g [126], also called the *vacuum Rabi frequency* [109]. Assuming the evolution of the system in the adiabatic limit, the propagation of a single quantum of light through a medium containing N atoms follows a simple solution [108]

$$\Psi(z,t) = \cos\vartheta(t)\mathcal{E}(z,t) - \sin\vartheta(t)\sqrt{N}\rho_{ca}(z,t)\mathrm{e}^{i\Delta k\cdot z}, \tag{2.30}$$

where the mixing coefficients are

$$\cos\vartheta(t) = \frac{\Omega_c}{\sqrt{\Omega_c^2 + g^2N^2}}, \qquad \sin\vartheta(t) = \frac{gN}{\sqrt{\Omega_c^2 + g^2N^2}}. \tag{2.31}$$

The collective atomic component ($\sqrt{N}\rho_{ca}$) shows a phase grating, $\Delta k \cdot z = (k_c - k_p)\, z$, given by the difference in phase from the quantum field wavevector (k_p) and the parallel projection of the coupling field in the quantum field direction of propagation ($k_c = \vec{k}\cdot\vec{e_z}$). This part of the polariton is commonly named the *spin wave*.

The dark-state polariton obeys a simple shape-preserving propagation equation [108] with velocity $v_g = c\cos^2\vartheta$,

$$\left[\frac{\partial}{\partial t} + c\cos^2\vartheta(t)\frac{\partial}{\partial z}\right]\Psi(z,t) = 0, \tag{2.32}$$

and it can be shown that its plane-wave decomposition, in the linear regime (where the excitation fraction is negligible), obeys *bosonic commutation relations* [108]. Even though we shall be interested in the single-photon case, we note that more complicated expressions exist for more general quantum states of the incoming light [109, 129, 130].

In light of the polariton picture, we can understand the connection between CPT and EIT: when the probe light propagates under the conditions of EIT, the photons from the probe field are borrowed to form part of the coherence between states $|a\rangle$ and $|c\rangle$. This rotates the dark-state in (2.21), initially in $|a\rangle$, to a superposition between $|a\rangle$ and $|c\rangle$. When the probe pulse reaches its maximum, the rotation is reversed. The stronger the coupling field, the smaller the rotation of the dark-state, and the smaller the time for the adiabatic return process, resulting in a smaller pulse delay [110].

2.3.5 Photon storage

As seen in the previous section, if a pulse of light enters the medium under the conditions of EIT, it is possible to transfer the excitation to the medium with a fraction $\sin\vartheta$ of the polariton state. Therefore, if we vary the mixture angle until $\vartheta = \pi/2$, we can store the pulse of light in the medium.

If a Fourier-limited pulse of duration τ enters the medium of length L in these conditions, it becomes compressed by a factor $c/v_g \gg 1$. For the pulse to fit within the medium, its (compressed) length should be smaller than the length of the medium. Its initial bandwidth should not exceed the EIT bandwidth to avoid absorption, thus $\tau^{-1} \lesssim |\Delta_{\text{trans}}|$. Both conditions read $L > \tau v_g \gg v_g \, |\Delta_{\text{trans}}|^{-1}$, which determine that OD $\gg 1$ [121]. Additionally, a large OD facilitates fulfilling the adiabaticity condition [108].

Once the pulse is completely inside of the medium, it is possible to transfer population between $|a\rangle$ and $|c\rangle$ by adiabatically changing the coupling laser $\Omega_c \to 0$.

When we do so, we borrow the photons from the field and transfer them to ρ_{ca}, which takes atoms in the ground state and transfers them to $|c\rangle$, making $\vartheta = \pi/2$. In the dark-state picture of (2.21), this amounts to changing adiabatically the mixing angle from the initial $0 < \theta < \pi/2$ to $\theta = \pi/2$, while reducing $v_g \to 0$ [121]. The pulse of light is then *stored* inside of the medium.

As long as the process remains coherent [131], it can be reversed by increasing the coupling Rabi frequency again. However, if the atoms in the medium show random motions, the phase factors arising in the spin wave (2.30) change in a way that makes the retrieval of the polariton in the forward direction inefficient [132]. This *dephasing* can be lessened if one limits the motion of the atoms, either by lowering the effective temperature or by reducing their range of motion by trapping them in a lattice, for example.

Since photon storage happens at the quantum level and preserves coherences,

it is possible to use this process to store quantum information [109, 133–136]. The most important limiting factor for the storage of photonic quantum information is the optical depth of the medium [126, 137], thus great care should be taken to obtain an optically thick sample when designing an EIT quantum memory.

This storage/retrieval protocol has been used in combination with strong dipole-dipole interactions (see Chapter 3) to generate single photons from an atomic ensemble [1, 79, 82]. Some interesting phenomena arise when EIT is combined with strong dipole-dipole interactions like, for example, those present when the uppermost state of the ladder is a Rydberg state [76–78, 87]. In fact, photons propagating in this system are predicted to interact [72, 81, 82, 89]. However, a complete description of the process of storage and retrieval, with the dynamic change of coupling Rabi frequencies, in the case of multiple stored polaritons is still lacking [1, 79, 86].

2.4 Summary

As we have seen in this chapter, a near-resonant probe EM field interacting with a two-level system (e.g. an atomic transition) can cause the population to cycle between the two levels being coupled. The Rabi frequency is a measurement of how strong the interaction between an EM field and a certain atomic transition is. The stronger these interactions are, the faster the cycling between the two levels.

In a non-interacting, three-level system a phenomenon called electromagnetically induced transparency arises, whereby a medium becomes transparent to light resonant with a certain transition due to the presence of a coupling field.

The light propagates within a transparency window that depends on the strength of this coupling field, as well as the lifetime of the intermediate

state. While doing so we can describe the combined system atom-light in a unified picture: dark-state polaritons. They are an mixture of a (quantised) EM field and an atomic coherence that obeys bosonic commutation relations. It is possible to change the mixing angle between light and atomic coherence by changing the strength of the coupling field. When the dark-state polariton is fully an atomic coherence, its propagation comes to a stop; we can use this effect to store the quantum information carried by a photon in a medium, and read it out again coherently.

Chapter 3

Atom-atom interactions

The key to our all-optical quantum computation is the mapping of states of light onto atomic excitations (polaritons) and making those excitations interact, thereby providing an effective, controlled photon-photon interaction.

One type of interaction that could offer such degrees of freedom is the dipole-dipole interaction. Despite lacking a permanent dipole moment, a pair of atoms can show dipole-dipole interactions when they are excited via a dipolar transition. During the excitation, a temporary dipole is formed in each of the atoms, and the field produced by each of them affects the other, changing the energy required to excite both of them together.

Dipole-dipole interactions depend crucially on the strength of the dipoles generated during the excitation and also on the distance between the atoms. Atomic dipole-dipole interactions induced on the ground to first excited state transition are weak at usual cold-atom densities ($\rho \sim 10^{10}\,\mathrm{cm}^{-3}$). To obtain dipole-dipole interactions that are comparable to the linewidths of usual transitions in one electron atoms, one either needs to have a very dense sample [138], where the interparticle distances are very small, or to excite atoms to states with high principal quantum numbers [42, 68], which exhibit large dipole matrix elements when coupled to neighbouring Rydberg states.

To obtain very dense samples, one can cool the sample until it reaches condensation ($\rho \sim 10^{14}\,\mathrm{cm}^{-3}$); alternatively, one could increase the temperature of the atomic reservoir in a hot atomic cell [138]. If one does the latter, however, the atoms move at high speeds, and coherent operations on the sample need to be fast to avoid thermal dephasing. When the interactions appear in very dense samples, the typical separation between atoms, l, is far below the diffraction limit ($l < \lambda/2$), making the addressing of individual excitations difficult to control.

On the other hand, Rydberg atoms [42] offer a way to use these strong interactions within a controllable system, due to the favourable scaling of the dipole-dipole interactions with principal quantum number n (the energy shift is about $-140\,\mathrm{GHz}$ for a pair of atoms separated by $1\,\mu\mathrm{m}$ at $n = 60$ in $^{87}\mathrm{Rb}$ [139]). These interactions can be exploited in a variety of scenarios, such as to perform very sensitive electrometric measurements [61, 140], to create novel forms of matter [57–59] and light [81], to generate non-classical states of light [1, 79, 80] and to realise universal quantum gates [95, 141].

In this chapter, we first describe the interaction between two atoms as that of four charged bodies (two nuclei and two electrons), and how this interaction is not-negligible, to first order, between dipole-connected levels. Later we apply perturbation theory to derive second order effects, which affect energies of pairs of atoms excited to the same state with large n. For more details, an in-depth analysis of the interactions between the atoms can be found in [142].

3.1 Atom-atom interactions

For large R (in the long-range region), we can write the Hamiltonian that describes the dynamics of two atoms at distance R as

$$H = H_0 + H_{\mathrm{int}}(R) \tag{3.1}$$

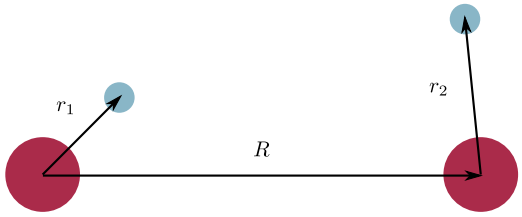

Figure 3.1: Two atoms and their electrons. Position vector of electrons 1 and 2 are labelled r_1 and r_2 respectively, and the distance between the nuclei is termed R.

where H_0 denotes the energies of the (noninteracting) atoms[1] and $H_{\text{int}}(R)$ is the interaction Hamiltonian between the two atoms, which is assumed to be $H_{\text{int}} \ll H_0$. To obtain an appropriate description of the system, we first consider the eigenfunctions of the Hamiltonian H_0 and then construct solutions for the full Hamiltonian based on these functions.

We consider the case of one-electron atoms. Let us denote the atoms by 1 and 2, separated by a distance R, each of them having one electron at positions r_1 and r_2 with respect to their respective nuclei, as seen in Figure3.1. The standard eigenfunctions of H_0 for one electron atoms under LS-coupling, are

$$\psi_{n,J,m_J}(r) = \sum_{m_S,m_L} C^{J,m_J}_{L,m_L,S,m_S} R_{nL}(|r|) Y_{L,m_L}(\hat{r})\, \chi_{m_S}, \tag{3.2}$$

where the total angular momentum $J = L + S$ is the sum of the orbital angular momentum, L, of the electron's wavefunction, and its spin, S; and m_J, m_L and m_S are their respective projections along the quantisation axis. The C^{J,m_J}_{L,m_L,S,m_S} are called Clebsh-Gordan coefficients, and are mixing factors that appear as a result of the combination of several angular momentum eigenfunctions; $R_{nL}(|r|)$ describes the radial part of the wavefunction and $Y_{L,m_L}(\hat{r})$ are the spherical harmonics, which encode the angular distribution of the wavefunction described by $\hat{r} = \frac{r}{|r|}$; finally, χ_{m_S} is the spinor for the

[1] Situation analogous to the two atoms being at an infinite distance apart

single electron.

Once we have the solutions for H_0, we take a look at the form of the interactions. The interaction between the four charged bodies (two valence electrons and two nuclei) is, in atomic units,

$$H_{\text{int}} = \frac{1}{|r_1 - (r_2 + R)|} - \frac{1}{|r_1 - R|} - \frac{1}{|r_2 + R|} + \frac{1}{|R|}, \tag{3.3}$$

where the first term represents the interaction between the valence electrons, H_{ee}; the second and third terms take into account the attraction of each of the electrons to the opposite nucleus, H_{ne}; and the final term is the repulsion between nuclei, H_{nuc}.

A bipolar expansion [143] of the first term leads to

$$\hat{H}_{\text{int}} = \sum_{k_1,k_2=1}^{\infty} \frac{(-1)^{k_2}}{R^{k_1+k_2+1}} \sqrt{\frac{(4\pi)^3(2k_1+2k_2)!}{(2k_1+1)!(2k_2+1)!(2k_1+2k_2+1)}} \times \sum_{p=-(k_1+k_2)}^{k_1+k_2} \sum_{p_1=-k_1}^{k_1} \sum_{p_2=-k_2}^{k_2} C^{k_1+k_2,p}_{k_1p_1,k_2p_2} |r_1|^{k_1} |r_2|^{k_2} Y_{k_1,p_1}(\hat{r_2}) Y_{k_2,p_2}(\hat{r_2}) Y_{k_1+k_2,p}(\hat{R}), \tag{3.4}$$

where the terms with $k_1 = k_2 = 0$; $k_1 = 1$, $k_2 = 0$; and $k_1 = 0$, $k_2 = 1$, cancel the contributions from H_{nuc}, H_{ne}. The lowest, non-zero order term in the series ($k_1 = k_2 = 1$) represents the dipole-dipole interactions, with a functional form of the energy proportional to $\propto R^{-3}$. The bipolar expansion is valid as long as there is no overlap between the electron clouds of the atoms, with sizes of the order of $\sim 0.2\,\text{nm}$ for ground state atoms, and a scaling of $\propto n^2$ with principal quantum number for Rydberg atoms. For typical cold-atom densities ($10^{10} - 10^{11}\,\text{cm}^{-3}$) this expansion is valid at moderate principal quantum numbers ($n \sim 60 - 70$)[2]. If we only retain the lowest order contribution with $k_1 = k_2 = 1$, the interaction Hamiltonian finally

[2] For larger principal quantum numbers or higher densities, neighbouring ground state atoms can interact with the Rydberg wavefunctions giving rise to ultralong-range Rydberg molecules [58].

becomes

$$\begin{aligned}\hat{H}_{\rm int} = &\frac{-1}{R^3}\sqrt{(4\pi)^3\frac{2}{15}} \\ &\times \sum_{p=-(2)}^{2}\sum_{p_1=-1}^{1}\sum_{p_2=-1}^{1} C^{2,p}_{1p_1,1p_2}|r_1||r_2|Y_{1,p_1}(\hat{r_1})Y_{1,p_2}(\hat{r_2})Y_{2,p}(\hat{R}),\end{aligned} \tag{3.5}$$

The form (3.5) of the Hamiltonian (3.3) is now much simpler. The $|r_1|Y_{1,p_1}(\hat{r_1})$ and $|r_2|Y_{1,p_2}(\hat{r_2})$ present in the formula shows that the non-zero matrix elements will be those between dipole-connected levels. The energy shifts have a functional form

$$\Delta E_{int} = \sum_N \frac{C_N}{R^N}, \tag{3.6}$$

where the C_N are state-dependent, constant coefficients. Thus, we can apply perturbation theory to find the C_N coefficients by matching functional forms.

3.2 First order perturbation theory

In order to apply perturbation theory, we need to move from the individual atom basis, where atom 1 is in state ψ_1 and atom 2 is in state ψ_2, to a pair state basis, where the combined state of the system is $\psi = \psi_1\psi_2$.

Let us begin by setting an arbitrary initial state $\psi^{(0)}$, with energy $H_0|\psi^{(0)}\rangle = E^{(0)}|\psi^{(0)}\rangle$, as the product of the initial states of atom 1, $\psi_1^{(0)}$, and 2, $\psi_2^{(0)}$. The first order energy shift associated with (3.1) is given by

$$\Delta E^{(1)} = \langle\psi^{(0)}|H_{\rm int}|\psi^{(0)}\rangle. \tag{3.7}$$

Inspecting (3.5) we identify a $\propto R^{-3}$ functional form, obtaining C_3 as the sum of the dipole transition amplitudes $\langle\psi_1^{(0)}|r_1|\psi_1^{(0)}\rangle\langle\psi_2^{(0)}|r_2|\psi_2^{(0)}\rangle$ with some angular factors, of order unity, which can add to zero for some orientations.

The first-order perturbation term is often called *resonant DD interaction* [144].

This allows us to make the following remarks:

- If both atoms are in the same eigenstate of H_0, $\psi_1^{(0)} = \psi_2^{(0)}$, $\Delta E^{(1)} = 0$, and resonant DD interactions are prevented.
- $C_3(\psi^{(0)})$ will be nonzero if the states of both atoms are such that $\psi^{(0)}$ is dipole connected with itself. These kind of states arise, for example, when one excites an ensemble of two atoms from an initial state ψ_i to a final state ψ_f via a dipolar transition: before both atoms can be transfered to that final state $\psi_{f1}\psi_{f2}$, they have to populate the intermediate state $\psi_{\text{inter}} = \psi_{i1}\psi_{f2} + \psi_{f1}\psi_{i2}$, which has $C_3(\psi_{\text{inter}}) \neq 0$.

3.3 Second order perturbation theory

Since (3.5) couples dipole-connected levels, we can apply second-order perturbation theory to obtain the energy shifts to the initial state in the coupled basis $\psi^{(0)}$ due to virtual processes involving an intermediate, dipole-coupled level ψ' with energy E'. A simple graphical explanation for the first- and second-order perturbation terms is shown in Figure 3.2. Let us remember that, in the pair state basis, an intermediate dipole connected level $\psi' = \psi_1'\psi_2'$ is connected to the initial state $\psi^{(0)} = \psi_1^{(0)}\psi_2^{(0)}$ via the Hamiltonian H_{int} such that $\langle\psi^{(0)}|H_{\text{int}}|\psi'\rangle \neq 0$.

The expression for the second-order energy shift to the state $\psi^{(0)}$ in the pair state basis, usually called *van der Waals* (vdW) interaction, is

$$\Delta E^{(2)} = \sum_{\psi' \neq \psi^{(0)}} \frac{\langle\psi^{(0)}|H_{\text{int}}|\psi'\rangle\langle\psi'|H_{\text{int}}|\psi^{(0)}\rangle}{E^{(0)} - E'}, \tag{3.8}$$

where the denominator $\Delta = E^{(0)} - E'$ is usually called Förster defect, and

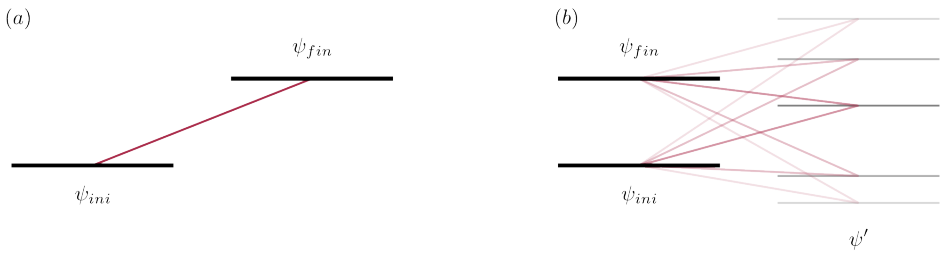

Figure 3.2: Graphical explanation of the contributions towards first- and second-order perturbation terms. (a) First order energy contributions only take into account dipole-connected levels. In this case, the initial pair state ψ_{ini} is connected via H_{int} to the final state ψ_{fin} and $\Delta E^{(1)} \neq 0$ (b) Second order energy contributions come from an infinite sum of dipole-coupled, intermediate states ψ' with $\langle\psi_{\text{ini}}|H_{\text{int}}|\psi'\rangle, \langle\psi'|H_{\text{int}}|\psi_{\text{fin}}\rangle \neq 0$. If we want to calculate the energy shift to the state ψ_{ini}, then $\psi_{\text{fin}} = \psi_{\text{ini}}$. The strongest contribution usually comes from a nearby, dipole-connected state with the smallest Förster defect.

measures the energy inbalance in these virtual processes. When the processes are resonant – that is, when $\Delta = 0$ – perturbation theory no longer holds, and we arrive at a situation called *Förster resonance*. These resonances occur whenever the *virtual* transitions to the intermediate dipole-coupled states have the same energy. This degeneracy in energy between the initial and the intermediate dipole-coupled state prompts oscillations between the two mediated by H_{int}, and causes energy shifts [145].

In Figure 3.3 we can observe several of these resonances appearing in the series corresponding to the states $|r\rangle = nS_{1/2}(n+a)S_{1/2}$ with $a = 1$ (red), 2 (purple), and 3 (blue)). These resonances show as a change of sign in the value of C_6, and are shown as abrupt peaks or dips in the graph. In contrast, the states $nS_{1/2}nS_{1/2}$ (broken line) do not show these resonances.

Second order perturbations are important whenever first order effects are suppressed, or when the Förster defect $\Delta = 0$. We can factor out the R dependence from both terms to give a functional form $\propto R^{-6}$.

To understand the actual functional form of this contribution, let us look at a simplified example [146, 147]. If we imagine that our initial state is

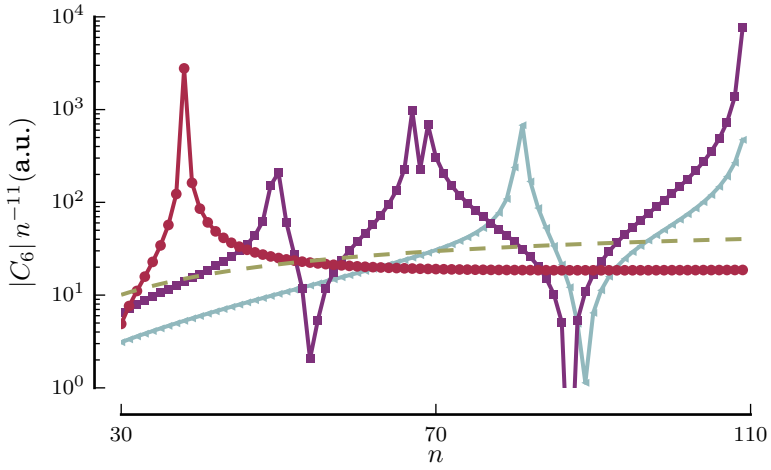

Figure 3.3: Scaled C_6 values, in atomic units, for the states $|r\rangle = nS_{1/2}(n+a)S_{1/2}$ in ^{87}Rb. In red circles, $a = 1$, in purple squares, $a = 2$; and, in blue triangles, $a = 3$. The broken line in yellow is the standard $a = 0$, for comparison. The values shown are an average of the eigenvalues with total magnetic quantum number $M = 0$ and $M = 1$. These results have been obtained by using modified code originally written by Christophe Vaillant [142].

$\psi^0 = |rr\rangle$, where both atom 1 and 2 are in state $|r\rangle$; the biggest contribution to the energy of this state, $\langle\psi^{(0)}|H_{\rm int}|\psi'\rangle$ comes from the state whose Förster defect is the smallest (assuming similar dipole moments). Let us call this state $|r'r''\rangle$, where either of the atoms can be connected to both $|r'\rangle$ and $|r''\rangle$. In the basis $|rr\rangle$, $|r'r''\rangle$, the Hamiltonian describing the dipole-dipole interaction is

$$\mathcal{H} = \hbar \begin{pmatrix} 0 & H_{\rm int} \\ H_{\rm int} & \Delta \end{pmatrix}. \tag{3.9}$$

Looking at the eigenvalues of $\mathcal{H}$,

$$\lambda = \frac{\Delta \pm \sqrt{\Delta^2 + 4H_{\rm int}^2}}{2}, \tag{3.10}$$

we can observe two different behaviours depending on the interatomic distance

- Short distance ($H_{\rm int} \gg \Delta$): the interaction is dominated by the off-diagonal contribution, where one expects excitation hopping [46, 47, 83]

between the atoms. The energy shifts are $\lambda \sim \pm H_{\text{int}}$. This goes as $\propto R^{-3}$, and the equivalent $C_3' \propto n^4$, since each of the dipole matrix elements scale with $\propto n^2$.

- Long distance ($\Delta \gg H_{\text{int}}$): in this case, the differences in energy with respect to the unperturbed case are $\lambda \sim -H_{\text{int}}^2/\Delta$. We extract the $\propto R^{-6}$ functional form from H_{int}^2, and the associated $C_6 \propto n^{11}$, since we have the contributions from the dipoles squared, and the Förster defect scales as $\propto n^{-3}$ due to the Rydberg series energy scaling as $E_n \propto 1/n^2$.

3.4 Dipole blockade and dephasing

If the DD interaction between excitations in a medium is stronger than the (broadened) linewidth of the exciting transition, a phenomenon called *dipole blockade* occurs [66, 68]. The blockade phenomenon prevents more than one excitation within certain volume (called *blockade volume*), where the DD interactions shift multiply excited states out of resonance with the exciting field. We can define the blockade volume as the region where the DD interaction energy is larger than the (broadened) linewidth Ω of the transition. For spherically symmetric interactions of the form C_n/R^n (like the ones in (3.6)) the *blockade sphere*[3] characterised by its radius

$$R_{\text{b}}^{(n)} = \sqrt[n]{\frac{C_n}{\hbar\Omega}}. \tag{3.11}$$

The spatial properties of the blockade effect due to the resonant DD interaction are then characterised by C_3, whereas those of the vdW interactions are characterised, in the long distance regime, by its C_6 coefficient. These two

[3] The angular distribution of the vdW interaction in the $nS_{1/2}nS_{1/2}$ state leads to an *almost* spherically symmetric blockade volume, because the DD interaction couples differently to different orbital angular momentum states, which are zero for the S state pair (see [116, 142]).

give rise to qualitatively different blockade volumes: in the vdW case, the R^{-6} potential gives rise to a blockaded volume resembling a hard-core potential, with a very thin *skin* between the blockaded and non-blockaded volumes [148]; on the other hand, the resonant DD case (with an R^{-3} potential) shows a much larger transition volume, in which the potential $C_3/R^3 \sim \hbar\Omega$. In this last case, the strength of the DD interactions is not enough to completely block multiple excitations within this volume.

In the intermediate regime where $C_3/R^3 \sim \hbar\Omega$, the long-range potential causes inhomogeneous phase shifts to multiply excited states. The accumulated phases decouple these multiply excited states from the phase-matched mode during the retrieval process. This DD induced *dephasing* also generates loss, and can be used to suppress efficiently multiple excitations [149] for the generation of single photons in a cloud with dimensions not smaller than, but comparable to, the blockade radius [79].

The strong DD interactions between Rydberg states (e.g. $C_6 \sim 100\,\mathrm{GHz}/\mu\mathrm{m}^6$ can give rise to macroscopic blockade radii $\sim 10\,\mu$m for typical experimental conditions, which has been exploited in recent experiments (e.g. [1, 86]).

3.5 Summary

In this chapter we have briefly discussed the theory of dipole-dipole interactions in one-electron atoms. We have derived functional forms for the first- and second-order terms of the perturbative expansion of the dipole-dipole interaction Hamiltonian. First-order effects can become important when Rydberg atoms are dipole-coupled to each other. Second-order effects are usually much weaker, but prevalent when the first-order contribution is zero, which is normally the case at large distances, or when the Förster defect is almost zero. The notion of Förster resonance has been introduced, and why this situation can change the state of the system. We have also presented

the dipole blockade and dipole induced phenomena, and the related concept of blockade radius.

Both first- and second-order effects have been shown to have an impact in recent experiments [1, 86], and are discussed in more depth in the next chapter appealing to the concept of blockade radius. They are also important in the functioning of the phase-gate, and they will be used in Chapter 6.

Chapter 4

Interference phenomena and photon statistics

To fully characterise the quantum state of a system in a general case, it is necessary to perform quantum tomography [150]. This requires making measurements on a minimal set of observables [151] (often termed *quorum* [152]) with which we can reconstruct the full density matrix (or any other quantity holding the same information). For a given light mode (polarisation, spatial and temporal), the electromagnetic field Hamiltonian is equivalent to that of a harmonic oscillator, and we can distinguish different Fock states, which are states with a well defined number of excitations in that particular mode. This description sets the state as a vector in an infinite-dimensional Hilbert space, and the number of observables in the quorum for such a system is infinite [151–153]. However, there are many techniques that allow us to reconstruct the state from a finite set of measurements, that lead to varying degrees of fidelity, depending on the chosen approximation [150].

Homodyne tomography allows one to reconstruct the state of a weak signal field in the Fock-state basis by measuring its quadratures [153], comparing them with a *local oscillator* in the same spatial and temporal mode as the signal. The measured quadratures hold indirect information about the state,

but to reconstruct the state (in the Fock-state basis, or any other particular representation), one needs to process that data: this procedure is called *quantum state reconstruction*. In our experiments [1, 86], we are interested in measuring the weak signal corresponding to the stored and retrieved photons in a cloud of cold atoms. The fidelity of the tomographic reconstruction of the state in Fock space – i.e. how accurately the reconstruction represents the actual state – depends on the modal overlap between the local oscillator and the signal. For weak signals, where the vacuum state contribution overwhelms the state, one can compensate a bad mode matching between the signal and the local oscillator by spatially and temporally filtering the signal using heralded detection [150]. However, in our experiment this is not possible, since we cannot herald the detection with sufficient fidelity.

Despite not being able to reconstruct the state completely, the nonclassical changes undergone in the state of the probe light during the storage and retrieval process can be measured in many ways. These measures of *quantumness* rely on quantities that have some classical bound which is normally broken by purely quantum systems. One of these bounds is associated with the *intensity autocorrelation function*, $g^{(2)}$, of the light field [154, 155]. We have used this quantity in our experiments [1] to ascertain the quantum nature of the light output as well as to hint at possible processes that are important during the storage and propagation of polaritons with Rydberg character in a cloud of cold atoms (see [86] and Chapter 5).

In this Chapter, we first describe the importance of interference phenomena. Then, we review the basics of the quantum theory of radiation: we describe Fock-states as the states with a well defined number of photons, and arrive at the concept of single-photon wavepacket, the basic information carrier in the phase-gate scheme proposal. Finally, discuss how intensity correlation measurements test the quantum nature of the field, knowledge that will become useful in Chapters 5 and 8.

4.1 Interference phenomena

The interference fringes appearing in the double-slit experiment by Young are considered to be one of the most successful proofs of the particle-wave duality, as it shows interference phenomena even at the single-photon level [156]. This kind of experiments have also been performed in electrons and neutrons, or even large molecules [157], thus confirming de Broglie's description. Interference is possible assuming the superposition principle, i.e. the linear nature of electromagnetic field propagation, where the field amplitude at a given point is the sum of the independent contributions from each source. If the fields are *in phase*, the interference will be *constructive*, whereas if the fields are *out of phase*, the result will be *destructive* interference. The possibility of destructive interference (even in probability amplitude fields), due to out-of-phase contributions, is very important in the quantum framework as it is one of the main aspects that sets it apart from the classical description.

Typical photodetectors (like photodiodes) count the number of photons via photon absorption. The effect of the photons in the material is then amplified to obtain a classical signal. However, since the typical bandwidths for this process are orders of magnitude smaller than the frequency of light ($\sim$ 100 THz), photodetectors do not measure the instantaneous nature of the electric field at any given time, but rather a time-averaged intensity. Therefore, in order to obtain a stationary interference pattern in the optical region of the spectrum, the light fields involved should meet certain *coherence* requirements.

In the strict sense of the word, coherence means connection or consistency between things. In physical terms, coherence describes the correlation between the physical quantities of a wave. We can describe light as a wave, according to Maxwell's equations. However, the emission of light is intrinsically random, because of the quantum nature of the emitters. In order to study light,

we resort to statistical methods, such as averaging and correlation, that can give us information about the physics behind it [155, 158]. If the conditions of coherence are adequate we might be able to observe directly the effects of interference within the statistical description of light.

The statistical properties of the light generated in our experiment, which are the subject of our study, are connected to the temporal dynamics of the light output[1]. Therefore, if we neglect the spatial properties of the beam, we can reduce the problem to that of temporal interference.

4.2 Review of the quantum theory of radiation

To understand interference phenomena at the quantum level, it is necessary to describe some basic concepts like that of electromagnetic mode, creation, annihilation and number operators, and their algebraic properties. Furthermore, in the development of the phase-gate we require the use of single-photon wavepackets to carry quantum information. These concepts will be shown in this part of the Chapter. The following review of the quantum theory of radiation, required to understand the results in the remaining chapters, is based heavily on the treatment in [121]. Other very useful references are [160–163].

The quantisation of Maxwell's equations for the electromagnetic field in a box of length L give rise to a denumerable, infinite set of eigenstates of the form of harmonic oscillators with frequency ω_k and wavevector $\boldsymbol{k}$ (related through $\omega_k = ck$) and two transversal polarisation vectors, denoted by $\lambda = 1, 2$. Solutions of the spatial part have the form $\exp(\pm \mathrm{i}\boldsymbol{k} \cdot \boldsymbol{r})$, and those of the temporal part have the form $\exp(\mp \mathrm{i}\omega_k t)$, where boundary conditions only allow wavevectors $\boldsymbol{k}$ that fullfil $k_j = 2\pi n_j / L$ for $j = x, y, z$.

[1] The first experimental example of such effect was Mandel and Kimble's demonstration [159] of the single-photon nature of the emission of light by an atom.

The spatial eigenfunctions $\boldsymbol{u}_{\boldsymbol{k}\lambda}(\boldsymbol{r}) = \boldsymbol{e}_{\boldsymbol{k}\lambda}\exp(\pm \mathrm{i}\boldsymbol{k}\cdot\boldsymbol{r})$ for the different modes satisfy the orthogonality condition

$$\frac{1}{V}\int_V \mathrm{d}^3 r \boldsymbol{u}^*_{\boldsymbol{k}\lambda}(\boldsymbol{r})\boldsymbol{u}_{\boldsymbol{k}'\lambda'}(\boldsymbol{r}) = \delta_{\boldsymbol{k}\boldsymbol{k}'}\delta_{\lambda\lambda'}, \tag{4.1}$$

and for each wavevector, the two orthogonal unit vectors $\boldsymbol{e}_{\boldsymbol{k}\lambda}$ (called polarization vectors) satisfy

$$\boldsymbol{e}_{\boldsymbol{k}\lambda}\cdot\boldsymbol{e}_{\boldsymbol{k}\lambda'} = \delta_{\lambda\lambda'}, \tag{4.2}$$

$$\boldsymbol{e}_{\boldsymbol{k}\lambda}\cdot\boldsymbol{k} = 0. \tag{4.3}$$

The quantisation of the temporal part gives rise to the creation, $a^\dagger_\alpha$, and annihilation, a_α, operators in the modes $\alpha = (\boldsymbol{k}\lambda)$, which create and annihilate elementary excitations (*quanta*) of the electromagnetic field oscillating at a frequency ω_k. The quanta of the EM field are called *photons*. These operators obey bosonic commutation relations:

$$[a_{\boldsymbol{k}\lambda}, a^\dagger_{\boldsymbol{k}'\lambda'}] = \delta_{\boldsymbol{k}\boldsymbol{k}'}\delta_{\lambda\lambda'}, \tag{4.4}$$

$$[a_{\boldsymbol{k}\lambda}, a_{\boldsymbol{k}'\lambda'}] = [a^\dagger_{\boldsymbol{k}\lambda}, a^\dagger_{\boldsymbol{k}'\lambda'}] = 0. \tag{4.5}$$

The electric field operator written in terms of the creation and annihilation operators takes the form

$$\boldsymbol{E}(\boldsymbol{r},t) = \mathrm{i}\sum_{\boldsymbol{k}\lambda}\boldsymbol{e}_{\boldsymbol{k}\lambda}\sqrt{\frac{\hbar\omega_k}{2\epsilon_0 V}}\left[a_{\boldsymbol{k}\lambda}\mathrm{e}^{\mathrm{i}(\boldsymbol{k}\cdot\boldsymbol{r}-\omega_k t)} - a^\dagger_{\boldsymbol{k}\lambda}\mathrm{e}^{-\mathrm{i}(\boldsymbol{k}\cdot\boldsymbol{r}-\omega_k t)}\right], \tag{4.6}$$

$$= \boldsymbol{E}^{(+)}(\boldsymbol{r},t) - \boldsymbol{E}^{(-)}(\boldsymbol{r},t), \tag{4.7}$$

where the positive frequency part $\boldsymbol{E}^{(+)}(\boldsymbol{r},t)$ contains the sum of annihilation operators oscillating as $\mathrm{e}^{-\mathrm{i}\omega_k t}$, and $\boldsymbol{E}^{(-)}(\boldsymbol{r},t) = \left(\boldsymbol{E}^{(+)}(\boldsymbol{r},t)\right)^\dagger$.

Using (4.7) and the analogous expression for the magnetic field $\boldsymbol{B}$, we can write the Hamiltonian [121, 161] of the quantised electromagnetic field in

terms of the creation and annihilation operators of the electromagnetic field modes α as

$$H = \frac{1}{2}\sum_{\alpha} \hbar\omega_k \left(a_\alpha^\dagger a_\alpha + a_\alpha a_\alpha^\dagger\right) = \sum_{\alpha} \hbar\omega_k \left(a_\alpha^\dagger a_\alpha + \frac{1}{2}\right), \tag{4.8}$$

where the summation over the modes α is a short-hand notation for the summation over all $\boldsymbol{k}$ and the two polarisations λ. Since the number of modes is infinite, and the lowest energy of the quantised harmonic oscillator is not zero, but half a quantum ($\hbar\omega_k/2$), it gives rise to an infinite *zero point energy* of the vacuum state. However, as long as the processes to be described involve differences in energies, we can omit the zero point energy in the Hamiltonian, obtaining

$$H = \sum_{\alpha} \hbar\omega_k a_\alpha^\dagger a_\alpha. \tag{4.9}$$

It is convenient to define the Hermitian *number operators* $N_\alpha = a_\alpha^\dagger a_\alpha$, which *count* the number of photons in each mode α. It is then possible to rewrite (4.9) as

$$H = \sum_{\alpha} \hbar\omega_k N_\alpha. \tag{4.10}$$

4.2.1 States of the field

To describe the general state of the system, we can choose the basis consisting on the tensor product of the eigenstates of the different modes. If we denote the eigenstates of mode α by $|n_\alpha\rangle$, an eigenstate of the system can be written as

$$|\{n_\alpha\}\rangle \equiv |n_{\alpha_1}\rangle \otimes |n_{\alpha_2}\rangle \otimes \cdots = \bigotimes_{\alpha} |n_\alpha\rangle, \tag{4.11}$$

called a *multimode number state*, which is an eigenstate of (4.8) with eigenvalue

$$\langle\{n_\alpha\}|H|\{n_\alpha\}\rangle = \sum_\alpha \hbar\omega_k n_\alpha. \tag{4.12}$$

We can define the multimode number operator $\mathcal{N} \equiv \sum_\alpha N_\alpha$, whose expectation value gives the number of photons in all the field modes

$$\langle\mathcal{N}\rangle = \sum_\alpha n_\alpha. \tag{4.13}$$

The eigenstates of the number operator are called *Fock* states.

The simplest example of these Fock states is the single-photon state $|1\rangle$ given by

$$|1\rangle \equiv \sum_\alpha c_\alpha |1_\alpha\rangle; \tag{4.14}$$

i.e. a normalised ($\sum_\alpha |c_\alpha|^2 = 1$) superposition of states $|1_\alpha\rangle \equiv a_\alpha^\dagger|0\rangle$ with a single quantum in each mode. Obviously, the eigenvalue of this state is $\langle 1|\mathcal{N}|1\rangle = 1$. We can define the spatio-temporal envelope of the *single-photon wavepacket* $\boldsymbol{F}(\boldsymbol{r},t)$ using the positive frequency part of the electric field:

$$\boldsymbol{F}(\boldsymbol{r},t) \equiv \langle 0|\boldsymbol{E}^{(+)}(\boldsymbol{r},t)|1\rangle = \mathrm{i}\sum_\alpha \boldsymbol{e}_\alpha \epsilon_k c_\alpha a_\alpha \mathrm{e}^{\mathrm{i}(\boldsymbol{k}\cdot\boldsymbol{r}-\omega_k t)}, \tag{4.15}$$

with $\epsilon_k \equiv \sqrt{\frac{\hbar\omega_k}{2\epsilon_0 V}}$ denoting the vacuum field at frequency ω_k. In experimental settings, quasi-monochromatic, beam-like radiation is commonly encountered; that is, light propagating chiefly in a single direction, with the electric field confined in the plane transverse to the propagation direction, and populating only modes with a narrow distribution of frequencies around some central frequency ω. In these conditions, we can write

$$\mathrm{i}\epsilon_\omega f(\boldsymbol{r},t) \equiv F(\boldsymbol{r},t) = \mathrm{i}\epsilon_\omega \sum_{\boldsymbol{k}} c_{\boldsymbol{k}} \mathrm{e}^{\mathrm{i}\boldsymbol{k}\cdot\boldsymbol{r}}. \tag{4.16}$$

In this expression we can identify $c_{\boldsymbol{k}}$ as the Fourier coefficients in the mode

expansion of the (normalised) *envelope function* $f(\boldsymbol{r}, t)$. This approximation is valid, for example, for the description of the emission of an atom, which typically has a bandwidth several orders of magnitude smaller than the frequency of the atomic transition; it is also valid in the description of the emission of a single-photon by a cavity, whose linewidth (determined by the decay rate of the cavity) is typically orders of magnitude smaller than the frequency.

The photon-sources required for the phase-gate scheme that will be presented in Chapter 6 can be described in this way. In Section 2.3.5 we saw that we can store (single-photon) wavepackets in a medium using EIT if the bandwidth of the pulse satisfies certain conditions. Since the blockade effect is non-local [78], we shall assume that the effect of the gate on the wavepackets does not alter its modal structure significantly if the wavepacket lies within the blockaded region.

It is possible to deal with more complicated wavepackets (that help in describing other scenarios when localised space-time interactions are considered) by introducing non-orthogonal, non-monochromatic, spatial-temporal modes [163], related through certain non-unitary transformations to the orthogonal, monochromatic, plane-wave modes we have described above. However, this description is beyond the scope of this Chapter.

The most important relations for the action of the creation, annihilation and number operators in the different modes are,

$$a_\alpha^\dagger |n_\alpha\rangle = \sqrt{n_\alpha + 1}|n_\alpha + 1\rangle, \tag{4.17}$$

$$a_\alpha |n_\alpha\rangle = \sqrt{n_\alpha}|n_\alpha - 1\rangle, \quad a_\alpha|0\rangle = 0, \tag{4.18}$$

$$N_\alpha |n_\alpha\rangle = n_\alpha |n_\alpha\rangle, \tag{4.19}$$

where $|0\rangle$ is the vacuum state. The application of the creation operator to the vacuum state gives rise to the different photon number states in each

mode:

$$|n_\alpha\rangle = \frac{(a_\alpha^\dagger)^{n_\alpha}}{\sqrt{n_\alpha!}}|0\rangle. \tag{4.20}$$

Let us mention that these expressions shown above relate to the quantisation of the electromagnetic field in a box of length L. The physical field does not have any boundaries, and thus its spectrum is continuous. The simplest way to account for this fact is to let the dimension of the box $L \to \infty$. Then, the summation of the field modes can be replaced by an integral over $\boldsymbol{k}$-space,

$$\sum_{\boldsymbol{k}} \to \left(\frac{L}{2\pi}\right)^3 \int \mathrm{d}^3k, \tag{4.21}$$

with the volume element $\mathrm{d}^3k = \mathrm{d}k_x\,\mathrm{d}k_y\,\mathrm{d}k_z$.

4.3 Correlation functions

The absorption of a photon from an initial pure state $|\psi\rangle$ of the field results in a state $|\psi_f\rangle$ which is obtained from the initial one by the application of $E^{(+)}(\boldsymbol{r},t)$, which contains the annihilation operators of the field modes, $|\psi_f\rangle \propto E^{(+)}(\boldsymbol{r},t)|\psi\rangle$.

A valuable tool to unravel the temporal properties of our electromagnetic fields is the degree of coherence. It is the normalised correlation of the electric field operators. The degree of first-order coherence for a pure state is defined as

$$g^{(1)}(t_1,t_2) = \frac{\left\langle E^{(-)}(\boldsymbol{r},t_1)E^{(+)}(\boldsymbol{r},t_2)\right\rangle}{\langle|E^{(-)}(\boldsymbol{r},t_1)E^{(+)}(\boldsymbol{r},t_1)|\rangle}, \tag{4.22}$$

where the angular brackets denote the ensemble average. For stationary fields, the ensemble average can be substituted by a time average. The degree of first-order coherence can be obtained as the visibility of the interference pattern in a Michelson or a Mach-Zehnder interferometer, where one combines in the detector time-delayed versions of the same EM field, so $g^{(1)}$

only depends on the time difference $\tau = t_2 - t_1$. It can range from $g^{(1)}(\tau) = 1$ for total coherence, to $g^{(1)}(\tau) = 0$ for total incoherence; anything in between would be partially coherent. It is related to the power spectrum of the light of by the Fourier transform.

Despite the useful information given by $g^{(1)}(\tau)$, it does not distinguish the quantum, single-photon nature of our source [164].

4.3.1 Intensity correlation measurements

One of the ways to ascertain the quantum nature of light is the one that, in 1977, Mandel used to justify the existence of photons [165]. He briefly discusses an experiment performed by Clauser where, using a Hanbury Brown-Twiss [166] interferometer, the intensity correlation of the fluorescence of Hg atoms is measured.

In a Hanbury Brown-Twiss interferometer, a beam of light is sent through a beamsplitter and is detected by two photodetectors, one at each of the output ports. It is then possible to measure the temporal correlation between the signals at the two detectors to obtain the intensity correlation.

Within the semiclassical theory of the photoelectric detection of light [155, 165], it is asserted that the statistics of the photoelectrons detected are directly related to the statistics of the field. Furthermore, whenever there are coherences in the light field, the photoelectron counts would show them as well. From these facts, we can justify the use of detectors based on photoelectron counts to study the statistical properties of light.

Mandel derives inequalities, in terms of intensity correlation measurements, that classical electromagnetic waves should fullfil. A violation of this inequality would point to a purely quantum effect [165]. The second order

(intensity) correlation function is usually [167] defined as

$$G^{(2)}(t+\tau,t) = \left\langle :: \hat{I}(t+\tau)\hat{I}(t) :: \right\rangle \tag{4.23}$$

$$= \left\langle E^{(-)}(t)E^{(-)}(t+\tau)E^{(+)}(t+\tau)E^{(-)}(t) \right\rangle , \tag{4.24}$$

where :: denote that the average must be computed for the normal- and time-ordered product of the electric field operators. In the classical picture, the field operators are substituted by the field amplitudes. The light intensity is related to the photoelectron counts at the detector. Therefore, $G^{(2)}(t+\tau,t)$ measures the correlation between the photoelectron counts at times t and $t+\tau$.

Mandel's inequality for a classical field in stationary regime, based on the Cauchy-Schwarz inequality, reads:

$$G^{(2)}_{cl}(\tau) \leq G^{(2)}_{cl}(0) \ . \tag{4.25}$$

This means that, for a classical, stationary radiation field, the probability of obtaining simultaneous coincidences must be greater than or equal to the probability of obtaining time-delayed coincident counts.

A non-classical behaviour would be characterised, therefore, by

$$G^{(2)}(\tau) > G^{(2)}(0). \tag{4.26}$$

An intuitive argument behind these inequalities in intensity correlation measurements can be understood as follows: if the light consists of *photons*, when one of them passes through a beam splitter it cannot be detected by the two sensors; rather, it can only be registered by one of the photodetectors. If we have, for example, a single atom emitting these photons, there would be a time delay between successive emissions and this would set a delay for successive detections in the two photodetectors. Therefore, we would not

see simultaneous events in the two detectors (except for background counts). This behaviour of light arriving in discrete units leading to a lack of multiple simultaneous detections is called *antibunching*. Alternatively, if one considers an electromagnetic wave, i.e. a classical field, as our input beam, the probability of detecting a photon in each of the detectors is proportional to $I(t)$, irrespective of the detections in the other one. With no destructive interference between the two detections, only positive correlations can arise near $\tau \approx 0$, and thus $G^{(2)}_{cl}(\tau) \leq G^{(2)}_{cl}(0)$.

It is usual to work with the normalised form of this correlation function, $g^{(2)}(\tau)$, also called the *intensity correlation function*, defined as

$$g^{(2)}(\tau) = \frac{\left\langle : \hat{I}(t+\tau)\hat{I}(t) : \right\rangle}{\left\langle : \hat{I}(t+\tau) : \right\rangle \left\langle : \hat{I}(t) : \right\rangle}. \tag{4.27}$$

The nonclassicality bound in (4.26) can be expressed as

$$g^{(2)}(0) < 1, \tag{4.28}$$

whereas a classical behaviour reads

$$g^{(2)}(0) \geq 1. \tag{4.29}$$

The field of a single-mode, monochromatic, continuous-wave laser can be described as coherent state $|\alpha\rangle$. A coherent state $|\alpha\rangle$ is the eigenstate of the annihilation operator a with the complex eigenvalue $\alpha = |\alpha|\, e^{\mathrm{i}\theta}$. We can represent this field in terms of the number states $|n\rangle$ of the mode as

$$|\alpha\rangle = \mathrm{e}^{-|\alpha|^2/2} \sum_{n=0}^{\infty} \frac{\alpha^n}{\sqrt{n!}} |n\rangle. \tag{4.30}$$

For the coherent state, the condition (4.29) is fulfilled, since $g^{(2)}(0) = 1$. In fact, this state lies in the boundary between the phenomena which have

classical description and those which do not. Not surprisingly, if the initial state of the field is that of a single-photon $|1\rangle$, the correlation function is $g^{(2)} = 0$, clearly violating the classical bound in (4.28). In fact, an n-photon Fock state $|n\rangle$ gives rise to

$$g^{(2)}(0) = 1 - \frac{1}{n} < 1. \tag{4.31}$$

4.4 Summary

In this Chapter we have reviewed some of the fundamental knowledge regarding the quantisation of the electromagnetic field. We have described the states of the electromagnetic field as excitations in an infinite number of modes. Some of their coherence properties have been shown using correlation measures. We have defined single-photon wavepackets, which shall be used in the description of the phase-gate in Chapter 6. Furthermore, we have shown the (arguably) most important inequality involving the intensity correlation function, (4.26), which can be used as measure of nonclassicality.

In Chapter 5 we shall use the knowledge presented in this chapter to make predictions about the process of retrieval of multi-photon component polariton from a cold atomic ensemble after the interactions induced by resonant microwave fields. Finally, in Chapter 8 we will describe the experimental setup and calibrations required to measure $g^{(2)}$ in our experiments [1, 86].

Chapter 5

Retrieval of multi-photon component polariton

There are models to describe the propagation of Rydberg polaritons in a 1D cloud [72, 80, 91] which have resulted in the observation of "bound" states of light [168]. Also, there are models that describe how the interaction-induced dephasing works in ensembles of stored polaritons [149], which led the way to the first demonstration of antibunched light generated from a Rydberg ensemble [79]. Since the strong DD interaction between Rydberg excitations leads spatial correlations [73, 169, 170] these should be evident in 1D media. When these spatial correlations arise as a result of polariton propagation, they open the possibility to affect the photon statistics by applying local operations in different parts of the cloud [171].

Previous experiments in Durham University have led the way to controlled interactions between stored Rydberg polaritons using microwave fields [1]. These microwave fields couple the Rydberg states used for storage (which show strong vdW interactions) to other states in the Rydberg manifold; this coupling, in turn, triggers direct DD interactions between polaritons, which leads to very interesting dynamics (see Figure 5.1).

In experiments performed in our group [1, 86] we store photons as dark-state polaritons in Rydberg states and apply a microwave pulse of duration t that couples these states to nearby Rydberg states. Afterwards, we retrieve the photons, and Figure 5.1 shows the number of retrieved photons as a function of microwave Rabi frequency Ω_μ.

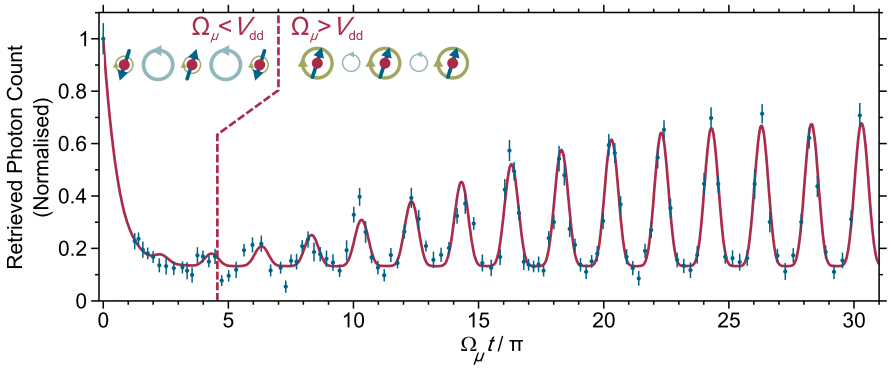

Figure 5.1: Nontrivial oscillations in the number of retrieved photons as a function of microwave pulse area $\Omega_\mu t$. After the photons are stored as polaritons in the state $|r\rangle = |60S_{1/2}\rangle$ of a cloud of ^{87}Rb, the polaritons are coupled to a neighbouring Rydberg state by a microwave field, and then retrieved (taken from [1]).

Our understanding of the dynamics of this system is still in its infancy, and more theoretical and experimental work is required in this area to fully understand the implications that it might have on QIP.

This Chapter presents a simple model to understand qualitatively the experiments in [1, 86]. It is possible to derive a more rigorous model [172], although quantitative agreement with experiments is still challenging.

5.1 Description of the system

We store 780 nm photons, resonant with the $|5S_{1/2}\rangle \leftrightarrow |5P_{3/2}\rangle$ transition of ^{87}Rb, in a cold atomic cloud. The photon propagate through the cloud as dark state polaritons under the conditions of EIT using a coupling laser resonant with the $|5P_{3/2}\rangle \leftrightarrow |60S_{1/2}\rangle$ transition in the ladder configuration

(see Figure 2.2), where the EIT bandwidth Δ_{EIT} (see (2.25)) gives a blockade radius $R_{\text{b}}^{(6)} \sim 7\,\mu\text{m}$.

The cloud is cigar-shaped, with longitudinal and trasversal standard deviations of the density distribution being given by $l \sim 30\,\mu\text{m} > R_{\text{b}}^{(6)}$ and $w_r \sim 2.8\,\mu\text{m} < R_{\text{b}}^{(6)}$ respectively. Since the cloud is elongated, let us assume that there are N atoms in a unidimensional region of space of length l (see Figure 5.2).

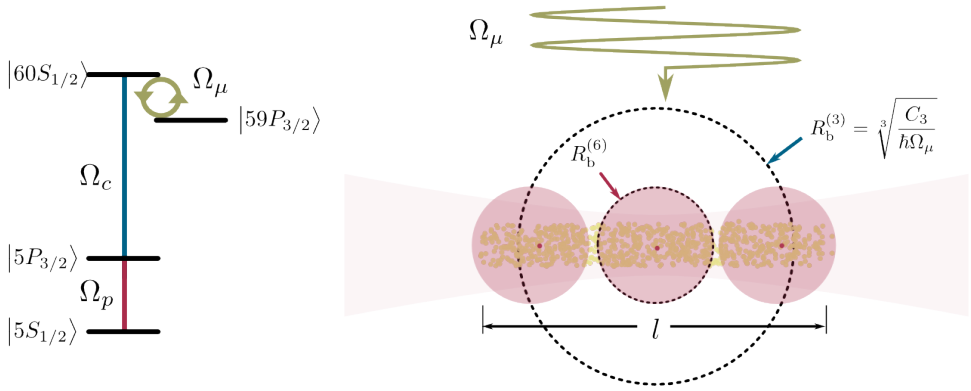

Figure 5.2: (Left) Probe photons are stored using a coupling field with Rabi frequency Ω_c into the Rydberg state $|r\rangle = |60S_{1/2}\rangle$. The resonant microwave field couples that state to $|p\rangle = |59P_{1/2}\rangle$ with Rabi frequency Ω_μ. (Right) Photons from a Gaussian beam (dim red) are stored as polaritons in an elongated cloud (yellow) with length l. The blockade effect due to vdW interactions prevents more than one excitation within each blockade radius $R_{\text{b}}^{(6)}$, limiting the number of excitations in the cloud. An applied microwave field with Rabi frequency Ω_μ couples the excitations to nearby Rydberg states, which induces resonant DD interactions, characterised by the blockade radius $R_{\text{b}}^{(3)}$. The radius, which depends on the resonant DD interaction coefficient C_3, can be controlled by changing the microwave Rabi frequency.

Then, the coupling laser is turned *off*, and the photons are stored as dark state polaritons in the cloud (see chapter 3). If the cloud were $l < R_{\text{b}}^{(6)}$, the dipole blockade effect [66] prevents more than one excitation to happen within the blockade radius $R_{\text{b}}^{(6)}$. This restriction allows us to write the evolution of the system during storage of the probe as an evolution from the ground state $|g\rangle = |g_1 g_2 \dots g_N\rangle$ to the singly-excited state $|s\rangle = \frac{1}{\sqrt{N}} \sum_{j=1}^{N} e^{i\phi_j} |r^j\rangle$ via a

two-photon EIT process (see Chapter 2). The state $|s\rangle$ is a symmetric mixture of the states with a single excitation at atom j, $|r^j\rangle = |g_1 g_2 \dots r_j \dots g_N\rangle$. The initial bandwidth of the process, which determines the distance between the stored excitations, is the two-photon EIT bandwidth, Δ_{EIT}. Since the excitation is stored as a polariton in the cloud (see chapter 2), the wave vector of the imprinted spin-wave is the sum of the excitation lasers $\mathbf{k} = \mathbf{k}_p + \mathbf{k}_c$, and the phase at the location of the j-th atom, $\mathbf{r}_j$ is just $\phi_j = \mathbf{k} \cdot \mathbf{r}_j$.

5.2 Storage into the first Rydberg state

The blockade radius $R_{\mathrm{b}}^{(6)}$ is a measure of the ratio between the vdW interaction energy between spatially-separated excitations and the EIT bandwidth (see (3.11)). If the energy shift due to DD interactions is larger than the transition linewidth, it prevents more than one excitation within one blockade sphere.

If we assume that the cloud is smaller than the blockade radius, $l \ll R_{\mathrm{b}}^{(6)}$, the storage of an excitation within one blockade radius transfers the system into this singly-excited state $|s\rangle$ with a negligible probability of having more than one excitation in the cloud.

If the cloud size is comparable or bigger than the blockade radius, $l \geq R_{\mathrm{b}}^{(6)}$, it is possible to have multiple excitations in the ensemble. Since the number of excitations may vary from shot to shot, the mean number of blockade spheres M depends roughly on the ratio $l/R_{\mathrm{b}}^{(6)}$.

5.3 Microwave coupling

Once the photons are stored in $|r\rangle = |60S_{1/2}\rangle$, we can couple them via an electric dipole transition to $|p\rangle = |59P_{3/2}\rangle$ using a microwave field. The microwave field couples each Rydberg state $|r_j\rangle$ to the lower one $|p_j\rangle$, and

induces long-range resonant DD interactions between pairs of excitations at a distance R, with strength $V_{\mathrm{DD}} = C_3(rp)/R^3$, where $C_3(rp)$ is the first-order DD coefficient for the states $|r\rangle$ and $|p\rangle$. Furthermore, this coupling doesn't introduce a position-dependent phase as the size of the cloud is much smaller than the wavelength of the transition.

A singly-excited, many body state $|s\rangle$ undergoes a complete rotation when a single atom 2π rotation is applied using the microwave field [149]. This is independent of the number of atoms present in the ensemble, so no collective effects are present, and we can treat each excitation as a simple two-level system.

If $l < R_{\mathrm{b}}^{(6)}$, only a single excitation is present in the cloud, and the application of microwaves couples singly-excited, symmetric states $|s\rangle$ and $|p\rangle = \frac{1}{\sqrt{N}} \sum_{j=1}^{N} e^{i\phi_j} |p^j\rangle$.

If $l \geq R_{\mathrm{b}}^{(6)}$ and the presence of more than one excitation in the cloud is appreciable, we need to make a distinction between the cases where the DD interactions are stronger than the coupling power and viceversa.

At low microwave powers the resonant DD interactions are large compared to the transition linewidth, $V_{\mathrm{DD}} > \Omega_\mu$. This prevents more than one excitation in the cloud if the distance $d < R_{\mathrm{b}}^{(6)}$ between two excitations is much smaller than the resonant blockade radius $R_{\mathrm{b}}^{(3)}(sp) = \sqrt[3]{C_3(sp)/\Omega_\mu}$. As explained in Section 3.4, if the distance between the excitations is similar to the blockade radius, DD interactions can also dephase multiply excited states, so even when separated by distances $d \sim R_{\mathrm{b}}^{(3)}$ they lead to loss during the retrieval process.

Since loss happens at distances $d \lesssim R_{\mathrm{b}}^{(3)}$, we will describe this effect with the effective lengthscale $R_{\mathrm{b}}^{(3)}$ (see Figure 5.2). Increasing the microwave coupling Ω_μ reduces the size of the new lengthscale. If $V_{\mathrm{DD}} < \Omega_\mu$, $R_{\mathrm{b}}^{(6)} > R_{\mathrm{b}}^{(3)}$, and the shift due to the resonant DD interactions is only effective within the original dipole blockade radius. Therefore, the microwaves can transfer the

populations from the original states $|s\rangle$ to the new Rydberg level $|s'\rangle$.

The transition between these two regimes is clearly visible in Figure 5.1.

5.4 Dicke states

The picture that we are left with in the limit $V_{\mathrm{DD}} < \Omega_m$ is a number of blockade spheres M which support a single excitation each. These cycle between the singly excited states $|s\rangle$ and $|p\rangle$ in the levels $|r\rangle$ and $|p\rangle$ respectively. This system is like a group of M two-level systems that interact with a radiation field, and since the wavelength of the field is bigger than cloud the systems are indistinguishable. Therefore, this system is the one described by the Dicke Hamiltonian [173].

The Dicke states in our system are the eigenstates of the following operators:

$$\mathbf{J}^2 |J, m_J\rangle = J(J+1) |J, m_J\rangle , \tag{5.1}$$

$$\mathbf{J_z} |J, m_J\rangle = M |J, m_J\rangle . \tag{5.2}$$

These operators are defined as

$$\mathbf{J_x} = \frac{1}{2} \sum_{j=1}^{M} \left(|s_j\rangle \langle s'_j| + |s'_j\rangle \langle s_j| \right) , \tag{5.3}$$

$$\mathbf{J_y} = \frac{i}{2} \sum_{j=1}^{M} \left(|s_j\rangle \langle s'_j| - |s'_j\rangle \langle s_j| \right) , \tag{5.4}$$

$$\mathbf{J_z} = \frac{1}{2} \sum_{j=1}^{M} \left(|s'_j\rangle \langle s'_j| - |s_j\rangle \langle s_j| \right) , \tag{5.5}$$

$$\mathbf{J}^2 = \mathbf{J_x}^2 + \mathbf{J_y}^2 + \mathbf{J_z}^2, \tag{5.6}$$

where the label j runs through the different blockaded ensembles. If we have M excitations and all of them are in the upper state ($|s\rangle$), the representation is $|J = M/2, m_J = -M/2\rangle$.

The evolution of Dicke states is related to the Wigner rotation matrices [174, 175]. The reduced rotation matrix $d^J_{m'_J m^j}$ between states with the same J with projections m'_j; and m_j is

$$d^J_{m'_J m_j} = \frac{(-1)^{m'_J - m_J}}{(m'_J - m_J)!}\sqrt{\frac{(J-m_J)!\left(J+m'_J\right)!}{(J+m_J)!\left(J-m'_J\right)!}}\cos^{2J+m_J-m'_J}\left(\tfrac{\phi}{2}\right)\sin^{m'_J-m_J}\left(\tfrac{\phi}{2}\right) \times {}_2F_1\left(m'_J - J, -m_J - J; m'_j - m_J + 1; -\tan^2(\phi/2)\right),$$

where the angle $\phi = \Omega_m t$ is the rotation provided by the microwave coupling and ${}_2F_1$ designates Gauss' hypergeometric function.

To retrieve the pulse in the same mode that it was stored in, it is necessary to preserve the initial phase structure. By turning the coupling field *on* again, radiation is retrieved when the original mode is present in the upper Rydberg state $|s\rangle$. Since our state is $|J = M/2, m_J = -M/2\rangle$, the probability of retrieval (that is, being in the same state) is proportional to the matrix element square,

$$P \propto \left|d^{M/2}_{M/2\,M/2}\right|^2 = \cos^{2M}\left(\frac{\phi}{2}\right) = \cos^{J}\left(\frac{\phi}{2}\right), \tag{5.7}$$

where the hypergeometric function takes the value 1 in the particular case where $m_J = -J$. The frequency of the oscillations corresponds to the single-atom microwave Rabi frequency, thus it does not depend on the number of excitations, or the number of atoms in each blockade sphere. This feature is important, since it allows us to observe the oscillations in a non-deterministically loaded sample.

The power of the cosine depends only on the mean number of excitations appearing in the first stage of the storage at high Ω_μ. Since the microwaves only change the state of the excitation, but not the number of excitations themselves, the number of blockade spheres is determined by the initial storage process. Therefore, once the microwave coupling is stronger than the

DD interactions, the shape of the oscillations should not change unless the microwave driving dephases any single excitation, thus reducing the number of blockades. Even if the number of excitations might vary shot to shot, the period of the oscillations remains constant; the only changing aspect when averaging $\cos^{2M}$ over different M is the *sharpness* of the peaks in the oscillations, and the width of the troughs. Therefore, the functional form of these oscillations can be seen as an indirect evidence for the amount of excitations present or surviving the microwave rotation process.

5.5 Impact on photon statistics

This intuitive picture where the dynamics in the Rydberg manifold is only determined by the blockade radii $R_{\mathrm{b}}^{(6)}$ and $R_{\mathrm{b}}^{(3)}$ manifold has some implications on the photon statistics of the retrieved field.

The first of them is the reduction of $g^{(2)}(0)$ at low microwave powers due to dephasing. Since resonant DD interactions between different excitations are much stronger at low microwave powers, these dephase multiple excitations [149, 174] without affecting the cases where either 0 or 1 excitations are present in the medium. Therefore, if the initial excitation corresponds to that of a Gaussian state, restricting the Fock state contributions to that of $n = 0$ and $n = 1$, thus resulting in a reduction of $g^{(2)}(0)$.

On the other side, with increasing microwave powers, an increasing number of excitations would survive the process, and so an increase in $g^{(2)}$ should be observed (bounded by the number of excitations available from the initial storage process, as in (4.31)). The relationship between $g^{(2)}$ and microwave Rabi frequency has not yet been observed in an experiment, but there is indirect evidence that the number of excitations surviving increases with the microwave power, as can be extracted from the functional form of the oscillations in Figure 5.1. Fitting the functional form of each individual peak

with a function of the form (5.7) shows an increasing exponent between 1 and 3 with increasing microwave power [86, 176].

5.6 Shortfalls of the model

The description above is not complete. One of the deficiencies of this simplified model is that it does not account for the effect of the DD interactions in the absence of the microwave field: even if the rotation in the Rydberg manifold with Rabi frequency Ω_μ is taking place, which adds a phase $\Omega_\mu t$ during the time t the field is turned on, resonant DD interactions are also present. The interactions should contribute $\sim V_{\mathrm{DD}} t$ towards the dynamics. The effect of the DD interactions cannot be neglected, and should contribute to dephasing even if $\Omega_\mu = 0$, and thus the oscillations in (5.7) only arise in the case where $V_{\mathrm{DD}} = 0$.

A more complex description is given by the XXZ-model Hamiltonian in [172], which shows some qualitative agreement with the data. Given the signal to noise ratio in the oscillations data, we cannot discard the possibility that the trend described in [86] could be described in some other way within the XXZ-model, although precise quantitative agreement between this theory and the experimental data is still lacking.

5.7 Summary

A simple model for the description of the dynamics of the experiments in [1, 86] has been developed. The dynamics can be described as a combination of two processes with different length scales: the storage/retrieval of photons on/from the cloud, where the vdW blockade radius $R_{\mathrm{b}}^{(6)}$ appears; and the microwave rotation in the Rydberg manifold, where the resonant DD interactions, showing a different length scale $R_{\mathrm{b}}^{(3)}$, prevail.

During the storage process the dipole blockade effect due to the vdW interactions between the excitations in the storage state limits the number of excitations in the cloud to M. Then, the application of microwaves coupling the storage state to a nearby Rydberg state during a finite time t leads to the description of the excitations as M spin-1/2 particles rotating under the influence of the microwave Rabi frequency Ω_μ. Coupling to a neighbouring state also induces resonant DD interactions, which leads to another blockade length scale that is a function of Ω_μ. In the limit of large Ω_μ, $R_{\rm b}^{(6)} \gg R_{\rm b}^{(3)}$ and the dynamics resemble that of the Dicke Hamiltonian, leading to oscillations in the number of retrieved counts as a function of Ω_μ with a functional form $\sim \cos^{2M}(\Omega_\mu t)$. On the other hand, in the limit of weak microwave power, $R_{\rm b}^{(6)} \ll R_{\rm b}^{(3)}$, and resonant DD interactions induce dephasing between the excitations in the cloud, reducing the number of retrieved photons.

The physics of multiple stored polaritons interacting with a microwave field can be exploited to design a universal phase gate, as will be shown in the following two chapters. The description of the system in terms of the different blockade radii will be used throughout.

Chapter 6

Photonic controlled-Z gate using Rydberg ensembles

In this Chapter, we present a photon gate scheme that decouples light propagation and interaction, allowing the realisation of high-fidelity photon-photon gates with negligible loss or distortion. We convert two photonic qubits (control and target) in the dual rail encoding into collective excitations (also called the dark-state polaritons [108, 126]) with Rydberg character in different positions in an ensemble of cold atoms. We subsequently perform a 2π-rotation on the target qubit using a microwave field coupled to an auxiliary state, which by default gives an overall phase shift of π-radians to the qubit pair. The microwave field also induces resonant DD interactions [1] between the target and control sites that are closest together, preventing the rotation for one of the four qubit-pair states, and thereby implementing a controlled-Z (CZ) gate. The excitations are then converted back to photons and emitted by the ensemble in the phase-matched direction.

Our scheme relies on the ability to modify the range of the DD interactions between highly-excited Rydberg atoms using a resonant microwave field [1, 50, 149]. Using this field to couple to an auxiliary Rydberg state, we exploit the spatial independence of the dipole-blockade mechanism [78] to induce a

homogeneous phase shift on the stored photon, and thereby circumvent the local-field limitation of the optical Kerr effect [33, 34].

This chapter is organised as follows:

- First, we outline the physical principle in 6.1 and explain how, for two photons stored in adjacent sites in an atomic cloud, resonant DD interactions can be used to obtain a π phase shift to the desired qubit state. We then derive some conditions and limits for the optimal performance of the gate.
- In section 6.2 we perform a fidelity estimation using a master equation approach. The results are showed in 6.2.2.
- We finish the chapter by looking at some limitations of the scheme and a discussion of the points for further study.

6.1 Physical principle

6.1.1 Controlled phase gate

A universal quantum computer should be able to implement any unitary transformation in a discrete Hilbert space [9], via a single processor, or a number of distinct ones connected to each other forming a *quantum network* [36].

To implement any unitary operation, we can use the elements of a universal set of quantum gates [17]. An example of such a set is the two-qubit controlled-not (CNOT) gate plus single qubit rotations [177]. Since single qubit rotations can be efficiently implemented for photonic qubits using beamsplitters and phase shifters, the other element left to implement for photonic qubits is the CNOT gate. This can be done probabilistically using ancilla qubits [27] with fidelities exceeding 85% [178, 179]. However,

concatenating probabilistic gates can reduce the efficiency of such a scheme if the probability of success is not close to 1. Therefore, finding a (quasi) deterministic universal quantum gate is an important problem.

Our proposal implements a CZ gate, which is universal, and can be cast into the more familiar CNOT gate using the single qubit Hadamard gate (as seen in Figure 6.1). A Hadamard gate acts on a single qubit described by the Hilbert space $\mathcal{H}$ by mapping the basis states $|0\rangle$ to $\frac{|0\rangle+|1\rangle}{\sqrt{2}}$ and $|1\rangle$ to $\frac{|0\rangle-|1\rangle}{\sqrt{2}}$; it can be represented as the unitary matrix

$$\mathrm{H} = \frac{1}{\sqrt{2}} \begin{pmatrix} 1 & 1 \\ 1 & -1 \end{pmatrix} . \tag{6.1}$$

The CZ gate can be represented [14] as the following unitary matrix acting in the two-qubit Hilbert space $\mathcal{H}_2 = \mathcal{H} \times \mathcal{H}$:

$$\mathrm{CZ} = \begin{pmatrix} 1 & 0 & 0 & 0 \\ 0 & 1 & 0 & 0 \\ 0 & 0 & 1 & 0 \\ 0 & 0 & 0 & -1 \end{pmatrix} , \tag{6.2}$$

where the minus sign acts on the two-qubit state $|11\rangle \in \mathcal{H}_2$.

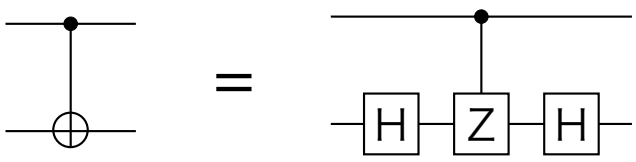

Figure 6.1: A CNOT gate (left) can be implemented by connecting two Hadamard gates to a CZ gate (right).

6.1.2 Qubit encoding

The photonic qubit (for example, from a Rydberg single-photon source [79]) is defined using the dual-rail encoding [14], where one photon travels in a superposition of two paths (*rails*) representing the computational basis states $|0\rangle$ and $|1\rangle$. Here, the paths travel through two spatially separated regions of an atomic cloud or through two different clouds, although care should be taken to make the density and shape of each cloud as similar as possible to match the modes of the qubits.

One can implement this scheme using coherent state inputs with low mean photon number $\langle n\rangle < 1$. This ensures that the multiphoton components ($n > 1$) are small compared to the single-photon contribution. In the Appendix A we discuss the expected change in fidelity when the inputs are coherent states, but for the rest of this chapter we assume single-photon inputs.

For a two-qubit gate we consider four separate spatial paths (see Figure 6.2). Similar geometries with two sites have already been implemented [94, 95]. We label the four channels as the elements of the basis set $\mathbb{B} = \{|1_{\mathrm{C}}\rangle, |0_{\mathrm{C}}\rangle, |1_{\mathrm{T}}\rangle, |0_{\mathrm{T}}\rangle\}$, where the subscript represent the (C)ontrol and (T)arget qubits. We arrange the paths for the $|1\rangle$ (*interacting*) components to be adjacent while the $|0\rangle$ paths are farther apart. We store the different photonic components in the medium as collective excitations (also called *dark-state polaritons*) with Rydberg character using electromagnetically induced transparency (EIT) in a ladder configuration [1, 76, 80, 84, 85], as has been already explained in Chapter 2. To this end, the signal light is resonant with the closed atomic transition $|g\rangle \leftrightarrow |e\rangle$, and classical coupling lasers resonant with the transitions $|e\rangle \leftrightarrow |r\rangle$ or $|e\rangle \leftrightarrow |r'\rangle$ are employed to store the control and target photons in two different Rydberg states $|r\rangle$ and $|r'\rangle$ (see Figure 6.3). These states can be of the form $|r\rangle = |nL\rangle$ and $|r'\rangle = |n'L'\rangle$, with $|L - L'| = 0, 2$, but, to simplify, we use $|r\rangle = |nS\rangle$ and $|r'\rangle = |n'S\rangle$, where n, n' are the principal quantum numbers and S denotes the $L = 0$

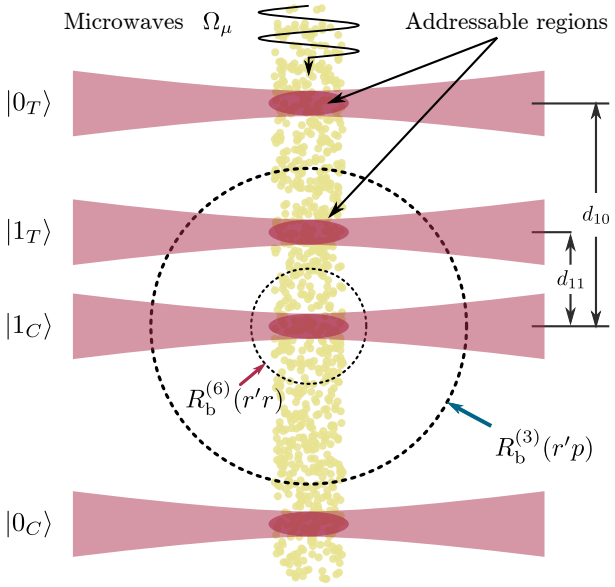

Figure 6.2: Optical layout: Control ($|C\rangle$) and Target ($|T\rangle$) photonic qubits, in dual-rail encoding, are stored as Rydberg polaritons (dark red) in a cold atomic ensemble (yellow). The spatial modes corresponding to the qubit states $|1_C\rangle$ and $|1_T\rangle$ are stored in adjacent sites at a distance d_{11}, and the others arbitrarily further apart from the interacting ones (d_{10}). After storage we attempt a 2π rotation on the target qubit using the microwave field with Rabi frequency Ω_μ and an intermediate state. This succeeds except for $|1_C 1_T\rangle$, in which the intermediate state is shifted by resonant DD interactions, which have a characteristic length scale $R_b^{(3)}$. We need to ensure that the van der Waals interactions between stored states (characterised by the blockade radius $R_b^{(6)}$) are small.

angular momentum state. Using different Rydberg states for target and control qubits allows us to perform operations on the individual qubits with a global microwave field.

There is at most one excitation in each site. This excitation is shared amongst all the atoms in that site, which maps the state into the superposition $|S_j\rangle = \frac{1}{\sqrt{N_j}} \sum_k^{N_j} |r_k^j\rangle e^{i\phi_k}$, where at each site $j \in \mathbb{B}$ with N_j atoms, the sum spans all possible singly-excited states $|r_k^j\rangle$ to the Rydberg level $|r^j\rangle$: $|r\rangle$ in the target qubit, $|r'\rangle$ in the control. The phase ϕ_k depends on the probe and coupling fields at the position of atom k. This process maps the photonic state $|CT\rangle = |C\rangle \otimes |T\rangle$ into a spin-wave state involving all of the four spatial channels $|S_{CT}\rangle = |S_C\rangle \otimes |S_T\rangle$, and can be achieved with efficiencies per site

exceeding 90% given sufficient optical depth [91] or using a low finesse optical cavity [180].

6.1.3 Microwave rotations and direct dipole-dipole interactions.

Once we have a mapping of the two-qubit state into the cloud, we make use of an auxiliary state $|p\rangle$ in the target qubit to perform the gate operation. A microwave pulse is applied to the system to attempt a $\int_0^t \Omega_\mu \mathrm{d}t = 2\pi$ rotation on the transition $|r\rangle \leftrightarrow |p\rangle$ in the target qubit, via the Hamiltonian $H_\mu = \hbar\Omega_\mu(|r\rangle\langle p| + |p\rangle\langle r|)$. Since there is only one excitation at each site, each ensemble behaves like an effective spin system, coupling the target states $|S_\mathrm{T}\rangle$ and the superposition of singly-excited $|p_k\rangle$ states, $|P_\mathrm{T}\rangle = \frac{1}{\sqrt{N}} \sum_k^{N_C} |p_k\rangle e^{\mathrm{i}\phi_k}$, with the single-atom Rabi frequency Ω_μ. Since the wavelength of the microwave field is much greater than the separation between sites, the coupling to both target sites is the same.

Performing the 2π-rotation adds a π-phase shift to the wavefunction, $|CT\rangle \rightarrow -|CT\rangle$. However, if the target state $|p\rangle$ is coupled to the control Rydberg state $|r'\rangle$ via an electric-dipole interaction at a distance d, the resonant DD interaction splits the energy between the states $|\pm\rangle = |r'p\rangle \pm |pr'\rangle$, shifting the energy of the coupled state by $\Delta_{r'p} = C_3(r'p)/d^3$, preventing the rotation, and thus the phase shift, conditional on the presence of a control excitation in a nearby channel. This operation, which implements a CZ gate[1], occurs with arbitrarily high fidelity if the distance between the adjacent control and target channels, d_{11}, is smaller than the characteristic length,

$$d_{11} < R_\mathrm{b}^{(3)}(r'p) = \sqrt[3]{C_3(r'p)/\hbar\Omega_\mu} < d_{10} \ , \tag{6.3}$$

[1] It actually implements a $(-1)\cdot$CZ gate according to the definition in (6.2). For the two-qubit setup described in this section, this global phase is irrelevant: any global phase can be obtained by properly tuning the path lengths travelled by the (photonic) qubits.

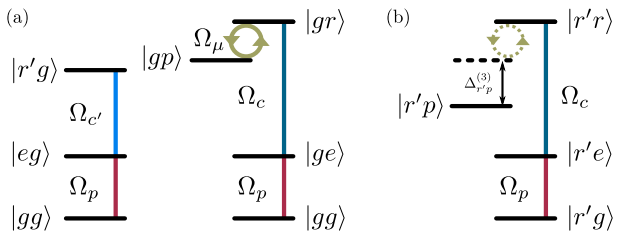

Figure 6.3: Coupled basis of the two inner polariton sites $|1_C 1_T\rangle$. (a) The control (left) and target (right) photonic qubits are stored in the atom cloud in two different Rydberg states, $|r'\rangle$ and $|r\rangle$, respectively. If the control qubit is in $|0\rangle$ (states $|gX\rangle$ in the pair state basis, with $X \in \{g, e, r, p\}$), we can perform a resonant 2π rotation on the $|r\rangle \leftrightarrow |p\rangle$ transition. (b) If the control qubit is in $|1\rangle$ (states $|r'X\rangle$), it shifts the auxiliary state $|p\rangle$ via a resonant DD interactions and the microwave 2π-pulse is no longer resonant. This gives rise to a homogeneous, conditional phase shift in the site.

where Ω_μ is the microwave Rabi frequency. The distance between non-interacting pairs, d_{10}, needs to be much larger than this length scale to prevent parasitic interactions.

6.1.4 Parasitic dipole-dipole interactions.

However the discussion outlined above is only valid if there are no other interactions between sites. As has been discussed in 3, if we have two excitations at a distance d in the medium (one for each qubit), vdW interactions between the Rydberg levels $|r\rangle$ and $|r'\rangle$ are important, and can degrade the gate fidelity by introducing spatially-dependent detunings. Such interactions detune the doubly-excited state $|r'r\rangle$ by an amount $\hbar\Delta_{r'r} = C_6(r'r)/d^6$ by coupling the states $|r'r\rangle \leftrightarrow |p'p\rangle$, where $|p\rangle$ and $|p'\rangle$ are dipole-coupled to both $|r\rangle$ and $|r'\rangle$ respectively. Here, $C_6(r'r) \propto 1/\delta_f$ is the vdW coefficient of an $|n'S, nS\rangle$ pair state, where δ_f is the Förster energy defect [51, 68].

If the energy shift $\hbar\Delta_{r'r}$ is comparable to the energy defect δ_f, DD interactions populate neighbouring states. Also, if this energy defect is zero (a situation called *Förster resonance*), we expect excitation hopping between

$|r'r\rangle$ and $|p'p\rangle$ to occur spontaneously [83]. This effect degrades the fidelity, as we lose control of the precise state the excitation is in. These scenarios can be avoided by choosing an appropriate level system. However, even for a system without Förster resonances, vdW interactions affect the proper functioning of the gate: during storage and retrieval processes and during the rotation in the microwave domain.

If we have an excitation $|r'\rangle$ in one site, the interaction shift between sites prevents the storage of the second photon [181] within a certain region characterised by the blockade length scale, $R_{\rm b}^{(6)}(r'r) = |C_6(r'r)/\hbar\Delta_{\rm EIT}|^{1/6}$, where $\Delta_{\rm EIT}$ is the linewidth of the EIT transparency window (see (2.25)). We minimise these inter-site interactions by ensuring that the distance d between any two spatial channels satisfies the inequality

$$d > R_{\rm b}^{(6)}(rr') \ . \tag{6.4}$$

This condition ensures that interactions during storage and retrieval are negligible, preventing spatial distortion of the spatial modes of the qubit wavepackets [33, 34].

The vdW interactions between $|r\rangle$ and $|r'\rangle$ are present also during the microwave rotation, when the coupling laser is off. This space-dependent energy shift causes a dephasing to the state $|11\rangle$ proportional to the 2π rotation time $\tau_{2\pi} = 2\pi/\Omega_\mu$, and to $\Delta_{r'r}$. But it decreases rapidly with the distance between interacting sites and is negligible when

$$d_{11} \gg R_\mu = |C_6(r'r)/\hbar\Omega_\mu|^{1/6} \ . \tag{6.5}$$

6.1.5 Conditions and limits.

Conditions (6.3), (6.4), and (6.5) suggest using

$$\frac{R_{\mathrm{b}}^{(3)}}{\max(R_{\mathrm{b}}^{(6)}, R_\mu)} = \left(\frac{C_6 \min(\Omega^2, \Omega_\mu^2)}{C_3^2 \Omega_\mu}\right)^{1/6} \tag{6.6}$$

as the figure of merit to maximise the gate fidelity for the following reasons:

- On the one hand, we need to maximise $R_{\mathrm{b}}^{(3)}$ to block any excitations to the $|r'p\rangle$ state in the interacting sites when the microwaves are applied. When the microwave rotation is "slow" ($\Omega_\mu < \Gamma$), this length scale is bounded by the lifetime of the state, $\max(R_{\mathrm{b}}^{(3)}) = (C_3/\Gamma)^{1/3}$.

- On the other hand, the effect of the vdW interactions is to impose a minimum distance $\sim \max(R_{\mathrm{b}}^{(6)}, R_\mu)$ that the two excitations can be apart. This distance depends not only on the excitation or the microwave rotation stages separately, but on the total time taken for the gate. For a sufficiently slow microwave rotation (to maximise $R_{\mathrm{b}}^{(3)}$), the denominator becomes $\max(R_{\mathrm{b}}^{(6)}, R_\mu) \to (C_6/\Gamma)^{1/6}$.

Dividing those expressions, and obviating the sixth root (which is a monotonous function) we obtain the dimensionless figure of merit

$$O = \left|\frac{C_3 (r'p)^2}{C_6 (r'r) \hbar \Gamma}\right| , \tag{6.7}$$

that can be used to compare between different systems. Note that O does not depend on any experimental parameters, only on the atomic species and the particular levels.

Figure 6.4 shows the figure of merit for different level systems of the form $|r'\rangle = |nS_{1/2}\rangle$, $|r\rangle = |(n+a)S_{1/2}\rangle$ and $|p\rangle = |nP_{1/2}\rangle$ as a function of the principal quantum number n in ^{87}Rb. The dipole-dipole interactions are calculated using perturbation theory, as shown in Chapter 3.

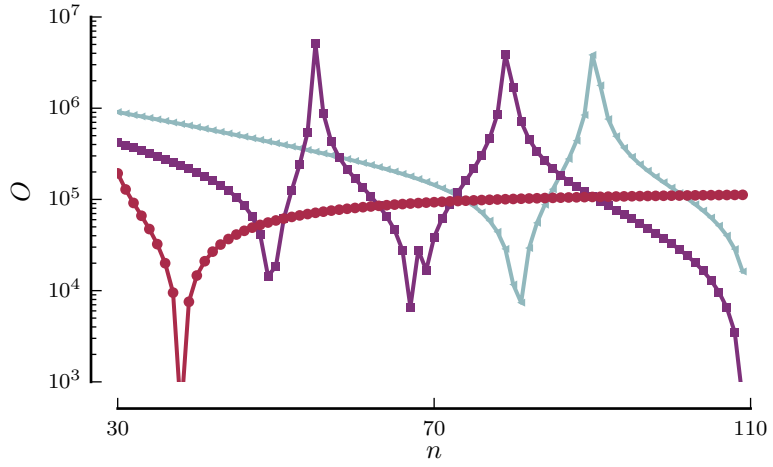

Figure 6.4: Figure of merit O for different level systems ($|r'\rangle = (n+a)S_{1/2}, |r\rangle = nS_{1/2}$ and $|p\rangle = nP_{1/2}$). In red circles, $a = 1$, which will be used for the estimation of the fidelity; in purple squares, $a = 2$; and, in blue triangles, $a = 3$. We observe multiple Förster resonances in the vdW coefficients which show as spikes and dips in the figure of merit. Note the Förster resonance from calculated values for the coupling $38s39s \leftrightarrow 38p_{3/2}38p_{3/2}$ in the red curve, which is in accordance with experimental values obtained elsewhere [145]. These simulations, based on the C_6 values in Figure 3.3, have been run using modified code originally written by Christophe Vaillant.

The following step is to estimate the fidelity. We restrict our study to the level system $|r'\rangle = |nS_{1/2}\rangle$, $|r\rangle = |(n+1)S_{1/2}\rangle$ and $|p\rangle = |nP_{1/2}\rangle$ to maximise O and avoid Förster resonances[2]. For $n = 70$ and a coupling of 10 MHz, we obtain $R_{\mathrm{b}}^{(6)} \sim 7\,\mu$m and $R_{\mathrm{b}}^{(3)} \sim 20\,\mu$m by coupling to the $M = 0$ state[3].

6.2 Fidelity estimation

If we condition the interaction between $|1_{\mathrm{C}}\rangle$ and $|1_{\mathrm{T}}\rangle$ by (6.3), and make sure that the effect of vdW interactions are negligible during the storage and retrieval (6.4) and microwave rotation (6.5), the photonic component $|11\rangle$

[2] The level system $nS\,(n+3)S$ shows a slightly higher O away from Förster resonances for $n < 80$ because its C_6 is smaller. However, since it shows more Förster resonances at higher n, we do not choose this level for our study (see Section 6.1.4)

[3] Away from Förster resonances, the scaling with principal quantum number of $C_6(nSnS)$ and $C_6(nS(n+1)S)$ are similar, thus one expects O to be constant with n. However, using higher n is more convenient, because the blockade radius is bigger, and thus the probe beams can be less focused.

picks up a homogeneous π-phase with respect to $|00\rangle$, $|10\rangle$ and $|01\rangle$, and the overall change in the system corresponds to that of the CZ-gate in (6.2) (whose global phase we neglect).

Since our aim is to estimate the fidelity of our scheme, we calculate the fidelity of achieving the state $|\psi'\rangle = (|00\rangle + |01\rangle + |10\rangle - |11\rangle)/2$ starting with the state $|\psi\rangle = (|00\rangle + |01\rangle + |10\rangle + |11\rangle)/2$. We choose this initial state because its evolution shows the main features of the gate; any choice of states not involving the $|11\rangle$ results in a (trivial) global phase, and does not show the conditional π phase.

6.2.1 Master equation approach

To better understand the possible implementation of the phase gate including real-world sources of decoherence, we estimate the fidelity using a simplified optical Bloch-equation approach. Our aim is not to provide a full many-body simulation of the gate protocol, but rather to estimate the errors in the case of a physical realisation using a cloud of cold ^{87}Rb atoms. We shall note that we do not fully simulate storage and retrieval processes; instead, we assume that the interacting sites are sufficiently far apart so that storage is successful.

There are four sites (two per qubit). The sites are excited sequentially, starting with the control sites. Since we neglect the atom-light coupling efficiency in this part of the calculation, in the absence of another excitation in the medium, we can transfer the photons at control sites to the Rydberg level $|r'\rangle$ following the EIT dark-state polariton picture (see 2.3.4. Thus we reduce the basis set for the sites of the control qubit to only two: "present", $|r'\rangle$, and "not present", $|g\rangle$.

Now, the transfer of the photons in the target sites to the levels $|r\rangle$, where a detuning given by the vdW shift is present, depends on the EIT transparency

linewidth Δ_{EIT} and the optical depth of the sample [109, 181]. The efficiency of the storage process is close to one if (6.4) is satisfied. To this end, for a given pair of states $|r'r\rangle$ we can either separate the interacting sites or we can choose a large Rabi frequency $\hbar\Omega_c > |C_6(r'r)|/d^6$. Conditional on the success of the storage procedure, we can use three states to describe the target sites: "not present", $|g\rangle$, Rydberg s-state, $|r\rangle$ and Rydberg p-state $|p\rangle$.

The operation of the phase gate then consists of three steps:

- storage of the target states,
- 2π rotation in the microwave domain of the control qubit, and
- retrieval of the target qubit.

During the storage and retrieval stages, we assume that the optical depth of the sample, OD, is large enough so that a small two-photon detuning does not affect the efficiency of the process [181]. However, the two-photon vdW interaction $H_{\mathrm{vdW}} = \Delta_{r'r}|r'r\rangle\langle r'r|$ only detunes the interacting pair, and this creates a phase-difference between the interacting and non-interacting regions; in the worst case scenario, when $\Delta_{r'r} \gg \Delta_{\mathrm{EIT}}$, it prevents the excitation of the target qubit in the interacting region, and when $|\Delta_{r'r}| \sim \Delta_{\mathrm{EIT}}$ it reduces the fidelity by changing the phase of the interacting pair.

Second, once the excitations are present, attempt to drive a 2π rotation of duration $\tau_{\mathrm{rot}} = 2\pi/\Omega_\mu$ in the $|r\rangle \to |p\rangle$ transition in the target sites. The dynamics are then described by $H_{\mathrm{rot}} = \frac{\Omega_\mu}{2}(|r\rangle\langle p| + |p\rangle\langle r|)$, where the effect of the direct dipole interaction is given, in the coupled basis, by $H_{\mathrm{res}} = \Delta_{r'p}|r'p\rangle\langle r'p|$. This interaction prevents the excitation of the interacting pair if $|\Delta_{r'p}| \gg \Omega_\mu$. Yet, if the linewidth of the transition is comparable to the direct-dipole interaction ($|\Delta_{r'p}| \lesssim \Omega_\mu$), some population can be transfered to the state $|r'p\rangle$ in the interacting pair, which can remain there during the de-excitation, limiting the fidelity of the final state.

Finally, a de-excitation in the same conditions as the excitation takes places to drive the atoms into the final state.

Let us note that during the 2π rotation stage, if $\Omega_\mu < \Delta_{\mathrm{EIT}}$, vdW interactions are important on the timescale of the rotation at distances $d_{11} \lesssim R_\mu$ (see (6.5). This causes oscillations due to the permanent detuning present on the $|r'r\rangle$ level. Furthermore, since vdW interactions depend on the distance, this creates an nonhomogenous phase across the sample in the interacting sites, and thus a transversal mode mismatch with respect to the noninteracting sites. Therefore, the optimal conditions for the phase gate requires condition (6.5). Also, to make a rough estimation of the effect of the finite size of the probe beam, we perform a Gaussian average with width $w = \sqrt{2}qR_{\mathrm{b}}^{(6)}(r'r) = \sqrt{2}w_0$, where $q = w_0/R_{\mathrm{b}}^{(6)}(r'r)$ is the ratio between the probe waist w_0 at each site and $R_{\mathrm{b}}^{(6)}(r'r)$. The $\sqrt{2}$ factor states that the interaction takes place between two sites. Writing the width w as a function of $R_{\mathrm{b}}^{(6)}(r'r)$ allows us to compare it with a meaningful quantity regarding the storage procedure at each n. Also, for the case where the initial qubit is derived from a coherent state (see Appendix A), multiple photons can be stored with significant probability when $q > 0.5$. This is, of course, not a problem with single-photon inputs.

6.2.2 Results

In Figure 6.6 the results of this exploration are shown, where we have calculated the fidelity of the final state ρ, $F_0 = \sqrt{\langle\psi'|\rho|\psi'\rangle}$, where the initial state $|\psi\rangle = (|00\rangle + |01\rangle + |10\rangle + |11\rangle)/2$ in the double-qubit basis becomes $|\psi'\rangle = (|00\rangle + |01\rangle + |10\rangle - |11\rangle)/2$ after the action of the gate. This state has been chosen so as to observe the effect of different processes (such as dephasing and decay) in multiple sites. Note that this does not constitute a measure of the process fidelity of the gate.

We initially obtain F_0 as a function of distance d_{11}, keeping the other pa-

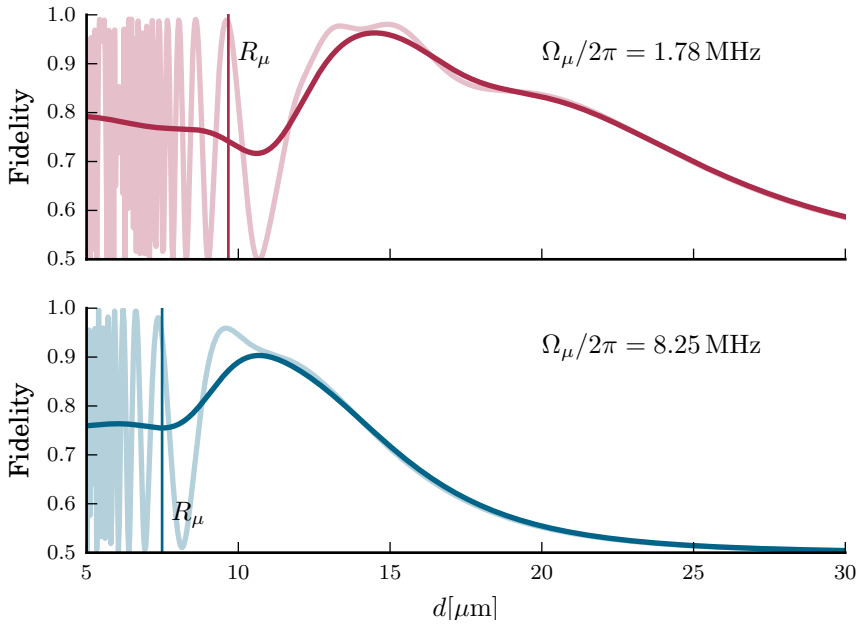

Figure 6.5: Comparison of the fidelity of the operation at different microwave powers. The results correspond to the level system with $n = 70$ and microwave Rabi frequencies of $\Omega_\mu/2\pi = 1.78\,\mathrm{MHz}$ (top) and $\Omega_\mu/2\pi = 8.25\,\mathrm{MHz}$ (bottom). The vdW interaction provides with an inhomogeneous detuning, which results in the interacting pair acquiring different phases at different distances, and a vertical line shows R_μ, a characteristic (maximum) length scale for this effect (see (6.5)). The raw results of the simulation are shown in light colours, and the Gaussian average of the fidelity for $w = \sqrt{2} \cdot 1.6\,\mu\mathrm{m}$ is shown in dark colours.

rameters constant (see Figure 6.5). The first significant effect is the presence of the oscillations at distances shorter than $\max(R_{\mathrm{b}}^{(6)}, R_\mu)$. These are mainly due to the effect of the vdW interaction in the state $|r'r\rangle$ which detunes this state with respect to the unperturbed state: as we have mentioned in the previous section, if the interaction time $\tau = 2\pi(1/\Omega_\mu)$ is fixed (by fixing Ω_μ) this time-dependent detuning is manifested in the form of distance-dependent oscillations. These oscillations become negligible when $\Delta_{r'r}\tau \sim 0$, and that is the reason why the oscillations stop when $d_{11} \gtrsim \max\left(R_\mu, R^{(6)}\right)$. For each n, Ω_μ we select the distance that shows the optimal fidelity, and the results are shown in Figure 6.6.

Since the stored excitations are spin-waves, these can suffer from motional

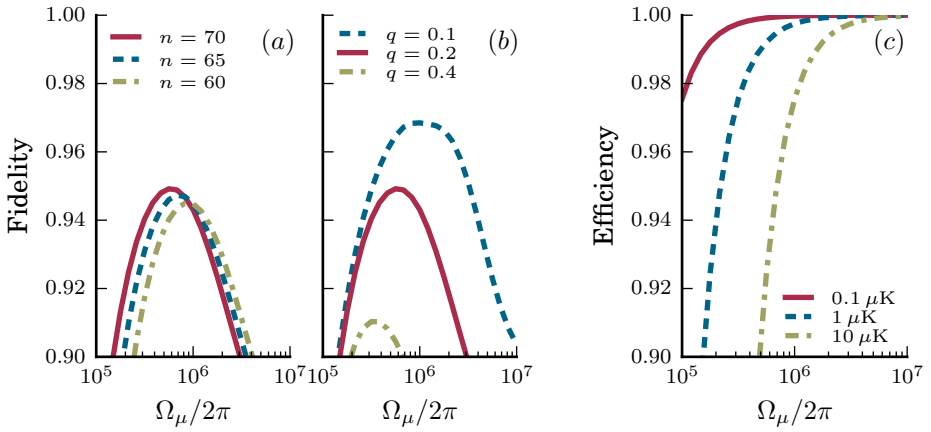

Figure 6.6: Estimation of the fidelity and efficiency of the gate protocol, including the effects of finite lifetimes of the Rydberg states and motional dephasing, as a function of the microwave Rabi frequency Ω_μ. The red, continuous line shows the case where $n = 70$ and $q = 0.2$ (see text for details). Plates (a) and (b) show the changes in fidelity by varying one parameter: (a) Principal quantum number n. (b) Different waist to blockade ratios $q = w_0/R_\mathrm{b}^{(6)}$ used in the Gaussian averaging. In plate (c) the changes in efficiency due to motional dephasing for different temperatures T are shown.

dephasing: atoms in an ensemble at a temperature T and average speed $v = \sqrt{k_\mathrm{B}T/m}$ (m is the atomic mass and k_B is the Boltzmann constant) can exit the site with mode diameter w_0 in a time $\xi = w_0/v$, or can move across the stored spin-wave with wavelength Λ in a time $\tau = \Lambda/2\pi v$. To quote some typical values, if we consider Rubidium atoms at $T = 1\,\mu$K travel with an average speed of $v \sim 9.9$ mm/s: an atom would take $\xi \sim 270\,\mu$s to exit an interaction region with mode diameter $w_0 = 2\,\mu$m; and since the stored spin wave has a wavelength $\Lambda \sim 1.2\,\mu$m, the time to move across the stored spin wave is $\tau \sim 20\,\mu$s. We can calculate a dephasing coefficient as $\eta_m \propto \exp\left[-(t^2/\tau^2)/(1 + t^2/\xi^2)\right]$ (taken from [132]): different gate times lead to different efficiencies. With these factors taken into account, we predict fidelities over 95% and low motional dephasing over a broad range of experimental parameters.

Inspecting Figure 6.6 we note the following general remarks: (c) The lower

the temperature, the larger the efficiency at a given Ω_μ: this is due to a reduction in motional difusion during the time $t_{2\pi} = 2\pi/\Omega_\mu$ taken to perform the gate operation. The lower dephasing allows lower microwave Rabi frequencies to be used, thereby enhancing the blockade effect (a) Increasing the principal quantum number increases the fidelity, although we expect a weak scaling with n, as seen inspecting O in Figure 6.4. This happens because we can drive transitions in the microwave domain with a weaker Ω_μ due to the favourable scaling of the lifetimes. However, this moves the peak of fidelity towards lower driving frequencies making the gate operation slower, which puts this parameter in competition with motional dephasing. Finally, (b) the smaller the waist of the sites, the higher the fidelity, but this is fundamentally limited by the diffraction limit; also, when the sites are very small, achieving a high OD is challenging and motional dephasing becomes a problem, although this could be reduced using a state-insensitive optical lattice [171].

6.3 Limitations and discussion

In addition to the limitations outlined above, a significant source of inefficiency is likely to arise from the mapping between the light field and the stored polaritons [91]. By making the cloud sufficiently dense ($\rho_0 \sim 10^{14}\,\mathrm{cm}^{-3}$), it is possible to obtain optical depths OD ~ 1000 that would give a theoretical efficiency per-channel of $\eta_c \approx 0.9$ and an overall [182] efficiency $\eta_c^2 \approx 81\%$. However, the densities required are similar to the ones achieved during BEC formation [183], and in that situation, the interactions between atoms become important: when the size of the wavefunction of the Rydberg state is comparable or bigger than the interparticle spacing, it can lead to the formation of Rydberg molecules [59] due to the interaction between the excited electron and neighbouring ground state atoms; this interaction can also be a source of dephasing [184]. The coupling efficiency can be improved by using photonic waveguides or by optimising the temporal shape of the

probe pulse [91]. Optimisation of the process of storage and retrieval of polaritons with Rydberg content might bring further improvements to our implementation.

The numbers quoted are comparable with previous implementations using linear optics [178, 185, 186], which have a 1/9 efficiency before post-selection, and experimentally achieves $\eta^2 \sim 85\%$ after post-selection. There are implementations of CNOT gates using Rydberg atoms as qubits [95] with demonstrated fidelities exceeding 70%, although different gate protocols predict fidelities greater than 95% [187] or even fidelity errors of order $\sim 10^{-3}$ [188]. Experimental constraints (especially atomic motion in the light field of the trap) are nowadays the limiting factor for the fidelity of these implementations. In the case of using Rydberg atoms as qubits, the gate protocols are not affected by mapping photons in and out of the atomic ensembles; at the same time, these implementations can only distribute quantum information locally, unless they are connected in some way to "flying qubits" able to transfer quantum information at long distances.

Looking forward, one can imagine using the scheme proposed in combination with integrated atom chip trapping and waveguides [189] to join several quantum gates, both sequentially and in parallel. Using existing waveguide technology, one could also implement single qubit operations [190, 191] in the same chip, which brings us closer towards a fully integrated quantum processor. Also, the proposed geometry and processing method could be extended to implement a photon switch and other operations.

In conclusion, we have shown that it is possible to realise a quasi-deterministic, high-fidelity universal quantum gate for photons. We circumvent the restrictions of conventional optical non-linearities by using the non-local dipole-blockade effect and by separating the propagation and interaction phases of the gate. We exploit microwave fields to neglect short range vdW

interactions and use longer range resonant DD interactions, which allows us to achieve a conditional phase shift on the stored target photon with fidelities in excess of 95% for currently achievable experimental conditions. The current limiting factor is the efficiency in mapping the flying qubits in and out of the atomic ensembles. Even if the efficiency of the protocol is not yet sufficient for error correction protocols, the scheme presented is a significant step forward for the realization of nearly deterministic quantum processing using photons.

Chapter 7

Multiqubit gates with dark-state polaritons and microwaves

The goal of universal quantum computation requires the generation of an arbitrary (and programable) unitary operation between an arbitrarily large number of input (N) and output qubits (M). It has been shown that any unitary for $N, M > 2$ can be approximated by a set of two-qubit, universal gates [192] with arbitrary accuracy. Furthermore, any two-qubit gate can be decomposed into three entangling gates, with the addition of single-qubit gates [192, 193].

Obviously, high-fidelity gates are needed to reach the goal of universal quantum computation. Even with error-correction codes, individual components should aim for error probabilities $p \lesssim 10^{-3}$ [194].

However, depending on the particular application, it might be possible to use a multiqubit, universal gate (with more than two qubits), such as the Toffoli [9, 195] or Fredkin gates [196], to aleviate the number of components required. For example, Shor's algorithm [10] was first devised using Toffoli gates.

A Toffoli gate (also called CCNOT gate) is a universal, reversible logic gate

[195]. Together with single-qubit gates, it can be used for universal quantum computation. The Toffoli applies a Pauli-X rotation matrix (the quantum analog of the NOT operation) conditional on the first and second qubits (called *control qubits*) being in the $|1\rangle$ state; this operation can be represented by the following unitary matrix:

$$\text{Toffoli} = \begin{pmatrix} 1 & 0 & 0 & 0 & 0 & 0 \\ 0 & 1 & 0 & 0 & 0 & 0 \\ 0 & 0 & 1 & 0 & 0 & 0 \\ 0 & 0 & 0 & 1 & 0 & 0 \\ 0 & 0 & 0 & 0 & 0 & 1 \\ 0 & 0 & 0 & 0 & 1 & 0 \end{pmatrix} . \tag{7.1}$$

A Toffoli gate be constructed using 6 CNOT gates [14, 197] optimally. Since a Toffoli gate made in this way concatenates CNOT gates with fidelity η_{CNOT}, the overall fidelity is degraded by a factor η_{CNOT}^6. Thus, if possible, it would be preferable to implement the 3-qubit gate directly with efficiency $\eta \sim \eta_{\text{CNOT}}$.

Implementations of multiqubit gates using Rydberg atoms and atomic qubit encoding have already been proposed [69, 198], with predicted errors smaller than 10%. However, these ideas have not yet been discussed in the context of photonic gates.

In this Chapter, we sketch a recipe to make a $(n+1)$-qubit entangling gate called C^nZ, where n qubits control a π phase picked up by a target qubit. The physical principle of this gate is similar to that used for the gate described in Chapter 6, where photonic qubits stored in a cloud of atoms in the form of Rydberg polaritons are subjected to multiple rotations in the Rydberg manifold by the use of microwaves. In this case, the geometric arrangement of the qubits is such that the vdW interactions for different states prevents the rotation of one of the qubit states of the *target* to happen conditional upon

all the other k *control* qubits being in state $|1\rangle$. The system described below gives rise to a number of conditions on the allowed dipole-dipole interactions for its implementation, but further research is necessary to understand its applicability.

First, we show the connection between the CZ of Chapter 6 and the C^nZ under consideration. Then we describe the microwave rotations to neighbouring transitions that both control and target qubits undergo. It will be seen that the precise geometrical arrangement of the qubits makes vdW interactions significant in all coupled basis states except for the case $|11\ldots1\rangle$. This gives rise to a π phase shift in the wave function in that singular case with respect to the rest, which implements the gate. Finally, the rest of the relevant DD interactions in the system are discussed, and conditions for the gate performance based on the blockade radii are derived.

7.1 Physical principle

7.1.1 C^nZ gate

The C^nZ is a symmetric, entangling gate that implements a Pauli-Z gate [14] in a target qubit conditional on n control qubits being in state $|1\rangle$. The operational matrix on the $n+1$ qubits is

$$C^nZ = \begin{pmatrix} 1 & 0 & \cdots & 0 & 0 \\ 0 & 1 & \cdots & 0 & 0 \\ \vdots & \vdots & \ddots & \vdots & \vdots \\ 0 & 0 & \cdots & 1 & 0 \\ 0 & 0 & \cdots & 0 & -1 \end{pmatrix} \tag{7.2}$$

The case $n = 1$ implements the same CZ gate analyzed in Chapter 6, although the optical layout and level systems are different in the two implementations.

The case $n = 2$ is the CCZ or the controlled-controlled-phase gate, which is the symmetric analogue to the Toffoli gate [197], and can be converted into the latter using only (single-qubit) Hadamard gates on the target qubit, as seen in Figure 7.1.

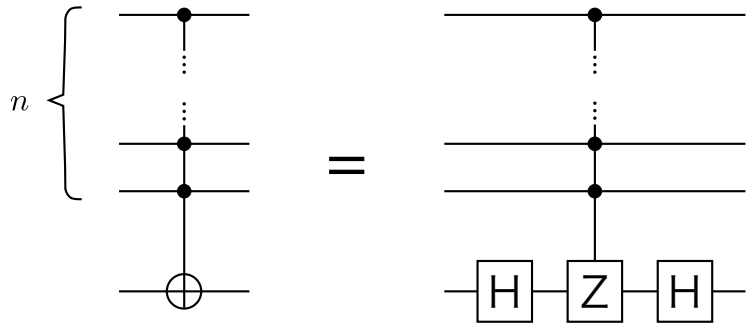

Figure 7.1: A C^{n}Z gate (left) implements a Pauli-Z rotation on the target qubit dependent upon n control qubits. It can be converted into the C^{n}NOT gate using two Hadamard gates (right).

7.1.2 Qubit encoding

The qubit encoding is similar to that in section 6.1.2. The *control* and *target* qubits are encoded using the dual-rail scheme as dark-state polaritons with Rydberg content in different states. This gives rise to $2(n + 1)$ paths that pass through one or multiple cold atomic clouds, encoding the $|0_k\rangle, |0_\mathrm{T}\rangle$ and $|1_k\rangle, |1_\mathrm{T}\rangle$ components of the control and target qubits respectively. The geometric arrangement is depicted in Figure 7.2.

Here, the $|0_k\rangle$ components of the control qubits are essentially equidistant to $|1_\mathrm{T}\rangle$ and $|0_\mathrm{T}\rangle$. Furthermore, the $|0_k\rangle$ and $|1_k\rangle$ components of the control qubits are, again, approximately equidistant to $|0_\mathrm{T}\rangle$. This geometric arrangement has the particularity that all the $|1_k\rangle$ components of the control qubits are approximately twice as far to $|1_\mathrm{T}\rangle$ than to $|0_\mathrm{T}\rangle$.

The storage of the target qubit uses a coupling laser Ω_t resonant with the transition $|e\rangle \leftrightarrow |r\rangle$. Subsequently, the other n control qubits use n differ-

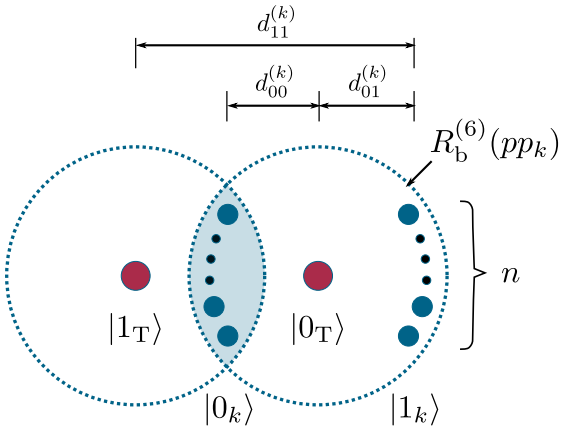

Figure 7.2: Transversal view of the optical layout: target (red) and control (blue) photonic qubits, in dual-rail encoding, are stored as Rydberg polaritons in a cold atomic ensemble. The $|0_k\rangle$ and $|1_k\rangle$ components of the n control qubits are stored at distances $d_{00}^{(k)}$ and $d_{01}^{(k)}$ (respectively) to $|0_{\mathrm{T}}\rangle$. Since those distances are smaller than $R_{\mathrm{b}}^{(6)}(pp_k)$, when attempting a 2π rotation in the target qubit it does not succeed. The only situation in which that rotation succeeds is the case where all of the qubits are in state $|1\rangle$, because the distance between the target $|1_{\mathrm{T}}\rangle$ and the controls $|1_k\rangle$, $d_{11}^{(k)}$, is larger than the blockade radius.

ent coupling lasers with $\Omega_c^{(k)}$ Rabi frequencies, resonant with the transitions $|e\rangle \leftrightarrow |r_k\rangle$. Figure 7.3 (a) shows the level systems for the noninteracting control (left) and target (right) qubit sites.

7.1.3 Microwave rotations

After the storage procedure, all qubits undergo rotations to neighbouring states. First, the control qubits perform a π rotation in the $|r_k\rangle \leftrightarrow |p_k\rangle$ with Rabi frequencies $\Omega_\mu^{(k)}$, which brings the population to $|p_k\rangle$. Then, the target qubit aims for a 2π-rotation in the transition $|r\rangle \leftrightarrow |p\rangle$ with Rabi frequency Ω_μ: if successful, the rotation adds a minus sign to the wavefunction. Finally, another π transition brings the population of the control qubits back to $|r_k\rangle$; in this case, the complete 2π rotation of the controls also add up to another minus sign on the wavefunction, which alongside with the one of the target gives a phase $(-1)^{(n+1)}$.

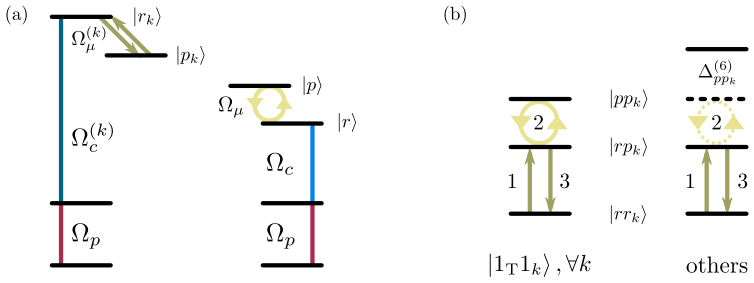

Figure 7.3: Basis states for target and coupling qubits. (a) The control (left) and target (right) photonic qubits are stored in the atom cloud in different states, $|r_k\rangle, k = 1 \cdots n$ and $|r\rangle$, respectively. The control qubits undergo a π rotation with Rabi frequency $\Omega_\mu^{(k)}$ to the states $|p_k\rangle$; then, the target qubits do a 2π rotation with Rabi frequency Ω_μ through state $|p\rangle$; finally, the control qubits return to the storage states with another π rotation. (b) If any of the control qubits is in $|0_k\rangle$, the vdW interactions between target and control sites shift the state $|pp_k\rangle$ of the coupled basis out of resonance, by an amount $\Delta_{pp_k}^{(6)}$, which prevents the probe's rotation (right). On the contrary, if all of the control qubits are in state $|1_k\rangle$ and the target qubit is in $|1_T\rangle$, vdW interactions are negligible, and the 2π rotation of the target takes place. This gives rise to a homogeneous conditional phase shift.

If the vdW interactions between the intermediate levels $|p\rangle \leftrightarrow |p_k\rangle$, $\Delta_{pp_k}^{(6)}$, are sufficiently strong (neglecting the rest of the interactions), then the 2π rotation of the target does not succeed, and the final wavefunction only gets a phase $(-1)^n$. In the same spirit as in Chapter 6, since we have stored the $|1_T\rangle$ and $|0_T\rangle$ states of the target qubit in different positions relative to the control qubits, it is in principle possible to obtain a π phase shift to the $|1_T, 1_k\rangle$ state with respect to the rest of the states, which implements a C^nZ gate[1].

The ideal gate succeeds if the distance $d_{11}^{(k)}$ between the $|1\rangle$ components of target and the k controls is bigger than the blockade radii $R_b^{(6)}(pp_k)$, and the rest of the target-control distances are smaller than that

$$d_{11}^{(k)} > R_b^{(6)}(pp_k) > d_{10}^{(k)}, d_{01}^{(k)}, d_{00}^{(k)}, \tag{7.3}$$

[1] The phase shifts discussed are only valid if the operation remains coherent the whole time. Decoherence in the sample leads to a decreased retrieval efficiency, and so it should be avoided

where $d_{AB}^{(k)}$ is the distance between the $|A_\mathrm{T}\rangle$ component of the target and $|B_k\rangle$ components of the control qubits.

7.1.4 Parasitic interactions and limitations

As in the previous gate scheme in Chapter 6, the DD interactions between intermediate levels can, in principle, affect the gate process. The success of the gate depends on the magnitude of these parasitic dipole interactions. If they are sufficiently small, those effects can be casted as inequalities affecting the blockade radii for transitions involving both first- and second-order DD interactions.

First, there are the vdW interactions between the storage sites' states (with blockade radii $R_\mathrm{b}^{(6)}(rr_k)$ and $R_\mathrm{b}^{(6)}(r_k r_j)$, $k \neq j$) and the microwave rotated states in the control qubits (with radii $R_\mathrm{b}^{(6)}(p_k p_j)$, $k \neq j$). The relevant resonant DD interactions are those between the storage states $|r\rangle, |r_k\rangle$ and the intermediate levels $|p\rangle, |p_k\rangle$.

By the geometrical construction in Figure 7.2, we know that the smallest distances between any two control sites, j and k, are $d_{00}^{(k,j)} \sim d_{11}^{(k,j)} \ll d_{01}^{(k,j)}$. Also, the $|1_\mathrm{T}\rangle$ site is further away from $|0_k\rangle$ than $|0_\mathrm{T}\rangle$. Therefore, the gate succeeds when the following conditions are met:

$$R_\mathrm{b}^{(3)}(rp_k), R_\mathrm{b}^{(3)}(pr_k), R_\mathrm{b}^{(6)}(rr_k) < \min\left(d_{01}^{(k)}, d_{00}^{(k)}, d_{01}^{(k)}\right), \tag{7.4}$$

$$R_\mathrm{b}^{(3)}(p_j r_k), R_\mathrm{b}^{(6)}(r_k r_j), R_\mathrm{b}^{(6)}(p_k p_j) < \min\left(d_{00}^{(k,j)}, d_{11}^{(k,j)}\right) \ (i \neq j). \tag{7.5}$$

These $3 \cdot n + 3 \cdot n(n-1)/2 = 3(n(n+1))/2$ inequalities complement the $4n$ inequalities of (7.3). For $n = 2$ (the CCZ), the number of inequalities is 17, whereas for the two-qubit gate CZ, $n = 1$, only 7 inequalities are required.

7.1.5 General remarks

In light of the huge number of inequalities appearing in the last section, some general comments must be made about these kind of gates.

First, it is necessary to find a physical system showing both strong and weak DD interactions between states. However, since both vdW and resonant DD coefficients depend on the dipolar transitions from some initial states, an open question remains: what are the physically possible ratios $C_3(ab)$ to $C_6(aa)$ and $C_6(bb)$ in transitions involving just two different states. These ratios should have a strong impact in this and other schemes mixing first and second order DD interactions. Looking at the DD interaction energies (3.7) and (3.8) suggests that there might be a general relationship between the two, although this relationship might depend on the particular quantum defects of the species under consideration.

Nevertheless, it might be possible to implement this scheme if an appropriate system that showed very strong vdW interactions in just one state $|pp'\rangle$, compared to the rest of the states. Then, coupling from the initial $|r_k\rangle$ to $|p'\rangle$ would reduce significantly the number of conditions required of the level system. However, as it was mentioned in Chapter 6, one should be careful to avoid Förster resonances that might lead to state-changing processes.

Finally, there is the issue of the finite size of the transverse photonic mode. For a probe beam with wavelength λ, the diffraction limit sets a minimum waist of $w_0 = 2r \sim \lambda/2$ in vacuum. In the total absence of DD interactions other than the ones required for the gate, the absolute maximum number N of qubits that can be entangled using this gate is $N \sim {R_\mathrm{b}^{(6)}}^2/(2r^2)$. For a blockade radius of $R_\mathrm{b}^{(6)} \sim 10\,\mu$m and $\lambda \sim 780\,$nm, the theoretical limit of modes is $N_\mathrm{max} \sim 1000$. However, obtaining that many diffraction limited spots is not feasible; for more realistic photonic modes with $r \sim 2\,\mu$m, a less substantial $N \sim 12$ holds.

7.2 Summary

In this Chapter an implementation of the multiqubit, entangling C^nZ gate using photonic qubits has been proposed. In the case where all of the qubits are in the $|1\rangle$ state, a 2π rotation in the target qubit succeeds; however, if any of the qubits are in the $|0\rangle$ state, strong vdW interactions suppress this rotation, and so a conditional π phase shift is obtained in the system. The geometrical conditions, which involve the blockade radii associated with the DD interactions present, have been derived.

Further research is required to show the possibility of implementing this scheme in a physical system using a specific atomic species.

Chapter 8

Experimental apparatus to measure $g^{(2)}$ for Rydberg polariton single photons

The coupling of weak light fields to Rydberg states of atoms under conditions of EIT leads to the formation of Rydberg polaritons, which are quasiparticles with tuneable effective mass and nonlocal interactions [199, 200]. These interactions affect the dispersive propagation of the photons [201], and under some conditions this propagation becomes dominated by a two-photon bound state [81].

If two propagating Rydberg polaritons under the conditions of EIT are sufficiently far apart, their propagation is not affected by the interactions in the medium. If, however, two or more excitations propagate at a distance smaller than the blockade radius, both the blockade effect and dipole-induced dephasing [82, 149] reduce the number of photons propagating to a maximum of one.

This heuristic explanation [116] suggests that if a steady-state, coherent state of photons traverse a cloud of atoms under the effects of EIT and the Rydberg

blockade (see Chapters 3 and 2), the output will be roughly a train of single photons separated by the time taken by a single photon to traverse a blockade sphere, τ_{b}. This output shows a degree of second order coherence, $g^{(2)}(0) \sim 0$, which, as we showed in Chapter 4, is quantum in nature. As a matter of fact, experiments performed in Harvard showed that this was the case [80], but the experimentally observed $g^{(2)}(\tau)$ suggested that the picture of a train of photons needed to be changed.

A similar, but different, process is that of polariton storage and retrieval in a cloud of strongly-interacting atoms [1, 79]. In this case, the Fock state content of the input light is mapped into polaritons in the cloud after the storage procedure. The strong interactions between these polaritons produce a similar quantum behaviour to that previously mentioned when the size of the cloud is comparable to the blockade radius: the probability of obtaining photon pairs in the same storage/retrieval cycle is smaller than the probability of obtaining pairs in consecutive cycles, thus the autocorrelation function $g^{(2)}(0) < 1$. As a matter of fact, for a fixed cloud size, $g^{(2)}(0)$ decreases with increasing blockade radius. In the limit where $g^{(2)}(0) \sim 0$, this system can be exploited as a quasi-deterministic source of single-photon wavepackets. But what happens when $0 < g^{(2)}(0) < 1$?

In our experiment, light is stored in an elongated cloud ($l \gg R_{\mathrm{b}}^{(6)}(rr)$) whose transverse size r is smaller than the blockade radius $R_{\mathrm{b}}^{(6)}(rr)$. This preferentially populates the state where several polaritons are stored along the cloud [86, 172], giving rise to $0 < g^{(2)}(0) \leq 1$. In the limit where the cloud is so big that a coherent state of polaritons can be populated, $g^{(2)}(0) = 1$.

In this Chapter we describe an experimental setup to measure the intensity autocorrelation $g^{(2)}$ of light using photon counting techniques. This setup has been used in recent experiments to study the quantum nature of the output light, and their results are presented elsewhere [1, 86, 176]. First, we describe our detection system based on single-photon avalanche diodes

(SPAD) required to convert single-photon detection events to standard electronic signals. Then, we describe the timing system used to *stamp* each of the electronic signals at the output of the SPADs with a time. The timing data enables us to perform a statistical analysis of the light output.

8.1 Experimental setup

A perfect detection system would be one that gives a *click* when it receives a photon, and is ready for another count immediatly afterwards, with a negligible dead time; furthermore, it would have the capability of distinguishing when two or more of these photons arrive simultaneously [202]. However, despite the best efforts of the scientific community, this ideal system is not available yet. Imperfect, *real* detection systems are characterized by several quantities that reflect in which ways they fail to reproduce perfect behaviour.

As mentioned above, we use a HBT interferometer shown in Figure 8.1, to split the light coming from the experiment. There, the photons are detected by *single-photon detectors*, which convert photons to standard electronic TTL pulses. These pulses are sent to a *timing module* to tag detections at the time they occur. Finally, we process the data and obtain the autocorrelation function. The process of data acquisition is controlled with a computer. In the two following sections, the characteristics of the photodetectors and the timing module are described in more detail.

8.2 Photodetectors and calibration

8.2.1 Single-photon detectors

To get information about the intensity correlation at the single-photon level, one must be able to detect repetitively single-photon events with a very good

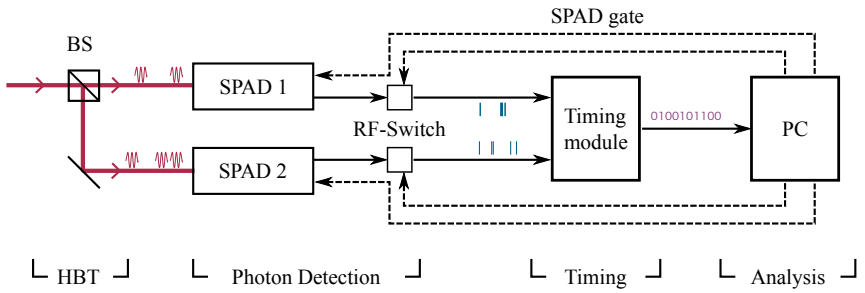

Figure 8.1: Detection system to determine $g^{(2)}$. A Hanbury-Brown-Twiss (HBT) interferometer divides the light using a beamsplitter (BS), which is then detected using single-photon avalanche photodiodes (SPADs) and the detections are converted to electronic pulses. The pulses are sent to the timing module. Finally, the data is collected in the computer for later processing.

time resolution [202].

Single-photon detectors must provide an amplification mechanism as noiseless as possible. The fraction of incident photons detected by the sensor is called the *quantum efficiency*, η. This is related to the number of electron-hole pairs generated by the arrival of a photon. It is therefore, a measure of the detector's sensitivity to light.

The *dark-count rate* is the number of counts that the detector records when there is no input light. It is mostly due to the thermal current in electronic components existing at any temperature greater than zero Kelvin, and is usually random (Poissonian) in nature. Dark counts can come from radioactive decay and cosmic rays. The effect of these dark counts is to increase the noise in the measurement. It is possible to reduce this dark-count rate by keeping the detectors as cold as possible.

The *signal-to-noise ratio* (SNR) is the ratio between the power of the signal and the power of the noise. This gives an account of the precision of the measurements, and can affect its accuracy. A low detection efficiency increases the amount of data required to separate the signal from the noise.

Apart from the amplification requirements, temporal requirements of single-

photon detectors are very important. The first requirement is a fast and consistent response to the arrival of a photon in order to obtain a precise time for the event and avoid *timing jitter*.

When one photon arrives at the detector, it triggers a current which will be detected later and its time recorded. Each time an event is detected, the instrument requires some time to be ready for detection again. This is called *dead time*.

Another important property of the detector is the *maximum repetition rate*, which is the maximum number of events that it can process in a given time without damage ocurring. This characteristic, usually provided by the manufacturer in the specifications, places important constraints on the power input at a given wavelength, and thus imposes a maximum upper limit to the amount of data available.

Amongst others, photomultiplier tubes (PMT) and single-photon avalanche diodes (SPAD) meet the requirements to perform this work [203].

In the case of PMTs, the detection of single photons is carried out in a vacuum tube where a photon incident on a photocathode releases an electron. This electron starts a cascade process in a series of dynodes that will increase the number of electrons (and thus the current) in a subnanosecond or nanosecond scale to be later detected. They usually operate [204] in the visible region of the spectrum, having a greater sensitivity in the green-blue region. The drawback of this detection scheme is the low quantum efficiency ($\eta < 25\%$), which is vastly reduced in the infrared part of the spectrum. PMTs are thus not suitable for our work.

In our experiment, we use a PerkinElmer SPCM-AQRH-14 SPAD. These are p-n junctions that operate biased above the breakdown voltage (Geiger mode) [205]. Under these circumstances, the electric field in the junction is high enough for a single photon to trigger a self-sustaining current avalanche by introducing a charge carrier in the depletion layer. SPADs require a

(pasive or active) quenching circuit able to:

- Sense the leading edge of the avalanche (ns or sub-ns time).
- Generate a standard, well synchronised output pulse (on the order of mA).
- Quench the avalanche by rapidly lowering the bias voltage. Otherwise, the diode would destroy itself.
- Restore the voltage to the operating level.

Sometimes, the circuits that control the current flowing through the detectors are not able to reduce it to an operative level before the bias voltage is restored, some carriers may be trapped in the junction. These trapped carriers may trigger another avalanche of electrons when restoring the voltage, thus giving rise to a phenomenon called *afterpulsing*.

The quoted photodetection efficiency is about $\eta \approx 65\%$ at 780nm, and the specifications quote a probability of afterpulsing of $p = 0.5\%$.

Finally, if one needs to turn on/off the SPADs at arbitrary frequencies, it is recommended to use an RF-switch at the output. The output of our SPADs is gated[1], but gating with a period of 1.2 s (near our experimental repetition rate) was problematic[2]. The solution to this problem is to use an RF-switch *after* the SPADs to regulate the output of the electronic pulses.

8.2.2 Data taking

To characterize the detectors, we used scheme shown in Figure 8.2. Light from a 780 nm NewFocus TLM7000 tunable diode laser is chopped in short pulses using a double-pass AOM layout [206]. The AOM RF input signal is

[1] Tests showed that the gating seemed to be affecting the quenching circuit, rather than the voltage bias. This lead to (undetected) afterpulsing effects accompanied by emission of photons. This *feature* is not shown in the specifications sheet.

[2] Neither was this other *feature*.

controlled by an RF switch that allows pulsing the laser using TTL signals. We can operate it in a continuous or pulsed regime, using the signal from a frequency generator or a custom-made LabView script. The rise and fall times of the AOM pulses are less than 50 ns, giving us a reasonably good pulse shape for testing purposes. The laser passes through a series of filters and pairs of half-wave plates and polarising beamsplitters to reduce, in a controlled way, the intensity of the beam. The light is then split in a beamsplitter and sent to the two SPADs using multimode fibers.

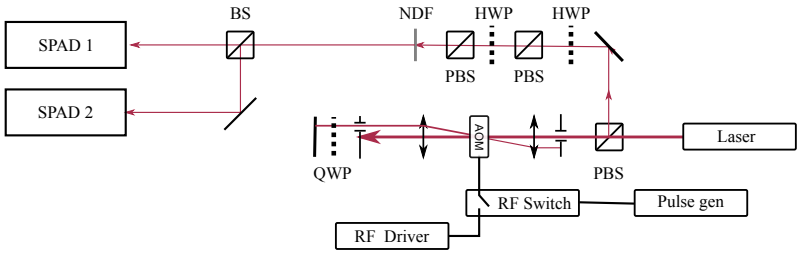

Figure 8.2: System to measure $g^{(2)}$ for a Poisson distribution. The output from a 780nm NewFocus TLM700 laser passes through a double-pass AOM to produce the pulses. The RF current driving the AOM is switched on/off using an RF switch controlled TTL signals either from a computer or a frequency generator (Pulse gen). To attenuate the beam, a series of half-wave plates (HWP) and polarising beamsplitters (PBS) are used, in combination with neutral density filters (NDF). The light is then detected using a Hanbury-Brown Twiss interferometer, as in Figure 8.1.

The counting of single photon requires a low background rate. Our detectors dark-count rates (measured with the light input covered by an opaque cap and averaged over 100s) are 42.6(7) Hz and 46.2(7) Hz respectively, where the errors have been given as the standard error after counting for 100 s. The attenuation and splitting stage of the layout is encased within an opaque box to minimize the amount of background light reaching the detectors. The small amount of leakage led to background counts below 500 Hz, compared to typical count rates of $0.1 - 5$ MHz.

8.2.3 Dead time and afterpulsing in the SPADs

To understand the effect of the dead time and afterpulsing in photodetected counts, we compare a set of photodetected counts in one of the SPADs with different theoretical probability distributions. The data was taken using a Tektronix DPO4034 oscilloscope connected to the SPADs. We obtain $\sim 10^4$ traces of $1\,\mu$s and analyse their contents later.

We can obtain information about the photodetectors by analysing the distribution of counts obtained. Each shot shows k number of counts, and the frequency of these events gives a probability mass function $P(X = k)$. As we will see in the following, this distribution can give us information about the dead time of the detectors, as well as the afterpulsing probability. With the information contained in each of the shots, it is also possible to construct a second order autcorrelation function $G^{(2)}(\tau)$, which provides a further source of information about the characteristics of the photodetectors.

The benefit of using an oscilloscope instead of the timing module is that we can take traces of photodetections without suffering from the dead time of the time-tagging. The obvious drawback is the expensive memory requirements to output each trace, and the slow acquisition, which makes this particular method not suitable generally.

We calibrate the resolution of the oscilloscope using a stable pulse generator. Using a sample rate of 2.5 GS/s we would ideally obtain a resolution of 400 ps, which in reality goes up to 700 ps due to the 8-bit precision of the signal analog-to-digital converter in the oscilloscope.

Poisson approximation Once the oscilloscope is calibrated, we sample the photodetection distribution X, counting the number of times we obtain k counts in the acquisition time of $S = 1\,\mu$s. The idealized process should

follow a Poisson distribution with probability mass function (pmf)

$$f(k;\theta) = \frac{\theta^k}{k!}e^{-\theta}, \tag{8.1}$$

where $\theta = \xi S$ is the observed mean photon number due to the flux ξ of photons during the acquisition time assuming a Poisson distribution.

Assuming that the errors are the square root of the number of counts, in Figure 8.3 we can see that neither the Poisson distribution with the observed mean flux, nor the one with fitted values actually model the process. This is mainly due to the effect of dead time present in the detectors, as will be shown next.

Dead time Our detectors are *non-paralyzable*: that is, during the dead time τ of an event, the presence of another count does not restart the dead time. It is possible to infer the dead time of the detectors as the minimum time observed between counts.

Theoretically, it is possible to derive a pmf [207, 208] based on the Poisson distribution. A notable simplification can be found [209, 210], where it is shown that the distribution of detected events for a non-paralyzable detector is a generalized Poisson distribution (GPD) of the form

$$g(k;\theta',\lambda) = \begin{cases} \frac{\theta'(\theta'+k\lambda)^{k-1}e^{-\theta'-k\lambda}}{k!} & k \leq n, \\ 0 & k > n \end{cases} \tag{8.2}$$

where the inequality $\max\{-1, \theta/n\} \leq \lambda < 1$ prescribes the truncation in n [209]. The factor $\lambda < 0$ for a non-paralyzable detector is

$$\lambda = -\tau\theta', \tag{8.3}$$

which accounts for the dead time τ of the detector. Then, the truncation

occurs in (8.2) occurs at $n = 1/\tau$. Since the dead time reduces the number of counts observed (that would appear otherwise during the dead time of the detectors), the observed mean $E[k] = \frac{\theta'}{1+\lambda}$ is smaller than the *true mean* θ'.

Afterpulsing If the avalanche caused by a photodetection is not quenched before the voltage is restored in the SPAD, another avalanche might start, giving a *fake* count, or afterpulse. This process can be thought of as a binomial selection of the underlying probability mass function $P'(X = k)$ happening with probability $p \ll 1$ [210], thus the final probability distribution is a mixture of the two distributions:

$$\begin{aligned} P_1(Y = y) &= \sum_{k=y}^{\infty} P(Y = y|X = k)P'(X = k), \\ &= \sum_{k=y} \binom{k}{y} p^y (1-p)^{k-y} P'(X = k), \qquad (8.4) \\ P_2(Y = y) &= \sum_{k=y}^{\infty} \binom{k}{y} p^{k-y} (1-p)^k P'(X = k). \qquad (8.5) \end{aligned}$$

The *selected* part P_1 shows the cases where afterpulsing happens, with probability p: in these cases, the number of counts must be doubled in the final distribution. The unselected part P_2 happens with probability $(1-p)$. If the underlying distribution is a Poisson distribution with parameter θ, both P_1 and P_2 are Poisson distributions with parameters $p\theta$ and $(1-p)\theta$ respectively.

8.2.4 Results

The dead time of the detectors can be directly obtained from the autocorrelation function $G^{(2)}$ of the photodetected counts (see Figure 8.4). Since the base process for the photodetected counts is a Poisson distribution, the probability of detecting a photon at any given time is not time dependent. Therefore, the dead time of the detectors, $\tau = 28.1\,\text{ns}$, corresponds to the minimum time difference (greater than zero) between any two counts, which

shows as the minimum time difference $\min\{\tau | G^{(2)}(\tau) > 0, \tau > 0\}$. We can

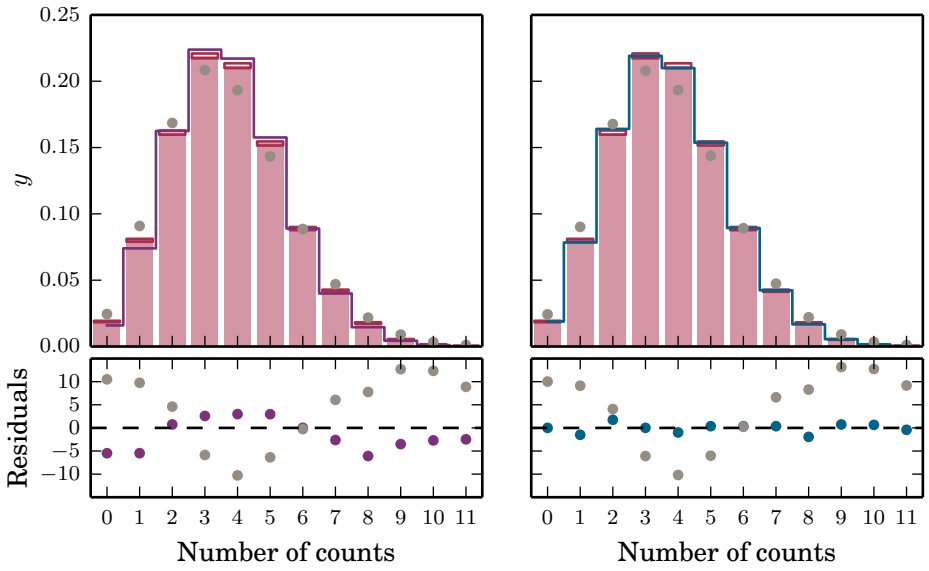

Figure 8.3: Comparison between experimental probability mass function (red bars) and theory. In the left graph, experimental data are compared with a Poisson process (circles) and a GPD (steps, purple) with their parameters given by extracted parameters. On the right, these two distributions have fitted parameters.

obtain information about both the dead time and the afterpulsing probability by analyzing the (normalized) frequencies for the number of counts, $P(X = k)$, as seen in Figure 8.3 in red. The errorbars correspond to the square root of the number of shots showing that number of counts.

First, we compare the data with Poissonian and GPD models. To make this comparison, we use a χ^2 test [211] . When comparing the data (x_i, y_i) with a model $y(x_i)$, the line of best fit minimizes the *goodness-of-fit* parameter

$$\chi^2 = \sum_i \left(\frac{y_i - y(x_i)}{\alpha_i} \right)^2, \tag{8.6}$$

where we have assumed that each data point has been drawn from a Gaussian with a width given by the standard error α_i. If there are N independent datapoints and we use a function with $\mathcal{N}$ parameters, the number of degrees of freedom is ν. The *reduced chi-squared statistic*, $\chi^2_\nu = \chi^2_{\min}/\nu$, gives a quick

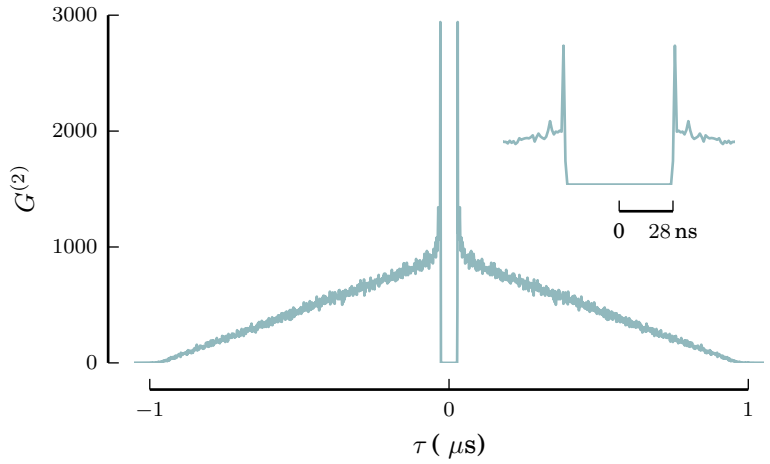

Figure 8.4: Autocorrelation function, $G^{(2)}(\tau)$ of photodetected counts in a single SPAD, histogrammed in 1 ns bins. It shows the effect of dead time – region without counts near zero time difference – and the non-stationary nature of the pulses – triangular envelope of the function.

Model	Data Mean	θ'	$\lambda/10^{-2}$	$p/10^{-4}$	χ^2_ν
Poisson (exp)	3.71				55.59
GPD (exp)		4.14	−12		14.42
Poisson	3.722 ± 0.008				60.39
GPD	3.70 ± 0.02	4.01 ± 0.01	-8.3 ± 0.4		1.41
Full model	3.72 ± 0.01	4.02 ± 0.01	-8.2 ± 0.4	8 ± 7	1.22

Table 8.1: Table with parameter values for different models. The final column corresponds to the goodness-of-fit parameter χ^2_ν. The upper Poisson and GPD values for parameters and reduced χ^2 correspond to those extracted from the data. The bottom ones have been fitted using a least-squares algorithm.

indication as to whether the null hypotheses should be rejected: $\chi^2_\nu \approx 1$, if the number of degrees of freedom is similar to the number of data points[3]. If the value of $\chi^2_\nu \gg 1$, it is likely that the null hypothesis should be rejected. Performing this test on the Poissonian and GPD models using the experimental data values for the mean ($E[x] = 3.71$) and the dead time of the detectors ($\tau = 28.1$ ns) shows that they do not fit the data (see Table 8.1). Following this simple analysis, we fitted the data with a Poisson model,

[3] This can be understood if we consider that, for a good fit, each point will differ from its expected value by typically the standard error. Therefore, each member in the summation of (8.6) should be of order one, and $\chi^2_{\min} \approx N$.

a GPD (which includes dead time) and a full model including afterpulsing. The maximum number of counts observed in the data was $k_{max} = 13$, but it was necessary to re-bin $k = 11, 12, 13$ because none of the last two bins had more than 5 counts. The errorbars in the Poisson and GPD models have been obtained from the $\Delta\chi^2 = 1$ surface [211], whereas the errors in the full model were extracted from the covariance matrix, for simplicity.

The results show that the GDP and the full model score much better in the χ^2 test. The dead time can be directly extracted in the GPD model from the fitted values of λ and θ using (8.3), and this gives $\tau' = 20 \pm 1\,\text{ns}$. We could do the same analysis in the full model, with similar results, since the probability of afterpulsing $p' = (8 \pm 7) \cdot 10^{-4} \ll 1$.

The theoretically extracted dead time τ' is smaller than the one extracted from the autocorrelation data, τ, seen in Figure 8.4. The reason behind this is still unknown, but it shows that one cannot trust the model completely to obtain the dead time and, probably, the afterpulsing probability. However, both of the theoretically extracted values seem to have the right order of magnitude, and can be used as an approximation.

8.3 Coincidence detection hardware and software

Once we have pulses out of the detector indicating the arrival of the photons, these are sent to a high resolution timing module model HRMTime from SensL [212]. This module takes as inputs the pulses from the two SPADs and converts the time of arrival of these to a digital format using a time-to-digital converter. It has a *maximum time resolution* between Start/Stop signals of 27 ps and a *saturated count-rate* of 4.5 MHz.

Despite the histogramming capabilities of the timer module, it is often useful to have the raw data and analyse it afterwards. Therefore, we used the FIFO ("first-in, first-out") modes of the module, where each count is recorded into a different position in the memory and then sent to the computer sequentially. These modes are Time-Correlated Single Photon Counting (TCSPC) or Time-Tagged Time-Resolved (TTTR), and we shall explain them next.

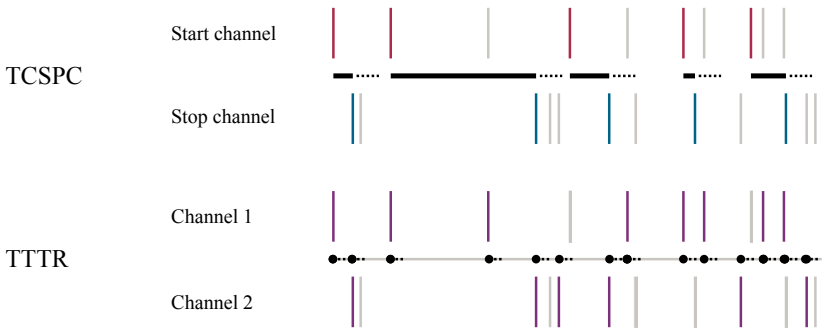

Figure 8.5: Diagrammatic comparison between the two FIFO modes of the coincidence detector hardware: time-correlated single photon counting (TCSPC) and time-tagged time-resolved (TTTR). The first obtains time differences between start (red) and stop (blue) channels; the second, obtains the time-tags of the events (purple) in each of the channels. After registering a time difference or a tag, the dead-time of the counting module prevents other detections from being immediately recorded.

8.3.1 TCSPC (with macro time)

In this mode, the module sets a *start* signal upon the arrival of a photodetection event in one of its channels. Afterwards, when a second photon arrives, a *stop* signal is generated. The timer then calculates the time between the Start and Stop signals and adds a count in memory with the *micro* time. This register has, in addition, a *macro* time with a maximun time resolution of 5 ns, that supplies information about the "absolute" timing of the *micro* time within the experiment.

These start-stop time differences can be directly histogrammed to obtain a

coincidence histogram $C(\tau)$, which holds information similar to $G^{(2)}$.

Nonetheless, this mode has several drawbacks. The first and most important effect is called *pile-up*, which leads to an over-representation of early photons in the histogram. When the time diferences obtained are binned, we obtain m bins. Each of the bins contains n_i counts, whereas the true number should be ns_i: n is the number of repetitions of the experiment, and s_i is the probability, per experiment, of a photon arriving in bin i. The measured (i.e. biased by pile-up) value of s_i is p_i; that is, the probability per experiment of obtaining, at least, one photon in bin i (and none in earlier channels). It can be shown [213] that these probabilities are

$$p_i = \frac{n_i}{n - \sum_{j=1}^{i-1}(1 - p_j)}. \tag{8.7}$$

If the count rate is greater than a few percent of the detector's maximum, the probability of detecting early photons is higher than the detection of later photons. Assuming that s_i is constant in each bin (for example, by making the bins very short), it is the mean of a Poisson distribution, and thus the *real* s_i have the form

$$s_i = -\ln(1 - p_i). \tag{8.8}$$

This simple picture only applies when the mean photon number of the pulses is constant. Some other approaches have been described elsewhere, using an iterative correction method [214] (which allows to combine shots at different powers) or Laplace transforms of the data [215].

Note that the assumption of Markovianity that leads to (8.8) might not be valid if the coherence time is larger than the bin width [216]. Pile-up can be corrected for short τ, but for τ longer than the average separation between counts no information is obtained.

Figure 8.6 shows an example of pile-up in TCSPC data. In this case, the data are a set of 1 μs-long square pulses separated by 5 μs. The triangular shapes correspond to the convolution of the square pulses. Wrap-up of the timing data over the maximum *micro* timer shows as a set of smaller, secondary peaks. In this particular dataset, we modulated the current of the laser using random noise, which appears as a higher peak at $g^{(2)}(0)$ [217].

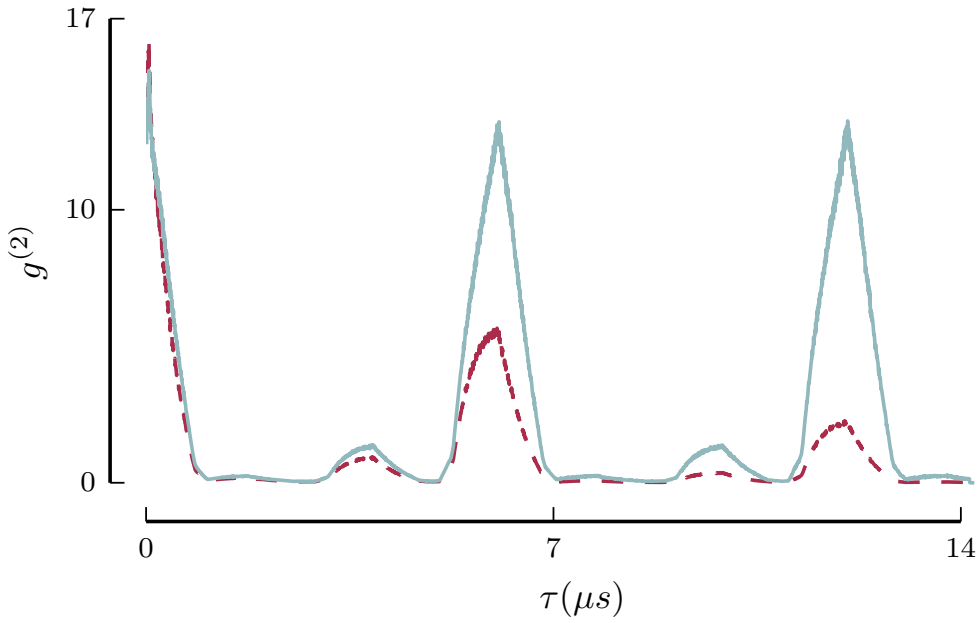

Figure 8.6: Plot showing $g^{(2)}$ data collected using TCSPC. Uncorrected data are shown in red (dashed) and corrected for pile-up is shown in blue (continuous).

A final drawback is the *dead time* of 190 ns after each stop pulse, much longer than the SPAD's, in which the timer has to process the event.

8.3.2 TTTR

In contrast with the previous case, the timing module only sets one *start* signal at the beginning of the experimental run and adds a tag for each consecutive *stop* signal. The time differences can thus be obtained by subtracting the tags' timings.

As the dead time of the timer after each stop pulse (5 ns) is the only one preventing data acquisition, the number of counts that we can get in this mode is much higher. The timer module has a buffer allowing it to process bursts in excess 100 MHz.

A special mode using the TTTR scheme is the *resync* mode, where a 250 kHz clock output provides start inputs, thus eliminating long term drift between the channels.

The timer can be controlled using two backends: SensL proprietary software or a custom-made LabView script. From a home-made LabView script we also control SPAD gating, which gives us the opportunity to define sequences of measurements.

The *memory* of our timer module *only* allows for $5 \cdot 10^5$ counts before these are read out, thus we must take into account the acquisition time not to saturate the memory. Using the LabView script, we can program sequences where this time is low (not to saturate the timer) but repeated many times, so that we get the desired amount of data; however, this poses constraints in the analysis of the data, as the normalisation factors should be taken individually on each acquisition through the entire sequence.

Nevertheless, the time-tag information allows us to directly compute $G^{(2)}$ from the time differences of the tags. This has allowed an easier (and better) interpretation of our results, and facilitated obtaining the $g^{(2)}$ variation *within* each light pulse in [86, 176].

8.4 Summary

In this Chapter we have described the setup and calibrations of a system to obtain the $g^{(2)}$ in recent experiments performed in our group [1, 86, 176]. We have reviewed the characteristics of single-photon detectors, and we focused our attention on SPADs. We have shown tests performed on these detectors

to calibrate them, and compared them with theoretically derived values.

Finally, we have described our coincidence detection system, based on the HRMTime module from SenSL. It was shown that TCSPC shows a number of problems which, even if solvable, prompt us to use TTTR counting techniques. The flexibility, along with the larger dataset obtained as a consequence of using this technique has enabled the group to obtain the results in [1] and [86]. This has lead to the theoretical insight necessary for the proposal of the phase-gate scheme (see Chapter 6).

Chapter 9

Conclusions and outlook

In this thesis we have shown how is it possible to devise schemes for universal photonic quantum gates using simple building blocks, namely EIT involving Rydberg states, microwave transitions in the Rydberg manifold and strong dipole-dipole interactions.

After deriving the relevant atom-atom (chapter 3) and atom-light (chapter 2) interactions, we could explain the storage and retrieval of multiple stored rydberg polaritons subject to resonant microwave fields in chapter 5. In chapter 6 we showed how to implement a controlled-phase gate (CZ gate), a two-qubit, universal quantum gate with photonic qubits; furthermore, in chapter 7 we sketched constructions to implement multi-qubit gates, such as the controlled-controlled phase gate.

Quantum information processing based on these schemes requires the ability to store different states of each photonic qubit in different regions of a cold atomic cloud (dual-rail encoding) as dark-state polaritons involving Rydberg states, and by the geometrical properties of the dipole blockade phenomenon. By carefully arranging the position of the different qubits, a conditional π-phase shift can be applied to a particular subset of states, therefore implementing a universal phase gate. The simplest of these gates can be readily implemented using realistic experimental parameters, with fidelities

exceeding 95% (not taking into account storage/retrieval efficiencies).

The two main sources of infidelity are the storage/retrieval efficiencies of the polaritons in/from the cloud, and the finite lifetime of the Rydberg levels. The second of these aspects is less important when using higher principal quantum number states due to the favourable scaling of the radiative lifetimes, τ, with n: $\tau \propto n^3$. A complete model for the storage and retrieval of dark-state polaritons in Rydberg levels in the case of multiple polaritons stored in regions that are larger than the blockade radius is still lacking. However, descriptions of the process of EIT involving Rydberg polaritons suggest that a high optical depth is required to increase the storage efficiency [82]. Therefore, increasing the optical depth should be at the focus of the new experiments implementing these schemes.

9.1 Future experimental setup

Ideally, the implementation of the CZ gate will take place on a chip that miniaturises all of the optics required and helps to concatenate several of these gates [189]. Additionally, integrated waveguide technologies would help to implement single-photon operations in a compact format [190, 191]. However, Rydberg states show very strong atom-surface interactions (see [54, 55, 218] and references therein) that can affect the gate functioning, thus more research in this direction is required to develop a way to make these interactions negligible or controllable even when the atoms are in the proximity of the chips.

However, even if we do not consider miniaturization, there are many experimental challenges that the new generation of the experiment aims to solve. These have been mentioned in the outlook of [176], and a new experimental setup has being built by Hannes Busche and Simon Ball to try and mitigate the weaknesses of the previous generation. The main areas in which the new

experiment aims to surpass the old one are: the optical depth of the ensemble in the dipole trap, the repetition rate of the experiment, and the control of the microwave fields.

As it was mentioned in chapter 2, the optical depth of the cloud is one of the limiting factors in the storage of light as dark-state polaritons. By implementing a 2D MOT atomic beam source [219–221] we aim to reduce the loading times, as well as to increase the number of the atoms in the MOT, and ultimately in the dipole trap, allowing for an increased optical depth in the ensemble and a higher repetition rate of the experiment (see Figure 9.1).

Furthermore, the previous experiments were performed with the microwave antenna located outside of the experimental vacuum chamber. This gave rise to interference due to multiple reflections inside of the chamber, which limited our abiliity to precisely control the power and polarization of the microwave field. To allow increased control, the new system will have microwave antennae inside the chamber. Multiple antennae are required to precisely control the polarization, especially in the presence of reflections inside the chamber. We could use the strong polarizabilities of Rydberg atoms to act as *probes* for the microwave field to gain more control over the system [62].

9.2 Single-photon capabilities

Using single-photon states as inputs to the experiments described would enormously decrease the complexity of the results, as one does not need to apply the largely-unknown theory of many-polariton storage and retrieval dynamics. Even if it is possible to use weak coherent states in the phase gate scheme proposed, due to the small size of the atomic ensembles required, this gives rise to errors that are detrimental to the scalability of the system (see Appendix A).

Therefore, one useful addition in the experimental setup would be a source

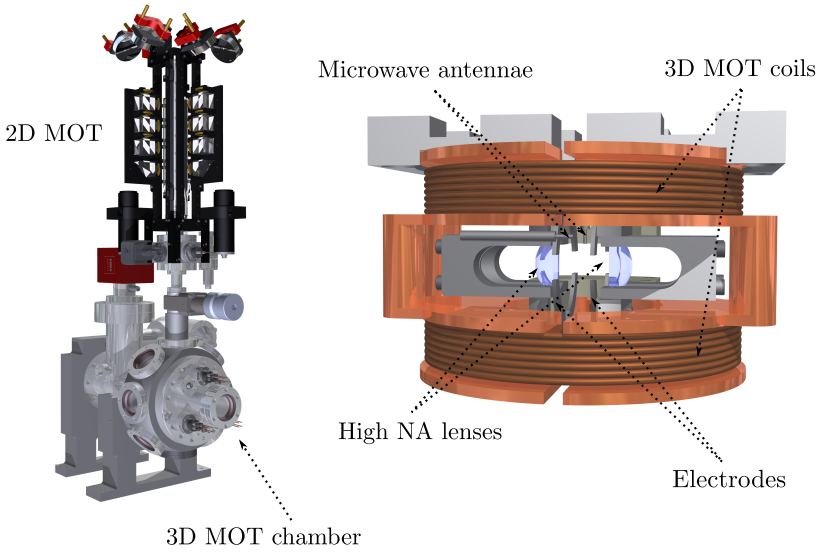

Figure 9.1: (Left) The new experiment uses a 2D MOT as a source of cold atoms, which are then further cooled and trapped in the 3D MOT chamber. (Right) Inside the main chamber we can find a block holding the MOT coils and the high numerical aperture (NA) lenses. The electrodes surrounding the lenses allow for the cancellation of stray electric fields, and the microwave antennae precisely control the polarization of the microwaves *(image rendered by Hannes Busche)*.

of single photons states compatible with our atomic species. Rydberg atoms could be used as a source of single-photons [1, 79, 80], although the experimental resources necessary make them unappealing. Standard single-photon sources based on quantum dots have bandwidths of the order of $\sim 1\,\mathrm{GHz}$ [222], but usually the wavelengths are not necessarily resonant with atomic transitions.

Cavity-enhanced downconversion might be exploited to obtain a heralded source of narrowband single photons resonant with an atomic transition [223], by using an interaction-free measurement scheme [224, 225] in a narrowband atomic filter [226]. The linewidth of the photons correspond, in this case, to the downconversion cavity linewidth, which can be made $\sim 7\,\mathrm{MHz}$ [227]. This method is more technically involved, but better suited to the task at hand.

A middle ground, in terms of the overheads required, could be achieved by combining the twin beam output of four-wave mixing in an atomic vapour with a narrowband cavity in the heralding beam. By filtering the idler output the spectral linewidth of the heralded photons is reduced, and bandwidths of 39 MHz, with a spectral brightness of 7700 photons per MHz per second have been shown [228].

9.3 Rydberg atoms and *fuzzy logic*

Most of the applications of the extraordinary properties of Rydberg atoms in QIP deal with the speed up promised by quantum computation in certain tasks, such as factorising large numbers. Certainly, classical computation is commonplace, and solving hard problems in this field is an important task. However, it is not the only model of computation, and in the past decades a number of speculative models that show different kinds of the underlying logic behind computations have been proposed.

One of such schemes is based on "*fuzzy logic*" [229, 230]. Such a logic aims to formalise *approximate reasoning* used in everyday life, and is related to multivalued logic, where intermediate truth values between 0 and 1 are allowed. It is possible to define a model of computation, the *fuzzy Turing algorithms* (similar to probabilistic Turing machines), that promises a performance beyond classical Turing machines [231]. Fuzzy systems and fuzzy control are widespread in industry, especially in those areas of *intelligent* controllers and imprecise language parsing [232, 233].

The spatial properties of the dipole-dipole interactions in Rydberg atoms (especially, the blockade phenomenon) shows some similarities to fuzzy sets: when trying to excite atoms to Rydberg states, the long-range nature of the dipole-dipole interactions can create regions where the double-excitation probability is close to one, close to zero, or values in between; these regions

can be tuned within some limits by changing the coupling Rabi frequency. These different regions can be regarded as the different *degrees of membership*, one of the fundamental characteristics of fuzzy sets [229].

The question of whether Rydberg atoms might be a suitable system to efficiently implement fuzzy logic is open. Of course, this is just a hypothesis, and further research is required in this area, with the first questions that need answering being that of the suitable encoding of fuzzy sets and the determination of a suitable set of operations that would allow the implementation of fuzzy logic.

Appendix A

Coherent state input to the CZ phase gate

The phase gate scheme in chapter 6 uses single-photons in two photonic modes (dual-rail encoding) as inputs. In the absence of single photons (which are not available in our laboratory), one can test the proof-of-principle capabilities of the gate using a weak coherent states with multiphoton components. In this appendix we estimate the effect of a multiphoton input to the CZ gate described in chapter 6, although similar arguments can be made for the multiqubit gates in chapter 7.

A.1 Basics

A photon creation operator in a certain mode is written as $a^\dagger$. A Fock state is then

$$|n\rangle = \frac{(a^\dagger)^n}{\sqrt{n!}}|0\rangle, \tag{A.1}$$

where the creation operators act on the vacuum state $|0\rangle$.

A coherent state, eigenstate of the annihilation operator a is represented as

$$|\alpha\rangle = e^{-\frac{|\alpha|^2}{2}} \sum_n \frac{\alpha^n}{\sqrt{n!}} (a^\dagger)^n |0\rangle. \tag{A.2}$$

The photonic qubit is defined using two basis states, with creation operators $a^\dagger$ and $b^\dagger$. If the other basis state is included, the state of a single photon with an arbitrary photonic state, described by the angle θ, is written as

$$|1;\theta\rangle = (a^\dagger \cos\theta + b^\dagger \sin\theta)|0\rangle. \tag{A.3}$$

We can describe a "qubit" state with a coherent input by substituting each of the creation operators in (A.2) with (A.3). Operating

$$|\alpha;\theta\rangle = e^{-\frac{|\alpha|^2}{2}} \sum_{n=0}^{\infty} \frac{\alpha^n}{\sqrt{n!}} (a^\dagger \cos\theta + b^\dagger \sin\theta)^n |0\rangle, \tag{A.4}$$

$$= e^{-\frac{|\alpha|^2}{2}} \sum_{n=0}^{\infty} \frac{\alpha^n}{\sqrt{n!}} \sum_{m=0}^{n} \sqrt{\binom{n}{m}} (a^\dagger \cos\theta)^m (b^\dagger \sin\theta)^{n-m} |0\rangle = 0. \tag{A.5}$$

This input state can lead to the presence of multiple photons per site ($m, n-m > 1$) as well as multiple photons per qubit ($n > 1$), which would cause errors in the performance of the phase gate. In the following two sections we take into account each of the contributions separately.

A.2 Multiple excitations per site

Each of the photonic qubits we have defined in Chapter 6 consists of a single photon that travels in a superposition of two paths. Therefore, each of the paths is only populated by, at most, one photon, which is to be stored in the cloud in the form of a polariton.

If the photonic qubit were defined by a weak coherent state ($|\alpha| \ll 1$) we can

use the dipole blockade effect to limit the number of photons to one per path as long as the waist of the beam is small compared to the blockade radius $w \ll R_{\mathrm{b}}^{(6)}(rr)$. This effect truncates (to second order in α) the state of a single qubit in equation (A.5) to the subspace where $m, n-m \leq 1$

$$|\alpha;\theta\rangle_{\mathrm{trun}} = e^{-\frac{|\alpha|^2}{2}} \left(1 + \alpha\left(a^\dagger \cos\theta + b^\dagger \sin\theta\right) + \alpha^2 a^\dagger b^\dagger \cos\theta \sin\theta\right)|0\rangle. \quad \text{(A.6)}$$

If the qubit travels only by one of the paths (i.e. when $\theta = 0$ or $\pi/2$), the probability to obtain a single photon at the output is

$$P_{\mathrm{single}} = e^{-|\alpha|^2}\alpha^2 \ . \quad \text{(A.7)}$$

This result should be corrected for storage and retrieval efficiency, as well as quantum efficiency of the detectors to obtain the probability of detection of a single photon per qubit.

A.3 Multiple excitations per qubit

The α^2 term in A.6 takes into account the events where a single qubit can store two photons, one in each path, with probability $P_{\mathrm{multiple}} = e^{-|\alpha|^2}\alpha^4$. This gives an signal to noise ratio that scales as $\mathrm{SNR} = \alpha^{-2}$ per qubit, which decreases linearly with increasing power, being 1 at $\langle n\rangle = 1$.

Appendix B

Two-level system physics

B.1 Sign change through a 2π-rotation.

One of the key results in this thesis lies in the acquisition of a minus sign (π phase shift) in the ground state probability amplitude in a two-level system undergoing a 2π-rotation. This section aims to show the origin of this sign change.

Let us begin with the Hamiltonian (2.13) which describes (in the rotating-wave approximation) the action of the semiclassical probe field with Rabi frequency Ω_p and detuning Δ_1 on the two-level system with basis states $|a\rangle$ and $|b\rangle$:

$$H_{\mathrm{2LS}} = \frac{\hbar}{2}\begin{pmatrix} 0 & \Omega_p \\ \Omega_p & -2\Delta_1 \end{pmatrix} .$$

The state of a two-level system is described as a state vector $|\psi(t)\rangle = c_a(t)|a\rangle + c_b(t)|b\rangle$ where the probability amplitudes for states $|a\rangle$ and $|b\rangle$ at time t are the complex quantities $c_a(t)$ and $c_b(t)$ respectively. In the absence of dissipation, the evolution of the system under the action of the

Hamiltonian $H_{2\mathrm{LS}}$ is given, in the Schrödinger picture, by

$$\frac{\mathrm{i}}{\hbar}\frac{d}{dt}|\psi\rangle = H_{2\mathrm{LS}}|\psi\rangle \ . \tag{B.1}$$

The following equations express the evolution of the probability amplitudes as given by (B.1):

$$\mathrm{i}\hbar\,\dot{c_a} = \frac{\hbar}{2}\,\Omega_p c_b \ , \tag{B.2}$$

$$\mathrm{i}\hbar\,\dot{c_b} = \frac{\hbar}{2}\left(\Omega_p c_a - 2\Delta_1 c_b\right) \ . \tag{B.3}$$

We are interested in the ground-state probability amplitude, but it is easier to first obtain the excited-state one and then substituting in (B.2). Differentiating the second equation and pluging in the first one yields the equation of the evolution of the excited state probability amplitude:

$$\ddot{c_b} - \mathrm{i}\Delta_1\dot{c_b} + \frac{\Omega_p^2}{4}c_b = 0 \ . \tag{B.4}$$

In the resonant case ($\Delta_1 \sim 0$), the solutions of (B.4) are of the form

$$c_b(t) = Ae^{\mathrm{i}\Omega_p t/2} + Be^{-\mathrm{i}\Omega_p t/2} \ , \tag{B.5}$$

where A and B are constants dependent upon the initial conditions. Now that we have $c_b(t)$ we need to substitute this solution in equation (B.3) to obtain the equation for c_a,

$$c_a(t) = -\frac{\mathrm{i}\Omega_p}{2}\int_0^t \left(Ae^{\mathrm{i}\Omega_p s/2} + Be^{-\mathrm{i}\Omega_p s/2}\right)\mathrm{d}s = -Ae^{\mathrm{i}\Omega_p t/2} + Be^{-\mathrm{i}\Omega_p t/2} \ . \tag{B.6}$$

From this last expression, together with (B.5), we can derive the relationship between the values of the probability amplitudes, c_a and c_b, at two different times $t = 0$ and $t_{2\pi} = 2\pi/\Omega_p$, the time to perform a 2π-rotation: $c_a(0) = -c_a(t_{2\pi})$ and $c_b(0) = -c_b(t_{2\pi})$, which implies $|\psi(0)\rangle = -|\psi(t_{2\pi})\rangle$.

B.2 Explicit form of the optical Bloch equations

In this section, the explicit forms for the equations (2.5) for a two-level system are shown for reference. We shall use the Hamiltonian in (2.13) for the unitary evolution of the system. The Lindblad operator in (2.6) accounts for the dissipation in the system via the lowering operator $\sigma_{ab} = \sqrt{\Gamma_b}|a\rangle\langle b|$, and we introduce $\gamma_b = \Gamma_b/2 + \gamma_p$ to account for the finite linewidth γ_p of the probe laser [116]. The equations are:

$$\dot{\rho}_{aa} = -\dot{\rho}_{bb} = \mathrm{i}\frac{\Omega_p}{2}\left(\rho_{ab} - \rho_{ba}\right) + \Gamma_b\rho_{bb}, \tag{B.7}$$

$$\dot{\rho}_{ab} = \dot{\rho}^{\dagger}_{ba} = \mathrm{i}\frac{\Omega_p}{2}\left(\rho_{aa} - \rho_{bb}\right) - \mathrm{i}\Delta_1\rho_{ab} - \gamma_b\rho_{ab}. \tag{B.8}$$

Bibliography

[1] D. Maxwell *et al.*, *Storage and control of optical photons using rydberg polaritons*, Phys. Rev. Lett. **110**, 103001 (Mar 2013), http://link.aps.org/doi/10.1103/PhysRevLett.110.103001

[2] Luigi F Menabrea and AA Lovelace, *Sketch of the analytical engine invented by charles babbage, esq., by lf menabrea, of turin, officer of the military engineers*, Translated and with notes by AA L. Taylor's Scientific Memoirs **3**, 666–731 (1843)

[3] A. M. Turing, *On computable numbers, with an application to the entscheidungsproblem*, Proceedings of the London Mathematical Society **s2-42**, 230–265 (Jan. 1937), ISSN 0024-6115, 1460-244X, http://plms.oxfordjournals.org/content/s2-42/1/230.full.pdf+html?frame=sidebar

[4] C. E. Shannon, *A mathematical theory of communication*, Bell System Technical Journal **27**, 379–423 (Jul. 1948), ISSN 00058580, http://ieeexplore.ieee.org/lpdocs/epic03/wrapper.htm?arnumber=6773024

[5] John O'Connor and Edmund F. Robertson, *MacTutor history of mathematics*, http://www-history.mcs.st-andrews.ac.uk/index.html

[6] Matthias Troyer and Uwe-Jens Wiese, *Computational complexity and fundamental limitations to fermionic quantum monte carlo simulations*,

Physical Review Letters **94**, 170201 (May 2005), http://link.aps.org/doi/10.1103/PhysRevLett.94.170201

[7] Richard P. Feynman, *Simulating physics with computers*, International Journal of Theoretical Physics **21**, 467–488 (Jun. 1982), ISSN 0020-7748, 1572-9575, http://link.springer.com/article/10.1007/BF02650179

[8] Carl Pomerance, *A tale of two sieves*, Biscuits of Number Theory **85** (2008)

[9] D. Deutsch, *Quantum computational networks*, Proceedings of the Royal Society of London. A. Mathematical and Physical Sciences **425**, 73–90 (Sep. 1989), ISSN 1364-5021, 1471-2946, http://rspa.royalsocietypublishing.org/content/425/1868/73

[10] P.W. Shor, *Algorithms for quantum computation: discrete logarithms and factoring*, in *, 35th Annual Symposium on Foundations of Computer Science, 1994 Proceedings* (1994) pp. 124–134

[11] Lov K. Grover, *A fast quantum mechanical algorithm for database search*, in *Proceedings of the Twenty-eighth Annual ACM Symposium on Theory of Computing*, STOC '96 (ACM, New York, NY, USA, 1996) p. 212–219, ISBN 0-89791-785-5, http://doi.acm.org/10.1145/237814.237866

[12] Mike Karvis, *The internet of things will radically change your big data strategy*, http://www.forbes.com/sites/mikekavis/2014/06/26/the-internet-of-things-will-radically-change-your-big-data-strategy/

[13] *Quantum algorithm zoo*, http://math.nist.gov/quantum/zoo/

[14] M.A. Nielsen and I.L. Chuang, *Quantum Computation and Quantum Information*, Cambridge Series on Information and the Natural

Sciences (Cambridge University Press, 2000) ISBN 9780521635035, http://books.google.co.uk/books?id=65FqEKQOfP8C

[15] Scott Aaronson and Alex Arkhipov, *The computational complexity of linear optics*, in *Proceedings of the 43rd annual ACM symposium on Theory of computing*, STOC '11 (ACM, New York, NY, USA, 2011) pp. 333–342, ISBN 978-1-4503-0691-1, http://doi.acm.org/10.1145/1993636.1993682

[16] Daniel Loss and David P. DiVincenzo, *Quantum computation with quantum dots*, Physical Review A **57**, 120–126 (Jan. 1998), http://link.aps.org/doi/10.1103/PhysRevA.57.120

[17] David P. DiVincenzo, *The physical implementation of quantum computation*, Fortschritte der Physik **48**, 771–783 (Sep. 2000), ISSN 1521-3978, http://onlinelibrary.wiley.com/doi/10.1002/1521-3978(200009)48:9/11<771::AID-PROP771>3.0.CO;2-E/abstract

[18] Hoi-Kwong Lo and Sandu Popescu, *Classical communication cost of entanglement manipulation: Is entanglement an interconvertible resource?*, Physical Review Letters **83**, 1459–1462 (Aug. 1999), http://link.aps.org/doi/10.1103/PhysRevLett.83.1459

[19] Ryszard Horodecki, Paweł Horodecki, Michał Horodecki, and Karol Horodecki, *Quantum entanglement*, Reviews of Modern Physics **81**, 865–942 (Jun. 2009), http://link.aps.org/doi/10.1103/RevModPhys.81.865

[20] Borivoje Dakić *et al.*, *Quantum discord as resource for remote state preparation*, Nature Physics **8**, 666–670 (Sep. 2012), ISSN 1745-2473, http://www.nature.com/nphys/journal/v8/n9/full/nphys2377.html

[21] Davide Girolami *et al.*, *Quantum discord determines the interferometric power of quantum states*, arXiv:1309.1472 [cond-mat, physics:math-ph, physics:nucl-ex, physics:physics, physics:quant-ph](Sep. 2013), `http://arxiv.org/abs/1309.1472`

[22] Victor Veitch, Christopher Ferrie, David Gross, and Joseph Emerson, *Negative quasi-probability as a resource for quantum computation*, New Journal of Physics **14**, 113011 (Nov. 2012), ISSN 1367-2630, `http://iopscience.iop.org/1367-2630/14/11/113011`

[23] Arnab Das and Bikas K. Chakrabarti, *Colloquium: Quantum annealing and analog quantum computation*, Reviews of Modern Physics **80**, 1061–1081 (Sep. 2008), `http://link.aps.org/doi/10.1103/RevModPhys.80.1061`

[24] Chetan Nayak *et al.*, *Non-abelian anyons and topological quantum computation*, Reviews of Modern Physics **80**, 1083–1159 (Sep. 2008), `http://link.aps.org/doi/10.1103/RevModPhys.80.1083`

[25] Yakir Aharonov, David Z. Albert, and Lev Vaidman, *How the result of a measurement of a component of the spin of a spin-1/2 particle can turn out to be 100*, Physical Review Letters **60**, 1351–1354 (Apr. 1988), `http://link.aps.org/doi/10.1103/PhysRevLett.60.1351`

[26] Hoi-Kwong Lo, Tim Spiller, and Sandu Popescu, *Introduction to quantum computation and information* (World Scientific, Singapore; [River Edge], NJ, 1998) ISBN 981024410X 9789810244101 981023399X 9789810233990

[27] E. Knill, R. Laflamme, and G. J. Milburn, *A scheme for efficient quantum computation with linear optics*, Nature **409**, 46–52 (Jan. 2001)

[28] Pieter Kok *et al.*, *Linear optical quantum computing with photonic*

qubits, Reviews of Modern Physics **79**, 135–174 (Jan. 2007), http://link.aps.org/doi/10.1103/RevModPhys.79.135

[29] E. Knill, *Bounds on the probability of success of postselected nonlinear sign shifts implemented with linear optics*, Physical Review A **68**, 064303 (Dec. 2003), http://link.aps.org/doi/10.1103/PhysRevA.68.064303

[30] Robert W. Boyd, *Nonlinear Optics* (Academic Press, 2003) ISBN 9780080479750

[31] Isaac L. Chuang and Yoshihisa Yamamoto, *Simple quantum computer*, Physical Review A **52**, 3489–3496 (Nov. 1995), http://link.aps.org/doi/10.1103/PhysRevA.52.3489

[32] Tim C Ralph and Geoff J Pryde, *Optical quantum computation*, Progress in optics **54**, 209–269 (2010)

[33] Jeffrey H. Shapiro, *Single-photon kerr nonlinearities do not help quantum computation*, Phys. Rev. A **73**, 062305 (Jun 2006), http://link.aps.org/doi/10.1103/PhysRevA.73.062305

[34] Julio Gea-Banacloche, *Impossibility of large phase shifts via the giant kerr effect with single-photon wave packets*, Phys. Rev. A **81**, 043823 (Apr 2010), http://link.aps.org/doi/10.1103/PhysRevA.81.043823

[35] Richard Hughes *et al.*, *A Quantum Information Science and Technology Roadmap, Part 1.*, Tech. Rep. LA-UR-04-1778 (Advanced Research and Development Activity (ARDA), 2004) version 2.0

[36] H. J. Kimble, *The quantum internet*, Nature **453**, 1023–1030 (Jun. 2008), ISSN 0028-0836, http://www.nature.com/nature/journal/v453/n7198/full/nature07127.html

[37] E. Amaldi and E. Segré, *Effect of pressure on high terms of alkaline spectra*, Nature **133**, 141 (Jan. 1934), ISSN 0028-0836, http://adsabs.harvard.edu/abs/1934Natur.133..141A

[38] Enrico Fermi, *Sopra lo spostamento per pressione delle righe elevate delle serie spettrali*, Il Nuovo Cimento **11**, 157–166 (Mar. 1934), ISSN 0029-6341, 1827-6121, http://link.springer.com/article/10.1007/BF02959829

[39] I. Martinson and L.J. Curtis, *Janne rydberg – his life and work*, Nuclear Instruments and Methods in Physics Research Section B: Beam Interactions with Materials and Atoms **235**, 17 – 22 (2005), ISSN 0168-583X, http://www.sciencedirect.com/science/article/pii/S0168583X05003617

[40] Niels Bohr, *Rydberg's discovery of the spectral laws*, in *Proceedings of the Rydberg Centennial Conference on Atomic Spectroscopy*, Vol. 50 (1954) pp. 15–21

[41] Peter J. Mohr, Barry N. Taylor, and David B. Newell, *CODATA recommended values of the fundamental physical constants: 2010*, Reviews of Modern Physics **84**, 1527–1605 (Nov. 2012), http://link.aps.org/doi/10.1103/RevModPhys.84.1527

[42] T.F. Gallagher, *Rydberg Atoms*, Cambridge Monographs on Atomic, Molecular and Chemical Physics (Cambridge University Press, 2005) ISBN 9780521021661, http://books.google.co.uk/books?id=8JIpEhHWT-cC

[43] Wenhui Li, I. Mourachko, M. Noel, and T. Gallagher, *Millimeter-wave spectroscopy of cold rb rydberg atoms in a magneto-optical trap: Quantum defects of the ns, np, and nd series*, Physical Review A **67** (May 2003), ISSN 1050-2947, doi:\bibinfo{doi}{10.1103/PhysRevA.67.052502}, http://pra.aps.org/abstract/PRA/v67/i5/e052502

[44] J. M. Raimond *et al.*, *Statistics of millimeter-wave photons emitted by a rydberg-atom maser: An experimental study of fluctuations in single-mode superradiance*, Physical Review Letters **49**, 1924–1927 (Dec. 1982), http://link.aps.org/doi/10.1103/PhysRevLett.49.1924

[45] P. Goy, J. M. Raimond, M. Gross, and S. Haroche, *Observation of cavity-enhanced single-atom spontaneous emission*, Physical Review Letters **50**, 1903–1906 (Jun. 1983), http://link.aps.org/doi/10.1103/PhysRevLett.50.1903

[46] W. R. Anderson, J. R. Veale, and T. F. Gallagher, *Resonant dipole-dipole energy transfer in a nearly frozen rydberg gas*, Physical Review Letters **80**, 249–252 (Jan. 1998), http://link.aps.org/doi/10.1103/PhysRevLett.80.249

[47] I. Mourachko *et al.*, *Many-body effects in a frozen rydberg gas*, Physical Review Letters **80**, 253–256 (Jan. 1998), http://link.aps.org/doi/10.1103/PhysRevLett.80.253

[48] J. Millen, G. Lochead, and M. P. A. Jones, *Two-electron excitation of an interacting cold rydberg gas*, Physical Review Letters **105**, 213004 (Nov. 2010), http://link.aps.org/doi/10.1103/PhysRevLett.105.213004

[49] G. Lochead *et al.*, *Number-resolved imaging of excited-state atoms using a scanning autoionization microscope*, Physical Review A **87**, 053409 (May 2013), http://link.aps.org/doi/10.1103/PhysRevA.87.053409

[50] M Tanasittikosol *et al.*, *Microwave dressing of rydberg dark states*, J. Phys. B **44**, 184020 (2011), http://stacks.iop.org/0953-4075/44/i=18/a=184020

[51] C L Vaillant, M P A Jones, and R M Potvliege, *Long-range rydberg–rydberg interactions in calcium, strontium and ytterbium*, J. Phys. B **45**, 135004 (2012), http://stacks.iop.org/0953-4075/45/i=13/a=135004

[52] C. Carr *et al.*, *Nonequilibrium phase transition in a dilute rydberg ensemble*, Phys. Rev. Lett. **111**, 113901 (Sep 2013), http://link.aps.org/doi/10.1103/PhysRevLett.111.113901

[53] L. Béguin *et al.*, *Direct measurement of the van der waals interaction between two rydberg atoms*, Physical Review Letters **110**, 263201 (Jun. 2013), http://link.aps.org/doi/10.1103/PhysRevLett.110.263201

[54] A Anderson *et al.*, *Measuring the van der waals forces between a rydberg atom and a metallic surface*, Physical Review A **37**, 3594 (1988)

[55] P. Nordlander, *Energies and lifetimes of atomic rydberg states near metal surfaces*, Physical Review B **53**, 4125–4132 (Feb. 1996), http://link.aps.org/doi/10.1103/PhysRevB.53.4125

[56] E. So, M. T. Bell, and T. P. Softley, *Wave-packet propagation study of the charge-transfer dynamics of rydberg atoms with metal surfaces*, Physical Review A **79**, 012901 (Jan. 2009), http://link.aps.org/doi/10.1103/PhysRevA.79.012901

[57] Chris H. Greene, A. S. Dickinson, and H. R. Sadeghpour, *Creation of polar and nonpolar ultra-long-range rydberg molecules*, Phys. Rev. Lett. **85**, 2458–2461 (Sep 2000), http://link.aps.org/doi/10.1103/PhysRevLett.85.2458

[58] Vera Bendkowsky *et al.*, *Observation of ultralong-range rydberg molecules*, Nature **458**, 1005–1008 (Apr. 2009), ISSN 0028-0836,

http://www.nature.com/nature/journal/v458/n7241/full/nature07945.html

[59] W. Li *et al.*, *A homonuclear molecule with a permanent electric dipole moment*, Science **334**, 1110–1114 (Nov. 2011), ISSN 0036-8075, 1095-9203, http://www.sciencemag.org/content/334/6059/1110

[60] Ashok K. Mohapatra *et al.*, *A giant electro-optic effect using polarizable dark states*, Nature Physics **4**, 890–894 (Nov. 2008), ISSN 1745-2473, http://www.nature.com/nphys/journal/v4/n11/full/nphys1091.html

[61] Jonathon A. Sedlacek *et al.*, *Microwave electrometry with rydberg atoms in a vapour cell using bright atomic resonances*, Nature Physics **8**, 819–824 (Nov. 2012), ISSN 1745-2473, http://www.nature.com/nphys/journal/v8/n11/full/nphys2423.html

[62] J. A. Sedlacek, A. Schwettmann, H. Kübler, and J. P. Shaffer, *Atom-based vector microwave electrometry using rubidium rydberg atoms in a vapor cell*, Physical Review Letters **111**, 063001 (Aug. 2013), http://link.aps.org/doi/10.1103/PhysRevLett.111.063001

[63] G. Pupillo *et al.*, *Strongly correlated gases of rydberg-dressed atoms: Quantum and classical dynamics*, Physical Review Letters **104**, 223002 (Jun. 2010), http://link.aps.org/doi/10.1103/PhysRevLett.104.223002

[64] N. Henkel, R. Nath, and T. Pohl, *Three-dimensional roton excitations and supersolid formation in rydberg-excited bose-einstein condensates*, Physical Review Letters **104**, 195302 (May 2010), http://link.aps.org/doi/10.1103/PhysRevLett.104.195302

[65] Jonathan B. Balewski *et al.*, *Rydberg dressing: Understanding of collective many-body effects and implications for experiments*,

arXiv:1312.6346 [cond-mat, physics:physics, physics:quant-ph](Dec. 2013), http://arxiv.org/abs/1312.6346

[66] M. D. Lukin *et al.*, *Dipole blockade and quantum information processing in mesoscopic atomic ensembles*, Phys. Rev. Lett. **87**, 037901 (Jun 2001), http://link.aps.org/doi/10.1103/PhysRevLett.87.037901

[67] E. Urban *et al.*, *Observation of rydberg blockade between two atoms*, Nature Physics **5**, 110–114 (Jan. 2009), ISSN 1745-2473, http://dx.doi.org/10.1038/nphys1178

[68] Daniel Comparat and Pierre Pillet, *Dipole blockade in a cold rydberg atomic sample*, J. Opt. Soc. Am. B **27**, A208–A232 (Jun 2010), http://josab.osa.org/abstract.cfm?URI=josab-27-6-A208

[69] M. Saffman, T. G. Walker, and K. Mølmer, *Quantum information with rydberg atoms*, Rev. Mod. Phys. **82**, 2313–2363 (Aug 2010), http://link.aps.org/doi/10.1103/RevModPhys.82.2313

[70] Hendrik Weimer *et al.*, *A rydberg quantum simulator*, Nature Physics **6**, 382–388 (May 2010), ISSN 1745-2473, http://www.nature.com/nphys/journal/v6/n5/abs/nphys1614.html

[71] Igor Lesanovsky, *Many-body spin interactions and the ground state of a dense rydberg lattice gas*, Physical Review Letters **106**, 025301 (Jan. 2011), http://link.aps.org/doi/10.1103/PhysRevLett.106.025301

[72] Alexey V. Gorshkov *et al.*, *Photon-photon interactions via rydberg blockade*, Phys. Rev. Lett. **107**, 133602 (Sep 2011), http://link.aps.org/doi/10.1103/PhysRevLett.107.133602

[73] Peter Schauß *et al.*, *Observation of spatially ordered structures in a two-dimensional rydberg gas*, Nature **491**, 87–91 (Nov. 2012), ISSN

0028-0836, http://www.nature.com/nature/journal/v491/n7422/full/nature11596.html

[74] D. Paredes-Barato and C. S. Adams, *All-optical quantum information processing using rydberg gates*, Physical Review Letters **112**, 040501 (Jan. 2014), http://link.aps.org/doi/10.1103/PhysRevLett.112.040501

[75] J. D. Pritchard *et al.*, *Hybrid atom-photon quantum gate in a superconducting microwave resonator*, Physical Review A **89**, 010301 (Jan. 2014), http://link.aps.org/doi/10.1103/PhysRevA.89.010301

[76] J. D. Pritchard *et al.*, *Cooperative atom-light interaction in a blockaded rydberg ensemble*, Phys. Rev. Lett. **105**, 193603 (Nov 2010), http://link.aps.org/doi/10.1103/PhysRevLett.105.193603

[77] David Petrosyan, Johannes Otterbach, and Michael Fleischhauer, *Electromagnetically induced transparency with rydberg atoms*, Physical Review Letters **107**, 213601 (Nov. 2011), http://link.aps.org/doi/10.1103/PhysRevLett.107.213601

[78] S. Sevinçli, N. Henkel, C. Ates, and T. Pohl, *Nonlocal nonlinear optics in cold rydberg gases*, Phys. Rev. Lett. **107**, 153001 (Oct 2011), http://link.aps.org/doi/10.1103/PhysRevLett.107.153001

[79] Y. O. Dudin and A. Kuzmich, *Strongly interacting rydberg excitations of a cold atomic gas*, Science **336**, 887–889 (2012), http://www.sciencemag.org/content/336/6083/887.full.pdf, http://www.sciencemag.org/content/336/6083/887.abstract

[80] T. Peyronel *et al.*, *Quantum nonlinear optics with single photons enabled by strongly interacting atoms*, Nature **488**, 57–60 (Aug. 2012)

[81] Ofer Firstenberg *et al.*, *Attractive photons in a quantum nonlinear*

medium, Nature **502**, 71–75 (Oct. 2013), ISSN 0028-0836, http://www.nature.com/nature/journal/v502/n7469/full/nature12512.html

[82] Alexey V. Gorshkov, Rejish Nath, and Thomas Pohl, *Dissipative many-body quantum optics in rydberg media*, Phys. Rev. Lett. **110**, 153601 (Apr 2013), http://link.aps.org/doi/10.1103/PhysRevLett.110.153601

[83] G. Günter *et al.*, *Observing the dynamics of dipole-mediated energy transport by interaction enhanced imaging*, Science, 1244843(Nov. 2013), ISSN 0036-8075, 1095-9203, http://www.sciencemag.org/content/early/2013/11/06/science.1244843

[84] C. S. Hofmann *et al.*, *Sub-poissonian statistics of rydberg-interacting dark-state polaritons*, Phys. Rev. Lett. **110**, 203601 (May 2013), http://link.aps.org/doi/10.1103/PhysRevLett.110.203601

[85] Simon Baur, Daniel Tiarks, Gerhard Rempe, and Stephan Dürr, *Single-photon switch based on rydberg blockade*, Physical Review Letters **112**, 073901 (Feb. 2014), http://link.aps.org/doi/10.1103/PhysRevLett.112.073901

[86] D. Maxwell *et al.*, *Microwave control of the interaction between two optical photons*, Phys. Rev. A **89**, 043827 (Apr 2014), http://link.aps.org/doi/10.1103/PhysRevA.89.043827

[87] Weibin Li, Daniel Viscor, Sebastian Hofferberth, and Igor Lesanovsky, *Electromagnetically induced transparency in an entangled medium*, Physical Review Letters **112**, 243601 (Jun. 2014), http://link.aps.org/doi/10.1103/PhysRevLett.112.243601

[88] Hannes Gorniaczyk *et al.*, *Single photon transistor mediated by inter-state rydberg interaction*, arXiv:1404.2876 [quant-ph](Apr. 2014), http://arxiv.org/abs/1404.2876

[89] Inbal Friedler, David Petrosyan, Michael Fleischhauer, and Gershon Kurizki, *Long-range interactions and entanglement of slow single-photon pulses*, Phys. Rev. A **72**, 043803 (Oct 2005), http://link.aps.org/doi/10.1103/PhysRevA.72.043803

[90] Ephraim Shahmoon, Gershon Kurizki, Michael Fleischhauer, and David Petrosyan, *Strongly interacting photons in hollow-core waveguides*, Phys. Rev. A **83**, 033806 (Mar 2011), http://link.aps.org/doi/10.1103/PhysRevA.83.033806

[91] Alexey V. Gorshkov, Rejish Nath, and Thomas Pohl, *Dissipative many-body quantum optics in rydberg media*, Phys. Rev. Lett. **110**, 153601 (Apr 2013), http://link.aps.org/doi/10.1103/PhysRevLett.110.153601

[92] Valentina Parigi *et al.*, *Observation and measurement of interaction-induced dispersive optical nonlinearities in an ensemble of cold rydberg atoms*, Phys. Rev. Lett. **109**, 233602 (Dec 2012), http://link.aps.org/doi/10.1103/PhysRevLett.109.233602

[93] D. Jaksch *et al.*, *Fast quantum gates for neutral atoms*, Phys. Rev. Lett. **85**, 2208–2211 (Sep 2000), http://link.aps.org/doi/10.1103/PhysRevLett.85.2208

[94] T. Wilk *et al.*, *Entanglement of two individual neutral atoms using rydberg blockade*, Phys. Rev. Lett. **104**, 010502 (Jan 2010), http://link.aps.org/doi/10.1103/PhysRevLett.104.010502

[95] L. Isenhower *et al.*, *Demonstration of a neutral atom controlled*−not *quantum gate*, Phys. Rev. Lett. **104**, 010503 (Jan 2010), http://link.aps.org/doi/10.1103/PhysRevLett.104.010503

[96] C. K. Hong, Z. Y. Ou, and L. Mandel, *Measurement of subpicosecond time intervals between two photons by interference*, Physical Review

Letters **59**, 2044–2046 (Nov. 1987), ISSN 0031-9007, http://prl.aps.org/abstract/PRL/v59/i18/p2044_1

[97] Mattias Marklund and Padma K. Shukla, *Nonlinear collective effects in photon-photon and photon-plasma interactions*, Reviews of Modern Physics **78**, 591–640 (May 2006), http://link.aps.org/doi/10.1103/RevModPhys.78.591

[98] Alexander I. Lvovsky, Barry C. Sanders, and Wolfgang Tittel, *Optical quantum memory*, Nature Photonics **3**, 706–714 (Dec. 2009), ISSN 1749-4885, http://dx.doi.org/10.1038/nphoton.2009.231

[99] Hugues de Riedmatten *et al.*, *A solid-state light–matter interface at the single-photon level*, Nature **456**, 773–777 (Dec. 2008), ISSN 0028-0836, http://www.nature.com/nature/journal/v456/n7223/full/nature07607.html

[100] K. F. Reim *et al.*, *Single-photon-level quantum memory at room temperature*, Physical Review Letters **107**, 053603 (Jul. 2011), http://link.aps.org/doi/10.1103/PhysRevLett.107.053603

[101] Y. O. Dudin, L. Li, and A. Kuzmich, *Light storage on the time scale of a minute*, Physical Review A **87**, 031801 (Mar. 2013), http://link.aps.org/doi/10.1103/PhysRevA.87.031801

[102] P. C. Maurer *et al.*, *Room-terature quantum bit memory exceeding one second*, Science **336**, 1283–1286 (Jun. 2012), ISSN 0036-8075, 1095-9203, http://www.sciencemag.org/content/336/6086/1283

[103] M. Steger *et al.*, *Quantum information storage for over 180 s using donor spins in a 28si "semiconductor vacuum"*, Science **336**, 1280–1283 (Jun. 2012), ISSN 0036-8075, 1095-9203, http://www.sciencemag.org/content/336/6086/1280

[104] Kamyar Saeedi *et al.*, *Room-temperature quantum bit storage exceeding 39 minutes using ionized donors in silicon-28*, Science **342**, 830–833 (Nov. 2013), ISSN 0036-8075, 1095-9203, http://www.sciencemag.org/content/342/6160/830

[105] D. G. England *et al.*, *High-fidelity polarization storage in a gigahertz bandwidth quantum memory*, Journal of Physics B: Atomic, Molecular and Optical Physics **45**, 124008 (Jun. 2012), ISSN 0953-4075, http://iopscience.iop.org/0953-4075/45/12/124008

[106] A. P. Lund and T. C. Ralph, *Nondeterministic gates for photonic single-rail quantum logic*, Physical Review A **66**, 032307 (Sep. 2002), http://link.aps.org/doi/10.1103/PhysRevA.66.032307

[107] A. Nicolas *et al.*, *A quantum memory for orbital angular momentum photonic qubits*, Nature Photonics **8**, 234–238 (Mar. 2014), ISSN 1749-4885, http://www.nature.com/nphoton/journal/v8/n3/full/nphoton.2013.355.html

[108] M. Fleischhauer and M. D. Lukin, *Dark-state polaritons in electromagnetically induced transparency*, Phys. Rev. Lett. **84**, 5094–5097 (May 2000), http://link.aps.org/doi/10.1103/PhysRevLett.84.5094

[109] M. Fleischhauer and M. Lukin, *Quantum memory for photons: Dark-state polaritons*, Physical Review A **65** (Jan. 2002), ISSN 1050-2947, http://pra.aps.org/abstract/PRA/v65/i2/e022314

[110] Michael Fleischhauer, Atac Imamoglu, and Jonathan P. Marangos, *Electromagnetically induced transparency: Optics in coherent media*, Reviews of Modern Physics **77**, 633–673 (Jul. 2005), http://link.aps.org/doi/10.1103/RevModPhys.77.633

[111] Jean Dalibard, Yvan Castin, and Klaus Mølmer, *Wave-function approach to dissipative processes in quantum optics*, Physical Review Let-

ters **68**, 580–583 (Feb. 1992), http://link.aps.org/doi/10.1103/PhysRevLett.68.580

[112] G. Lindblad, *On the generators of quantum dynamical semigroups*, Communications in Mathematical Physics **48**, 119–130 (Jun. 1976), ISSN 0010-3616, 1432-0916, http://link.springer.com/article/10.1007/BF01608499

[113] Ryogo Kubo, *Statistical-mechanical theory of irreversible processes. i. general theory and simple applications to magnetic and conduction problems*, Journal of the Physical Society of Japan **12**, 570–586 (Jun. 1957), ISSN 0031-9015, http://journals.jps.jp/doi/abs/10.1143/JPSJ.12.570

[114] Claude Cohen-Tannoudji, Jacques Dupont-Roc, and Gilbert Grynberg, *Atom-Photon Interactions: Basic Processes and Applications* (Wiley, 1998) ISBN 9780471293361

[115] Marlan O. Scully, *Quantum Optics* (Cambridge University Press, 1997) ISBN 9780521435956

[116] J. D. Pritchard, *Cooperative Optical Non-linearity in a blockaded Rydberg ensemble*, Ph.D. thesis, University of Durham (2011)

[117] B. R. Mollow, *Power spectrum of light scattered by two-level systems*, Physical Review **188**, 1969–1975 (Dec. 1969), http://link.aps.org/doi/10.1103/PhysRev.188.1969

[118] H. C. Torrey, *Transient nutations in nuclear magnetic resonance*, Physical Review **76**, 1059–1068 (Oct. 1949), http://link.aps.org/doi/10.1103/PhysRev.76.1059

[119] J. Keaveney *et al.*, *Maximal refraction and superluminal propagation in a gaseous nanolayer*, Physical Review Letters **109**, 233001 (Dec. 2012), http://link.aps.org/doi/10.1103/PhysRevLett.109.233001

[120] J. P. Marangos, *Electromagnetically induced transparency*, Journal of Modern Optics **45**, 471–503 (1998), ISSN 0950-0340, http://www.tandfonline.com/doi/abs/10.1080/09500349808231909

[121] Peter Lambropoulos and David Petrosyan, *Fundamentals of quantum optics and quantum information* (Springer Berlin, 2007)

[122] G. Alzetta, A. Gozzini, L. Moi, and G. Orriols, *An experimental method for the observation of r.f. transitions and laser beat resonances in oriented na vapour*, Il Nuovo Cimento B Series 11 **36**, 5–20 (Nov. 1976), ISSN 0369-3554, 1826-9877, http://link.springer.com/article/10.1007/BF02749417

[123] S. H. Autler and C. H. Townes, *Stark effect in rapidly varying fields*, Physical Review **100**, 703–722 (Oct. 1955), http://link.aps.org/doi/10.1103/PhysRev.100.703

[124] Julio Gea-Banacloche, Yong-qing Li, Shao-zheng Jin, and Min Xiao, *Electromagnetically induced transparency in ladder-type inhomogeneously broadened media: Theory and experiment*, Physical Review A **51**, 576–584 (Jan. 1995), http://link.aps.org/doi/10.1103/PhysRevA.51.576

[125] K.-J. Boller, A. Imamolu, and S. E. Harris, *Observation of electromagnetically induced transparency*, Physical Review Letters **66**, 2593–2596 (May 1991), http://link.aps.org/doi/10.1103/PhysRevLett.66.2593

[126] Alexey V. Gorshkov, Axel André, Mikhail D. Lukin, and Anders S. Sørensen, *Photon storage in λ-type optically dense atomic media. ii. free-space model*, Phys. Rev. A **76**, 033805 (Sep 2007), http://link.aps.org/doi/10.1103/PhysRevA.76.033805

[127] John David Jackson and John D Jackson, *Classical electrodynamics*, Vol. 3 (Wiley New York etc., 1962)

[128] S. E. Harris and Lene Vestergaard Hau, *Nonlinear optics at low light levels*, Physical Review Letters **82**, 4611–4614 (Jun. 1999), http://link.aps.org/doi/10.1103/PhysRevLett.82.4611

[129] A. S. Parkins, P. Marte, P. Zoller, and H. J. Kimble, *Synthesis of arbitrary quantum states via adiabatic transfer of zeeman coherence*, Physical Review Letters **71**, 3095–3098 (Nov. 1993), http://link.aps.org/doi/10.1103/PhysRevLett.71.3095

[130] M. D. Lukin, S. F. Yelin, and M. Fleischhauer, *Entanglement of atomic ensembles by trapping correlated photon states*, Physical Review Letters **84**, 4232–4235 (May 2000), http://link.aps.org/doi/10.1103/PhysRevLett.84.4232

[131] Chien Liu, Zachary Dutton, Cyrus H. Behroozi, and Lene Vestergaard Hau, *Observation of coherent optical information storage in an atomic medium using halted light pulses*, Nature **409**, 490–493 (Jan. 2001), ISSN 0028-0836, http://www.nature.com/nature/journal/v409/n6819/full/409490a0.html

[132] S D Jenkins, T Zhang, and T A B Kennedy, *Motional dephasing of atomic clock spin waves in an optical lattice*, J. Phys. B **45**, 124005 (2012), http://stacks.iop.org/0953-4075/45/i=12/a=124005

[133] M. D. Eisaman *et al.*, *Electromagnetically induced transparency with tunable single-photon pulses*, Nature **438**, 837–841 (Dec. 2005), ISSN 0028-0836, http://www.nature.com/nature/journal/v438/n7069/full/nature04327.html

[134] M. Lobino, C. Kupchak, E. Figueroa, and A. I. Lvovsky, *Memory for light as a quantum process*, Physical Review Letters **102**, 203601

(May 2009), http://link.aps.org/doi/10.1103/PhysRevLett.102.203601

[135] Ryan M. Camacho, Praveen K. Vudyasetu, and John C. Howell, *Four-wave-mixing stopped light in hot atomic rubidium vapour*, Nature Photonics **3**, 103–106 (Jan. 2009), ISSN 1749-4885, http://dx.doi.org/10.1038/nphoton.2008.290

[136] K. S. Choi, H. Deng, J. Laurat, and H. J. Kimble, *Mapping photonic entanglement into and out of a quantum memory*, Nature **452**, 67–71 (Mar. 2008), ISSN 0028-0836, http://www.nature.com/nature/journal/v452/n7183/full/nature06670.html

[137] Alexey V. Gorshkov *et al.*, *Universal approach to optimal photon storage in atomic media*, Physical Review Letters **98**, 123601 (Mar. 2007), http://link.aps.org/doi/10.1103/PhysRevLett.98.123601

[138] J. Keaveney *et al.*, *Cooperative lamb shift in an atomic vapor layer of nanometer thickness*, Phys. Rev. Lett. **108**, 173601 (Apr 2012), http://link.aps.org/doi/10.1103/PhysRevLett.108.173601

[139] Kilian Singer, Jovica Stanojevic, Matthias Weidemüller, and Robin Côté, *Long-range interactions between alkali rydberg atom pairs correlated to the ns–ns, np–np and nd–nd asymptotes*, Journal of Physics B: Atomic, Molecular and Optical Physics **38**, S295 (Jan. 2005), ISSN 0953-4075, http://iopscience.iop.org/0953-4075/38/2/021

[140] Harald Kübler *et al.*, *Atom based vector microwave electrometry using rubidium rydberg atoms in a vapor cell*, in *Research in Optical Sciences*, OSA Technical Digest (online) (Optical Society of America, 2014) p. JW2A.42, http://www.opticsinfobase.org/abstract.cfm?URI=HILAS-2014-JW2A.42

[141] I. E. Protsenko, G. Reymond, N. Schlosser, and P. Grangier, *Operation of a quantum phase gate using neutral atoms in microscopic dipole traps*, Phys. Rev. A **65**, 052301 (Apr 2002), http://link.aps.org/doi/10.1103/PhysRevA.65.052301

[142] Christophe Vaillant, *Long-Range Interactions in One- and Two-Electron Rydberg Atoms*, Doctoral, Durham University (2014), http://etheses.dur.ac.uk/10594/

[143] Robert J. Buehler and Joseph O. Hirschfelder, *Bipolar expansion of coulombic potentials*, Phys. Rev. **83**, 628–633 (Aug 1951), http://link.aps.org/doi/10.1103/PhysRev.83.628

[144] K. Afrousheh *et al.*, *Spectroscopic observation of resonant electric dipole-dipole interactions between cold rydberg atoms*, Phys. Rev. Lett. **93**, 233001 (Nov 2004), http://link.aps.org/doi/10.1103/PhysRevLett.93.233001

[145] Jianing Han and T. F. Gallagher, *Millimeter-wave rubidium rydberg van der waals spectroscopy*, Phys. Rev. A **79**, 053409 (May 2009), http://link.aps.org/doi/10.1103/PhysRevA.79.053409

[146] J.-Y. Zhang and J. Mitroy, *Long-range dispersion interactions. i. formalism for two heteronuclear atoms*, Physical Review A **76**, 022705 (Aug. 2007), http://link.aps.org/doi/10.1103/PhysRevA.76.022705

[147] Thad G. Walker and M. Saffman, *Consequences of zeeman degeneracy for the van der waals blockade between rydberg atoms*, Physical Review A **77**, 032723 (Mar. 2008), http://link.aps.org/doi/10.1103/PhysRevA.77.032723

[148] F. Robicheaux and J. V. Hernández, *Many-body wave function in a*

dipole blockade configuration, Physical Review A **72**, 063403 (Dec. 2005), http://link.aps.org/doi/10.1103/PhysRevA.72.063403

[149] F. Bariani, Y. O. Dudin, T. A. B. Kennedy, and A. Kuzmich, *Dephasing of multiparticle rydberg excitations for fast entanglement generation*, Phys. Rev. Lett. **108**, 030501 (Jan 2012), http://link.aps.org/doi/10.1103/PhysRevLett.108.030501

[150] A. I. Lvovsky and M. G. Raymer, *Continuous-variable optical quantum-state tomography*, Reviews of Modern Physics **81**, 299–332 (Mar. 2009), http://link.aps.org/doi/10.1103/RevModPhys.81.299

[151] U. Fano, *Description of states in quantum mechanics by density matrix and operator techniques*, Reviews of Modern Physics **29**, 74–93 (Jan. 1957), http://link.aps.org/doi/10.1103/RevModPhys.29.74

[152] James L Park and William Band, *A general theory of empirical state determination in quantum physics: Part i*, Foundations of Physics **1**, 211–226 (1971)

[153] K. Vogel and H. Risken, *Determination of quasiprobability distributions in terms of probability distributions for the rotated quadrature phase*, Physical Review A **40**, 2847–2849 (Sep. 1989), http://link.aps.org/doi/10.1103/PhysRevA.40.2847

[154] R. Loudon, *Non-classical effects in the statistical properties of light*, Reports on Progress in Physics **43**, 913 (Jul. 1980), ISSN 0034-4885, http://iopscience.iop.org/0034-4885/43/7/002

[155] Leonard Mandel and Emil Wolf, *Optical Coherence and Quantum Optics*, 1st ed. (Cambridge University Press, 1995) ISBN 0521417112

[156] G. I. Taylor, *Interference Fringes with Feeble Light*, Proc. Cam. Phil. Soc., 114(1909)

[157] Stefan Gerlich *et al.*, *Quantum interference of large organic molecules*, Nature Communications **2**, 263+ (Apr. 2011), http://dx.doi.org/10.1038/ncomms1263

[158] Bahaa E. A. Saleh and Malvin C. Teich, *Fundamentals of Photonics (Wiley Series in Pure and Applied Optics)*, 1st ed. (John Wiley & Sons, 1991) ISBN 9780471839651

[159] H. J. Kimble and L. Mandel, *Theory of resonance fluorescence*, Physical Review A **13**, 2123–2144 (Jun. 1976), http://dx.doi.org/10.1103/PhysRevA.13.2123

[160] Leonard Mandel and Emil Wolf, *Optical Coherence and Quantum Optics* (Cambridge University Press, 1995) ISBN 9780521417112

[161] Rodney Loudon, *The Quantum Theory of Light* (Oxford University Press, 2000) ISBN 9780191589782

[162] Wolfgang Schleich, *Quantum optics in phase space*, 1st ed. (Wiley-VCH, Berlin ; New York, 2001) ISBN 352729435X

[163] Brian J. Smith and M. G. Raymer, *Photon wave functions, wave-packet quantization of light, and coherence theory*, New Journal of Physics **9**, 414 (Nov. 2007), ISSN 1367-2630, http://iopscience.iop.org/1367-2630/9/11/414

[164] O. Steuernagel, *Quantum statistics can suppress classical interference*, Phys. Rev. A **65**, 013809 (Dec 2001)

[165] L. Mandel, *Photoelectric counting measurements as a test for the existence of photons*, J. Opt. Soc. Am. **67**, 1101–1104 (Aug 1977), http://www.opticsinfobase.org/abstract.cfm?URI=josa-67-8-1101

[166] R. Hanbury Brown and R. Q. Twiss, *A Test of a New Type of Stellar Interferometer on Sirius*, Nature **178**, 1046–1048 (Nov. 1956)

[167] Werner Vogel and Dirk-Gunnar Welsch, *Quantum Optics* (Wiley-VCH, 2006) ISBN 3-527-40507-0

[168] Ofer Firstenberg *et al.*, *Attractive photons in a quantum nonlinear medium*, Nature **502**, 71–75 (Oct. 2013), ISSN 0028-0836, http://www.nature.com/nature/journal/v502/n7469/full/nature12512.html

[169] T. Pohl, E. Demler, and M. D. Lukin, *Dynamical crystallization in the dipole blockade of ultracold atoms*, Physical Review Letters **104**, 043002 (Jan. 2010), http://link.aps.org/doi/10.1103/PhysRevLett.104.043002

[170] Y. O. Dudin, F. Bariani, and A. Kuzmich, *Emergence of spatial spin-wave correlations in a cold atomic gas*, Physical Review Letters **109**, 133602 (Sep. 2012), http://link.aps.org/doi/10.1103/PhysRevLett.109.133602

[171] L. Li, Y. O. Dudin, and A. Kuzmich, *Entanglement between light and an optical atomic excitation*, Nature **498**, 466–469 (Jun. 2013), ISSN 0028-0836, http://www.nature.com/nature/journal/v498/n7455/full/nature12227.html

[172] S. Bettelli *et al.*, *Exciton dynamics in emergent rydberg lattices*, Phys. Rev. A **88**, 043436 (Oct 2013), http://link.aps.org/doi/10.1103/PhysRevA.88.043436

[173] R. Dicke, *Coherence in spontaneous radiation processes*, Physical Review **93**, 99–110 (Jan. 1954), ISSN 0031-899X, http://prola.aps.org/abstract/PR/v93/i1/p99_1

[174] Jovica Stanojevic *et al.*, *Generating non-gaussian states using collisions between rydberg polaritons*, Physical Review A **86**, 021403 (Aug. 2012), http://link.aps.org/doi/10.1103/PhysRevA.86.021403

[175] Thomas Vanderbruggen, *Détection non-destructive pour l'interférométrie atomique et Condensation de Bose-Einstein dans une cavité optique de haute finesse*, Ph.D. thesis, Université Paris Sud-Paris XI (2012)

[176] Daniel Maxwell, *Light storage and control of photon-photon interactions in a cold Rydberg gas*, Doctoral, Durham University (2013), http://etheses.dur.ac.uk/7757/

[177] David P. DiVincenzo, *Two-bit gates are universal for quantum computation*, Phys. Rev. A **51**, 1015–1022 (Feb 1995), http://link.aps.org/doi/10.1103/PhysRevA.51.1015

[178] J. L. O'Brien *et al.*, *Demonstration of an all-optical quantum controlled–*NOT *gate*, Nature **426**, 264–267 (Nov. 2003), arXiv:quant-ph/0403062

[179] J. L. O'Brien *et al.*, *Quantum process tomography of a controlled-NOT gate*, Physical Review Letters **93**, 080502 (Aug. 2004), http://link.aps.org/doi/10.1103/PhysRevLett.93.080502

[180] Erwan Bimbard *et al.*, *Homodyne tomography of a single photon retrieved on demand from a cavity-enhanced cold atom memory*, Physical Review Letters **112**, 033601 (Jan. 2014), http://link.aps.org/doi/10.1103/PhysRevLett.112.033601

[181] Claudia Mewes and Michael Fleischhauer, *Two-photon linewidth of light "stopping" via electromagnetically induced transparency*, Physical Review A **66**, 033820 (Sep. 2002), http://link.aps.org/doi/10.1103/PhysRevA.66.033820

[182] J. Nunn *et al.*, *Multimode memories in atomic ensembles*, Phys. Rev. Lett. **101**, 260502 (Dec 2008), http://link.aps.org/doi/10.1103/PhysRevLett.101.260502

[183] Wolfgang Ketterle, *Nobel lecture: When atoms behave as waves: Bose-einstein condensation and the atom laser*, Rev. Mod. Phys. **74**, 1131–1151 (Nov 2002), http://link.aps.org/doi/10.1103/RevModPhys.74.1131

[184] Jonathan B. Balewski *et al.*, *Coupling a single electron to a bose-einstein condensate*, Nature **502**, 664–667 (Oct. 2013), ISSN 0028-0836, http://www.nature.com/nature/journal/v502/n7473/full/nature12592.html

[185] T. C. Ralph, N. K. Langford, T. B. Bell, and A. G. White, *Linear optical controlled*-NOT *gate in the coincidence basis*, Phys. Rev. A **65**, 062324 (Jun 2002), http://link.aps.org/doi/10.1103/PhysRevA.65.062324

[186] M. A. Pooley *et al.*, *Controlled*-NOT *gate operating with single photons*, Applied Physics Letters **100**, 211103 (May 2012), arXiv:1205.4899 [quant-ph]

[187] Matthias M. Müller *et al.*, *Implementation of an experimentally feasible controlled-phase gate on two blockaded rydberg atoms*, Physical Review A **89**, 032334 (Mar. 2014), http://link.aps.org/doi/10.1103/PhysRevA.89.032334

[188] X. L. Zhang *et al.*, *Fidelity of a rydberg-blockade quantum gate from simulated quantum process tomography*, Physical Review A **85**, 042310 (Apr. 2012), http://link.aps.org/doi/10.1103/PhysRevA.85.042310

[189] M. Kohnen *et al.*, *An array of integrated atom-photon junctions*, Nature Photonics **5**, 35–38 (Jan. 2011)

[190] Jeremy L O'Brien, Akira Furusawa, and Jelena Vučković, *Photonic quantum technologies*, Nature Photonics **3**, 687–695 (2009)

[191] Andrea Crespi *et al.*, *Integrated photonic quantum gates for polarization qubits*, Nature Communications **2**, 566 (2011)

[192] Adriano Barenco *et al.*, *Elementary gates for quantum computation*, Physical Review A **52**, 3457–3467 (Nov. 1995), http://link.aps.org/doi/10.1103/PhysRevA.52.3457

[193] D. Hanneke *et al.*, *Realization of a programmable two-qubit quantum processor*, Nature Physics **6**, 13–16 (Jan. 2010), ISSN 1745-2473, http://www.nature.com/nphys/journal/v6/n1/full/nphys1453.html

[194] Adam Paetznick and Ben W. Reichardt, *Fault-tolerant ancilla preparation and noise threshold lower bounds for the 23-qubit golay code*, arXiv:1106.2190 [quant-ph](Jun. 2011), arXiv: 1106.2190, http://arxiv.org/abs/1106.2190

[195] Tommaso Toffoli, *Reversible computing*, in *Automata, Languages and Programming*, Lecture Notes in Computer Science No. 85, edited by Jaco de Bakker and Jan van Leeuwen (Springer Berlin Heidelberg, 1980) pp. 632–644, ISBN 978-3-540-10003-4, 978-3-540-39346-7, http://link.springer.com/chapter/10.1007/3-540-10003-2_104

[196] Edward Fredkin and Tommaso Toffoli, *Conservative logic*, International Journal of Theoretical Physics **21**, 219–253 (Apr. 1982), ISSN 0020-7748, 1572-9575, http://link.springer.com/article/10.1007/BF01857727

[197] Vivek V. Shende and Igor L. Markov, *On the* CNOT*-cost of* TOFFOLI *gates*, arXiv:0803.2316 [quant-ph](Mar. 2008), arXiv: 0803.2316, http://arxiv.org/abs/0803.2316

[198] L. Isenhower, M. Saffman, and K. Mølmer, *Multibit* C_kNOT *quantum gates via rydberg blockade*, Quantum Information Processing **10**, 755–

770 (Dec. 2011), ISSN 1570-0755, 1573-1332, http://link.springer.com/article/10.1007/s11128-011-0292-4

[199] Johannes Otterbach, Matthias Moos, Dominik Muth, and Michael Fleischhauer, *Wigner crystallization of single photons in cold rydberg ensembles*, Physical Review Letters **111**, 113001 (Sep. 2013), ISSN 0031-9007, http://link.aps.org/doi/10.1103/PhysRevLett.111.113001

[200] P. Bienias *et al.*, *Scattering resonances and bound states for strongly interacting rydberg polaritons*, arXiv:1402.7333 [physics, physics:quant-ph](Feb. 2014), http://arxiv.org/abs/1402.7333

[201] Jovica Stanojevic *et al.*, *Dispersive optical nonlinearities in a rydberg electromagnetically-induced-transparency medium*, Physical Review A **88**, 053845 (Nov. 2013), http://link.aps.org/doi/10.1103/PhysRevA.88.053845

[202] Robert H. Hadfield, *Single-photon detectors for optical quantum information applications*, Nature Photonics **3**, 696–705 (Dec. 2009), ISSN 1749-4885, http://www.nature.com/nphoton/journal/v3/n12/abs/nphoton.2009.230.html

[203] ALV-GmbH, *Single Photon Detectors*, http://www.alvgmbh.de/Products/PMTs___APDs/tt_detekt/tt_detekt.html

[204] M. Wahl, *Time-Correlated Photon Counting Tech Note TCSPC 1.2*, PicoQuant GmbH (January 2000), http://www.picoquant.com/technotes/technote_tcspc.pdf

[205] S. Cova *et al.*, *Avalanche photodiodes and quenching circuits for single-photon detection.*, Appl Opt **35**, 1956–1976 (1996)

[206] E. A. Donley *et al.*, *Double-pass acousto-optic modulator system*, Review of Scientific Instruments **76**, 063112 (Jun. 2005), ISSN 0034-6748,

1089-7623, http://scitation.aip.org/content/aip/journal/rsi/76/6/10.1063/1.1930095

[207] Jörg W. Müller, *Counting statistics of a Poisson process with dead time*, Tech. Rep. (Bureau International des Poids et Mesures, 92-Sevres (France), 1970)

[208] Jörg W. Müller, *Some formulae for a dead-time-distorted poisson process: To andré allisy on the completion of his first half century*, Nuclear Instruments and Methods **117**, 401–404 (May 1974), ISSN 0029-554X, http://www.sciencedirect.com/science/article/pii/0029554X74902833

[209] V. G. Kornilov, *A statistical description of the non-linearity of photon counts*, Astronomy Reports **52**, 70–78 (Jan. 2008), ISSN 1063-7729, 1562-6881, http://link.springer.com/article/10.1134/S1063772908010083

[210] V. G. Kornilov, *Effects of dead time and afterpulses in photon detector on measured statistics of stochastic radiation*, Journal of the Optical Society of America A **31**, 7–15 (Jan. 2014), http://josaa.osa.org/abstract.cfm?URI=josaa-31-1-7

[211] Ifan G Hughes and Thomas Hase, *Measurements and their Uncertainties* (Oxford Univ. Press, 2010)

[212] SensL, *HRMTime Instalation and User Guide (Version 1.7)*

[213] P. B. Coates, *The correction for photon 'pile-up' in the measurement of radiative lifetimes*, Journal of Physics E: Scientific Instruments **1**, 878 (Aug. 1968), ISSN 0022-3735, http://iopscience.iop.org/0022-3735/1/8/437

[214] John G. Walker, *Iterative correction for 'pile-up' in single-photon lifetime measurement*, Optics Communications **201**, 271–277 (Jan.

2002), ISSN 0030-4018, http://www.sciencedirect.com/science/article/pii/S0030401801016637

[215] Michel Orrit, *Photon statistics in single molecule experiments*, Single Molecules **3**, 255–265 (Nov. 2002), ISSN 1438-5171, http://onlinelibrary.wiley.com/doi/10.1002/1438-5171(200211)3:5/6<255::AID-SIMO255>3.0.CO;2-8/abstract

[216] C. C. Davis and T. A. King, *Correction methods for photon pile-up in lifetime determination by single-photon counting*, Journal of Physics A: General Physics **3**, 101 (Jan. 1970), ISSN 0022-3689, http://iopscience.iop.org/0022-3689/3/1/013

[217] G. T. Foster, S. L. Mielke, and L. A. Orozco, *Intensity correlations of a noise-driven diode laser*, Journal of the Optical Society of America B **15**, 2646–2653 (Nov. 1998), http://josab.osa.org/abstract.cfm?URI=josab-15-11-2646

[218] K. A. Whittaker *et al.*, *Optical response of gas-phase atoms at less than* $\lambda/80$ *from a dielectric surface*, Physical Review Letters **112**, 253201 (Jun. 2014), http://link.aps.org/doi/10.1103/PhysRevLett.112.253201

[219] K Dieckmann, RJC Spreeuw, M Weidemüller, and JTM Walraven, *Two-dimensional magneto-optical trap as a source of slow atoms*, Physical Review A **58**, 3891 (1998)

[220] J. Schoser *et al.*, *Intense source of cold rb atoms from a pure two-dimensional magneto-optical trap*, Phys. Rev. A **66**, 023410 (Aug 2002), http://link.aps.org/doi/10.1103/PhysRevA.66.023410

[221] Simone Götz *et al.*, *Versatile cold atom target apparatus*, Review of Scientific Instruments **83**, 073112 (Jul. 2012), ISSN 0034-6748, 1089-

7623, http://scitation.aip.org/content/aip/journal/rsi/83/7/10.1063/1.4738643

[222] Brahim Lounis and Michel Orrit, *Single-photon sources*, Reports on Progress in Physics **68**, 1129 (May 2005), ISSN 0034-4885, http://iopscience.iop.org/0034-4885/68/5/R04

[223] Matthias Scholz, Lars Koch, and Oliver Benson, *Statistics of narrow-band single photons for quantum memories generated by ultrabright cavity-enhanced parametric down-conversion*, Physical Review Letters **102**, 063603 (Feb. 2009), http://link.aps.org/doi/10.1103/PhysRevLett.102.063603

[224] Avshalom C. Elitzur and Lev Vaidman, *Quantum mechanical interaction-free measurements*, Foundations of Physics **23**, 987–997 (Jul. 1993), ISSN 0015-9018, 1572-9516, http://link.springer.com/article/10.1007/BF00736012

[225] P. G. Kwiat *et al.*, *High-efficiency quantum interrogation measurements via the quantum zeno effect*, Physical Review Letters **83**, 4725–4728 (Dec. 1999), http://link.aps.org/doi/10.1103/PhysRevLett.83.4725

[226] Joanna A. Zielińska, Federica A. Beduini, Nicolas Godbout, and Morgan W. Mitchell, *Ultranarrow faraday rotation filter at the Rb d1 line*, Optics Letters **37**, 524–526 (Feb. 2012), http://ol.osa.org/abstract.cfm?URI=ol-37-4-524

[227] Florian Wolfgramm *et al.*, *Atom-resonant heralded single photons by interaction-free measurement*, Physical Review Letters **106**, 053602 (Feb. 2011), http://link.aps.org/doi/10.1103/PhysRevLett.106.053602

[228] A. MacRae, T. Brannan, R. Achal, and A. I. Lvovsky, *Tomography of a high-purity narrowband photon from a transient atomic collective excitation*, Physical Review Letters **109**, 033601 (Jul. 2012), `http://link.aps.org/doi/10.1103/PhysRevLett.109.033601`

[229] L. A. Zadeh, *Fuzzy sets*, Information and Control **8**, 338–353 (Jun. 1965), ISSN 0019-9958, `http://www.sciencedirect.com/science/article/pii/S001999586590241X`

[230] Bart Kosko and Satoru Isaka, *Fuzzy logic*, Scientific American **269**, 62–7 (1993)

[231] Jiří Wiedermann, *Characterizing the super-turing computing power and efficiency of classical fuzzy turing machines*, Theoretical Computer Science, Super-Recursive Algorithms and Hypercomputation **317**, 61–69 (Jun. 2004), ISSN 0304-3975, `http://www.sciencedirect.com/science/article/pii/S0304397503006315`

[232] Ebrahim H. Mamdani, *Application of fuzzy logic to approximate reasoning using linguistic synthesis*, IEEE Transactions on Computers **C-26**, 1182–1191 (Dec. 1977), ISSN 0018-9340

[233] Kevin M. Passino, *Fuzzy Control* (Addison-Wesley, 1998) ISBN 9780201180749